GDAŃSK UNIVERSITY OF TECHNOLOGY

The author of the doctoral dissertation: Mateusz Troka
Scientific discipline: Mechanical Engineering

DOCTORAL DISSERTATION

Title of doctoral dissertation: Unsupervised Machine Learning in Biomechanical Data Analysis. Medical Application of Self-Organising Maps

Title of doctoral dissertation (in Polish): Nienadzorowane Uczenie Maszynowe w Analizie Danych Biomechanicznych. Medyczne Zastosowanie Map Samoorganizujących.

Supervisor *signature*	Second supervisor *signature*
Dr hab. inż. Izabela Lubowiecka, prof. GUT	-
Auxiliary supervisor Not applicable *signature*	Cosupervisor Not applicable *signature*
-	-

Gdańsk, 2025

GDAŃSK UNIVERSITY OF TECHNOLOGY

STATEMENT

The author of the doctoral dissertation: Mateusz Troka

I, the undersigned, declare that I am aware that in accordance with the provisions of Art. 27 (1) and (2) of the Act of 4th February 1994 on Copyright and Related Rights (Journal of Laws of 2021, item 1062), the university may use my doctoral dissertation entitled:
Unsupervised Machine Learning in Biomechanical Data Analysis. Medical Application of Self-Organising Maps
for scientific or didactic purposes.[1]

Gdańsk,..... .....
signature of the PhD student

Aware of criminal liability for violations of the Act of 4th February 1994 on Copyright and Related Rights and disciplinary actions set out in the Law on Higher Education and Science(Journal of Laws 2021, item 478), as well as civil liability, I declare, that the submitted doctoral dissertation is my own work.

I declare, that the submitted doctoral dissertation is my own work performed under and in cooperation with the supervision of Izabela Lubowiecka.

This submitted doctoral dissertation has never before been the basis of an official procedure associated with the awarding of a PhD degree.

All the information contained in the above thesis which is derived from written and electronic sources is documented in a list of relevant literature in accordance with Art. 34 of the Copyright and Related Rights Act.

I confirm that this doctoral dissertation is identical to the attached electronic version.

Gdańsk,..... .....
signature of the PhD student

I, the undersigned, agree to include an electronic version of the above doctoral dissertation in the open, institutional, digital repository of Gdańsk University of Technology.

Gdańsk,..... .....
signature of the PhD student

[1] Art 27. 1. Educational institutions and entities referred to in art. 7 sec. 1 points 1, 2 and 4–8 of the Act of 20 July 2018 – Law on Higher Education and Science, may use the disseminated works in the original and in translation for the purposes of illustrating the content provided for didactic purposes or in order to conduct research activities, and to reproduce for this purpose disseminated minor works or fragments of larger works.

2. If the works are made available to the public in such a way that everyone can have access to them at the place and time selected by them, as referred to in para. 1, is allowed only for a limited group of people learning, teaching or conducting research, identified by the entities listed in paragraph 1.

GDAŃSK UNIVERSITY OF TECHNOLOGY

DESCRIPTION OF DOCTORAL DISSERTATION

The Author of the doctoral dissertation: Mateusz Troka

Title of doctoral dissertation: Unsupervised Machine Learning in Biomechanical Data Analysis. Medical Application of Self-Organising Maps

Title of doctoral dissertation in Polish: Nienadzorowane Uczenie Maszynowe w Analizie Danych Biomechanicznych. Medyczne Zastosowanie Map Samoorganizujących.

Language of doctoral dissertation: English

Supervisor: Izabela Lubowiecka

Date of doctoral defense: -

Keywords of doctoral dissertation in Polish: Uczenie maszynowe, Mapy Samoorganizujące, biomechanika, ściana brzucha, staw skroniowo-żuchwowy, pole odkształceń, pomiar pełnego pola przemieszczeń, cyfrowa korelacja obrazu

Keywords of doctoral dissertation in English: Unsupervised Machine Learning, Self-Organising Maps, biomechanics, abdominal wall, temporomandibular joint, strain fields, full-field measurement of displacement, Digital Image Correlation

Summary of doctoral dissertation in Polish: Niniejsza rozprawa doktorska dotyczy zastosowania map samoorganizujących się (SOM), modelu nienadzorowanej sieci neuronowej, do grupowania i wizualizacji eksperymentalnie uzyskanych danych biomechanicznych na podstawie ich podobieństwa. SOM osiąga to poprzez zachowanie relacji topologicznych, odwzorowując podobne dane na sąsiednie węzły dwuwymiarowej mapy. Jednocześnie, SOM redukuje wymiarowość analizowanego problemu.

Cele niniejszej rozprawy sformułowano dla dwóch zbiorów danych, na których przeprowadzono analizy za pomocą SOM. Pierwsza dotyczy identyfikacji obszarów ściany brzucha człowieka, które wykazują pewne podobieństwo pod względem mechanicznym. Badanie przeprowadzono na podstawie danych z pomiarów in vivo pełnego pola przemieszczeń wykonanych na ochotnikach przy użyciu techniki cyfrowej korelacji obrazu.

W dalszej części rozprawy poruszono kwestię metody klasyfikacji umożliwiającej ocenę pracy mięśni otaczających staw skroniowo-żuchwowy u ludzi na podstawie aktywacji mięśni wokół stawu skroniowo-żuchwowego. W badaniach wykorzystano istniejące dane z sygnału elektromiografii powierzchniowej i zastosowano SOM, co umożliwiło wgląd w potencjalne problemy związane z funkcjonalnością stawu.

Zawarte w pracy odkrycia pokazują znaczny potencjał proponowanych rozwiązań do tworzenia narzędzi wspierających diagnostykę medyczną i zindywidualizowane procedury leczenia.

Summary of doctoral dissertation in English: This dissertation concerned the application of Self-Organising Maps (SOM), unsupervised neural network model, to experimentally acquired biomechanical datasets to group and visualise the data based on their similarities.

SOM achieves this by preserving the topological relationships in the data, mapping similar data points to neighbouring nodes on a two-dimensional map. At the same time SOM reduces the dimensionality of the analysed problem.

The objectives of this dissertation were formulated for two sets of data on which analyses with SOM were performed. The first one concerned identification of areas of the human abdominal wall that reveal a certain similarity in terms of their mechanical behaviour. The study is based on full-field measured data obtained from in vivo experiments on human volunteers using the digital image correlation technique.

Following, the dissertation addresses the necessity for a classification method to evaluate the performance of muscles surrounding the temporomandibular joint (TMJ) in selected patients. The SOM technique was employed to group healthy patients based on their surface electromyography signal data, providing insights into potential issues related to TMJ functionality.

These findings demonstrate the significant potential of proposed approaches based on machine learning to enhance patient-specific solutions and to support medical diagnostics.

GDAŃSK UNIVERSITY OF TECHNOLOGY

Unsupervised Machine Learning in Biomechanical Data Analysis. Medical Application of Self-Organising Maps

DISSERTATION

Submitted in Fulfillment of

the Requirements for

the Degree of

DOCTOR OF PHILOSOPHY (Mechanical Engineering)

at the

GDAŃSK UNIVERSITY OF TECHNOLOGY
Doctoral School

by

Mateusz Troka

January 2025

Vita

Since 2019 when I have started PhD research and training in doctoral school a lot have changed. The world is a very different place right now and it is hard to predict what the future holds, hopefully only bright side of life are ahead of us.

Now, since 2019, I have met my wife, adopted our lovely dog, undergone two hip arthroscopic procedures, therefore I was partly forced to part ways, 20 years of continuous work, with my table tennis career for good, but to the dismay of my wife it fuelled my in-too-deep rabbit hole of a fascination with cycling and the science behind it.

Throughout my time in doctoral school I have actively attended five scientific conferences, published four original peer-reviewed articles (three of which I was the first author). Hopefully, my PhD dissertation shows my involvement to the academia, not only through this dissertation, but as well mentioned articles, abstracts and different kinds of contributions that are partly listed and described in this manuscript.

I firmly believe that I have just scratched the surface of what the scientific world has to offer. The world which I still hold a strong appreciation for.

Acknowledgements

First and foremost I would like to thank my wife for being for and with me since almost the beginning of my PhD course of life. My supervisor Iza without whom all of it would not in the faintest be possible. My co-workers, especially Kasia for all the help and knowledge. My family, my friends and colleagues, along with my dog (the best therapist!).

Apart from scholarship earned from the doctoral school my research and work was also partially funded and supported by the National Science Centre (Poland) [grant No. UMO-2017/27/B/ST8/02518]. Calculations were carried out partially at the Academic Computer Centre in Gdansk.

Yours Mateusz
January 2025

To all the PhD pursuing brave, but kind of crazy as well, souls.

Contents

List of Figures

List of Tables

Chapter 1

Introduction

1.1 Outline of the thesis

The thesis of this work can be formulated as follows: *The application of an unsupervised machine learning model, namely Self-Organising Maps, in experimentally acquired biomechanical data analysis offers a novel approach to uncovering hidden features within datasets.* Particularly concerning the two medical problems analysed in this dissertation, it is proposed that the Machine Learning-based methodology can be employed for the following analyses:

1. Identifying regions of similar mechanical behaviour in abdominal walls across individuals using full-field Digital Image Correlation measurements under dynamic loading conditions over time.

2. Evaluating potential temporomandibular joint dysfunction by analysing sEMG signals from the muscles surrounding the joint.

The work consists of seven chapters, bibliography and abstracts in Polish and English.

Apart from this **Chapter 1** where an introduction is made **Chapter 2** provides a literature background of state of the art in biomechanical data analysis in terms of Machine Learning (ML) review. Mainly, differences of application resulting from the choice of a particular algorithm are presented.

This thesis concerns machine learning algorithms, with a particular emphasis on a unsupervised and clustering method, that are discussed in **Chapter 3**. Unsupervised learning methodology is therefore used for the analysis of the biomechanical data, as the subject of this study.

The concepts of strain, stress, and deformation in bodies, as well as the background of continuum mechanics applied in this work, are introduced and presented in **Chapter 4**.

Chapter 5 is devoted to the research that aimed to make a step towards identification of mechanically similar regions of human anterior abdominal wall with the use of Self-Organising Maps (SOM), an unsupervised machine learning model. Experimentally obtained data of mechanical behaviour of human abdominal wall under changing pressure is discussed. Based on that, a methodology is developed and conducted to cluster strain data with Self-Organising Maps. SOM is particularly effective for grouping data and reducing dimensionality of the data space, which is critical when analysing complex deformation states across various loading levels in biomechanical experiments.

In **Chapter 6** the Self-Organising Maps technique was proposed to identify similarities between multiple patients in the performance of muscles around temporomandibular joint (TMJ). The performance was assessed by analysing the muscle activity with the use of surface electromyography (sEMG). sEMG data, collected beforehand, during tests where subjects performed four mandibular motions were provided in the form of post-processed signals. A methodology was then developed and conducted to cluster sEMG data with Self-Organising Maps.

Although a general summary of the dissertation and the whole work is presented in **Chapter 7**, conclusions regarding their specific medical issues are presented in the relevant chapters in Chapter 5 and Chapter 6.

The dissertation was realised in the years 2019-2024 at the Doctoral School led by Gdansk University of Technology. The research was funded by the National Science Centre (Poland) [grant No. UMO-2017/27/B/ST8/02518] and computation power was fueled by Academic Computer Centre (CI TASK) of Gdansk University of Technology. Presented data of temporomandibular joint was obtained within the project 3D-JAW (The study of 3D temporo-mandibular joint (TMJ) model of bone-cartilage-ligament system mapping for effective commercialization of results in dental prosthetics, orthodontic and orthognathic surgery; POIR.04.01.02-00-0029/17). For purpose of this dissertation entitled "Unsupervised Machine Learning in Biomechanical Data Analysis. Medical Application of Self-Organising Maps" all materials and findings are original and include nothing which is outcome of a work done previously by anyone else or in collaboration except otherwise indicated through reference.

Part of presented work in respective research Chapters was as well published in following peer reviewed articles:

- Troka M., Szepietowska K., Lubowiecka I.

  Self-organising maps in the analysis of strains of human abdominal wall to identify areas of similar mechanical behaviour,

  Elsevier, Journal of the Mechanical Behavior of Biomedical Materials,

  Volume 156, 2024,

  https://doi.org/10.1016/j.jmbbm.2024.106578

- Troka M., Wojnicz W., Szepietowska K., Lubowiecka I.

  Unsupervised Learning for Biomechanical Data Using Self-organising Maps, an Approach for Temporomandibular Joint Analysis,

  Springer Science and Business Media Deutschland GmbH, Lecture Notes in Networks and Systems,

  Volume 875, pp. 233 - 240, 2024,

  https://doi.org/10.1007/978-3-031-52382-3

- K. Szepietowska, M. Troka, M. Lichodziejewska-Niemierko, M. Chmielewski, and I. Lubowiecka.,

  Full-field in vivo experimental study of the strains of a breathing human abdominal wall with intra-abdominal pressure variation,

  Elsevier, Journal of the Mechanical Behavior of Biomedical Materials,

  Volume 147, 2023,

  https://doi.org/10.1016/j.jmbbm.2023.106148

1.2 Overview of the discussed problems

This dissertation addresses two distinct but equally important biomechanical problems: abdominal wall insufficiency and issues related to temporomandibular joint. Both of them present significant challenges.

Abdominal wall and its insufficiencies, particularly in the context of hernias or post-surgical complications, involves the failure of the abdominal wall to maintain its structural integrity. Unfortunately, the mechanical behaviour of the abdominal wall under varying conditions, such as different intra-abdominal pressures, is complex and not fully understood. Thus, machine learning methods, particularly Self-Organising Maps, can provide a promising way to analyse large datasets of mechanical quantities, and in this case, enabling the identification of regions of the abdominal wall that exhibit similar deformation characteristics.

On the other hand, temporomandibular joint, including issues related to jaw movement and muscle function, often cause significant discomfort, pain, and difficulty in performing essential functions like speaking and eating. Diagnosing TMJ and understanding the role of muscle activation is challenging due to the variability in how individual muscles perform during jaw movements. By analysing surface electromyography signals, this dissertation aims to apply machine learning techniques to classify patients muscle performance and identify patterns in the multidimensional datasets.

The overarching objective of this dissertation is to apply Self-Organising Maps, to these two biomechanical issues.

1.2.1 Human Abdominal Wall and Its Insufficiencies

A comprehensive understanding of abdominal biomechanics is crucial for improving the prevention and treatment of abdominal disorders and injuries. Despite extensive research, the precise mechanical behaviour of the abdomen and the underlying causes of many abdominal injuries remain unclear Peña et al. (2017). This uncertainty is partly attributable to the inherent limitations of experimental studies, such as high costs, difficulties in accurately measuring strain and stress, and challenges in replicating certain natural conditions. For example, finite element models have proven to be highly valuable, offering detailed insights into the mechanical properties of biological tissues and the behaviour of living organs, which are both cost- and time-efficient. Likewise the employment of Machine Learning

models can aid in gathering knowledge of abdominal intricacies.

The initial motivation to undertake this research study was to address the issue of recurring abdominal hernias and to develop medical implants that can effectively prevent such recurrences. As noted by Deeken and Lake (2017), hernia recurrences impact approximately 25-30% of patients. With around 20 million hernias being repaired worldwide each year (Kingsnorth and LeBlanc (2003)), which is a significant concern.

There are numerous surgical implants available on the market, each with varying material properties. The materials and surgical techniques are widely discussed in literature (e.g., Liu et al. (2021)). For example, laparotomy incisions through the linea alba are a common method for accessing the peritoneal cavity. However, this approach weakens the area where abdominal muscle fibers intersect, which increases the risk of incisional hernias. To repair hernias, surgeons typically place a surgical mesh in the affected area to reinforce the weakened abdominal wall. Here, the important aspect of this procedure is connected with the choice of the implant and its placement. However, as there is considerable variation in the mechanical properties of living tissues, there is also significant diversity in the mechanical performance of the abdominal walls of different individuals, as seen in both experimental studies (e.g., Lubowiecka et al. (2022)) and computational models (e.g., Karrech et al. (2023)). Given that different regions of the abdominal wall undergo varying levels of deformation Szymczak et al. (2012) and that commercial implants also exhibit different strain capacities Tomaszewska et al. (2013), it is likely that the challenge lies in the lack of precise information for selecting the most appropriate implant for a specific hernia location and patient.

To advance this patient-specific approaches, e.g. Jourdan et al. (2024) introduced a finite element based model of the abdomen using simplified geometry. The model employs seven ellipses aligned along the cranio-caudal axis, scaled to match the abdominal dimensions of three subject types with varying body mass indices.

In the context of human-technology interaction, especially for development of medical devices, implants, surgery strategies or ergonomic equipment, a comprehensive understanding of biomechanical *in vivo* behaviour is crucial. To gather such knowledge for the abdomen in that case, a study was conducted by Remus et al. (2024) that measured the continuous mechanical responses of the abdominal soft tissues of ten healthy participants in various lying positions—anterior, lateral, and posterior. With an experimental setup consisting of a mechatronic indenter

with hemispherical tip and two time-of-flight sensors for optical 3D displacement measurement of the surface. They found that the mean stiffness of the abdomen was significantly different when the trunk muscles were activated or relaxed. No significant differences were found between the anterior-lateral measurement regions. The exception were regions around linea alba and rectus abdominis below the inter-tubercular plane. The shapes and areas of deformation of the skin depended on the region and muscle activity. They used hyper-elastic Ogden model, to identify material parameters for tested regions (Remus et al. (2024)).

Considering the aformentioned studies, it should be noted that there is still a lack of works that provide material characteristics of the human abdominal wall. For example, taking into account the variability of the individual, or different loading conditions (passive/active behaviour). The problematic nature of *in vivo* studies on humans makes it difficult to obtain. Thus, it remains an open question.

Other example is a study by Berardo et al. (2024), where they developed first characterisation of the superficial fascia, a connective tissue layer found beneath the skin, through mechanical tests, revealing its anisotropic and viscoelastic properties. These characteristics mean that the fascia exhibits different mechanical responses depending on the direction of the applied forces and the duration or speed of the force application. The superficial fascia showed a site-specific variability when comparing the abdominal and thoracic districts.

Strain fields was utilised in studies to compare healthy abdominal walls with those containing implants (Podwojewski et al. (2014)) where higher strains were found along the linea alba versus the perpendicular direction. What is more, evaluating strains in multiple deformation states could be sufficient to determine the mechanical compatibility between the implant and abdominal wall, as strain range comparisons can reveal potential mismatches (Deeken and Lake (2017)). They found that in order for a biomaterial to be the most compliant it should be oriented in the longitudinal direction, and to be the stiffest it should be oriented in the medial-transverse direction. Finally, the human abdominal wall was found to be anisotropic, with anisotropy ratios as high as 8-9, reported for the human linea alba.

Furthermore, for example, to evaluate different methods for closing the abdominal wall after midline laparotomy Le Ruyet et al. (2020) performed a study on post mortem specimens. They used a digital image correlation based method for the comparison of strain fields on the external surface of the myofascial abdominal wall.

The results showed no significant difference between the 5x5 mm and 10x10 mm closure configurations. However, reinforcing the suture line with mesh led to stiffer midline behaviour under similar intra-abdominal pressures, particularly when a larger mesh overlap was applied. This strain-based approach allowed researchers to gather information from non-invasive *in vivo* experiments, without the need for additional assumptions about material properties.

Tensile properties, for another example, of the human abdominal wall were researched in Kriener et al. (2023) by studying it layer by layer, as well as considering it as a partial composite. Because the heterogeneity of the abdominal wall exists particularly due to the varying muscle layers with distinct mechanical properties across different regions of the abdomen and its wall (Fig. 1.1). In that study, the tissues were obtained from both fresh-never-frozen and fresh-frozen cadavers, and these samples were subjected to uniaxial tensile tests at a constant rate of 5 mm/min until the point of mechanical failure. The authors revealed from experimental results the significant variations in the tensile properties of abdominal wall tissues, both within individual tissues and between different tissue types.

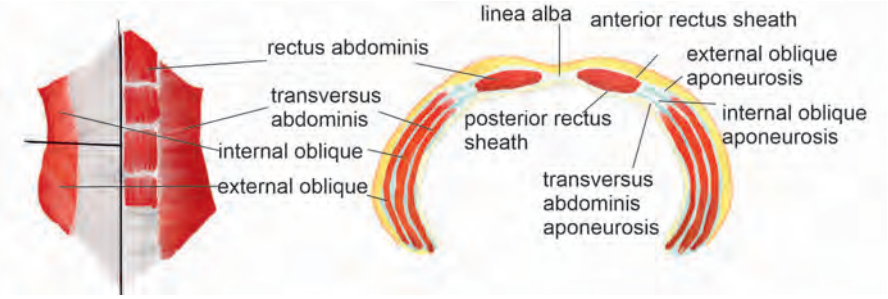

Figure 1.1: Abdominal wall scheme: left - anterior view with some layers of muscles partially removed, right: cross-section in region superior to arcuate line, modified from Troka et al. (2024a).

Finally, a work made by Spadoni et al. (2024) reviews state-of-the-art about numerical models used to study abdominal wall biomechanics. It highlighted various experimental techniques for validating these models. Such new studies consist of the use of electromyography (Janneke Schwaner et al. (2024)), ultrasound imaging (Carbonaro et al. (2023)) with recognised intra-abdominal pressure measurements, abdominal surface deformation analysis, and stiffness/compliance evaluations. At the same time Joppin et al. (2024) highlighted in their research that by coupling magnetic resonance image and pressure sensor in the abdominal wall during passive exercise (breathing) and active exercise (cough, Valsalva), they were able to study

correlation of the muscle motion, visceral area and intra-abdominal pressure change.

Also Machine Learning methods are common in studies of human abdominal wall. For example, Tang et al. (2022) proposed a non-invasive and contactless system to learn and predict the relationship between the passive mechanical behaviour of the abdominal wall with millimetre-wave frequency-modulated continuous wave radar and an intra-abdominal pressure sensor via a deep learning approach.

And recently, Nguyen and Lejeune (2024) has proposed a methodology for clustering strain and displacement fields using unsupervised machine learning methods, such as k-means clustering, spectral clustering, iForest clustering, and One-class Support Vector Machine. Their study, which focused on the analysis of heterogeneous, highly deformable materials like soft tissues, demonstrated both the effectiveness and limitations of these approaches using artificially generated data. They set the stage for future studies that can adapt more specifically these methods to mechanical data.

Objectives

The first aim of this dissertation is to identify regions of the living human abdominal wall that exhibit similar mechanical behaviour under varying intra-abdominal pressures. The study, conducted on multiple human subjects, highlights the diversity among the patients analysed. The methodology presented in the thesis methodology starts with full-field data collection through the digital image correlation technique during *in vivo* tests on patients undergoing peritoneal dialysis, as detailed in Szepietowska et al. (2023). However, analysing experimental data alone is challenging because of mechanical behaviours like those during breathing, involving abdominal muscles (Mikołajowski et al. (2022)), and changes in intra-abdominal pressure as the cavity fills with fluid. This raises the question of which measurements and deformation states should be considered to identify regions that behave similarly.

To address this, an unsupervised machine learning technique called Self-Organising Maps (Kohonen (1997)) was employed to cluster the data, thereby revealing regions in the abdominal wall that responded similarly during the experiment. SOM is particularly suitable for this purpose as it can reduce the dimensionality of the dataset, which enables the analysis of deformation states under different load levels at various time points during the experiment.

The SOM was applied to cluster data obtained from full-field measurement of the deformation of the human abdominal wall during changing intra-abdominal

pressure within an *in vivo* experiment. The experiment was non-invasive and was performed during a standard medical procedure of peritoneal dialysis performed in the university clinic. Initially, the grid points and surface geometry of the abdomen were mapped using the digital image correlation system. These grid points of strain datasets were then inputted into the SOM, which subsequently clustered them. The resulting clusters were visualised on the abdominal wall surface, representing groups of points that share similar mechanical responses based on principal strains and principal strain directions. The mentioned variables were analysed simultaneously to obtain comprehensive results of the abdominal wall behaviour. Strains were chosen as the basis for clustering because it is a measurable parameter that can be easily obtained from non-invasive full-field measurements. This innovative approach allowed us to analyse strain fields and consider deformation states at different time/load stages corresponding to changes in intra-abdominal pressure. By focusing on strain-based clustering, this method could also guide the selection and orientation of surgical implants, ensuring mechanical compatibility with the surrounding tissue.

Unlike previous studies that primarily emphasised passive mechanical responses, this analysis integrated dynamic data from breathing subjects, capturing the mechanical behaviour of the abdominal wall during both inhalation and exhalation phases. This inclusion introduces variations arising from active behaviour, such as muscle engagement during breathing, combined with a multidimensional analysis that considers the state of strains at different stages of loading. By accounting for the breathing cycle, the analysis captures dynamic changes, such as the shifting directions of principal strains. These variations potentially alter the observed mechanical response, resulting in more intricate clustering outcomes and offering deeper insights into the biomechanical behaviour of the human abdominal wall.

1.2.2 Temporomandibular Joint

Multivariate data analysis techniques provide a robust approach to tackling medical challenges, especially when exploring the complexities of biomechanical systems like the temporomandibular joint. Insights gained from such analyses can significantly enhance our understanding of occurring processes, as well as contribute to advancements in diagnostics and treatment strategies. Therefore, the subsequent objective of this dissertation is to analyse temporomandibular joint muscle sEMG signal data using machine learning.

The temporomandibular joint is a critical component of human anatomy, situated at the junction of the mandible and the temporal bone. It is unique in its duality, with both joints working in coordination yet influencing each other. This anatomical interdependence allows for complex movements, including translational and rotational displacements, which are essential for normal jaw function. However, any instability or dysfunction in one joint inevitably affects the other, leading to potential discomfort or impaired mobility.

Hence, temporomandibular joint disorders (TMDs) represent a significant musculoskeletal health issue, second only to chronic back pain in prevalence. These disorders impact 5–12% of the population, as highlighted by Bianchi et al. (2020). TMDs encompass a range of skeletal and muscular conditions that directly affect the performance of the TMJ. Common symptoms include pain, limited range of motion, and clicking or locking of the jaw. The constant positional adjustments required by the mandible to maintain coordinated movement further underscore the joint's vulnerability to dysfunction, as noted by Tanteri et al. (2020).

The temporomandibular joint is a highly specialised and complex joint that connects the mandible (lower jaw) to the temporal bone of the cranium, facilitating essential functions such as chewing, speaking, and swallowing. This joint is unique in that it consists of two synovial compartments that must work in harmony to perform both rotational and translational movements. The articular surfaces of the TMJ are lined with fibrocartilage, which, compared to hyaline cartilage, provides better resistance to wear and tear due to the joint's repetitive and high-stress activities Demerjian et al. (2018a).

The TMJ is divided into two compartments by the articular disc, a dense fibrous structure that lacks innervation and vascularization. This disc plays a crucial role in the biomechanics of the TMJ by acting as a viscoelastic shock and stress absorber, thereby contributing to load distribution across the joint during function Tanteri et al. (2020).

In the lower compartment of the TMJ, rotational (hinge-like) movement of the mandibular condyle occurs against the articular disc. In contrast, the upper compartment facilitates translational (sliding) movement of the disc against the glenoid fossa. This dual-compartment structure allows the TMJ to perform the complex movements necessary for mastication and speech Michael S. Detamore (2003); Tanaka et al. (2004).

The overall structure of the TMJ is supported by a fibrous capsule and various

ligaments that ensure joint stability while allowing the required range of motion. The combination of these anatomical features and the disc's viscoelastic properties makes the TMJ a remarkable joint capable of withstanding the mechanical demands of daily functions.

Temporomandibular joint disorders often manifest through various symptoms that extend beyond pain and restricted jaw movements. Audible joint noises, such as clicking and popping during jaw motions, are common indicators of TMD and should not be overlooked. These sounds can result from misalignment, disc displacement, or other structural issues within the joint. The pathophysiology of TMD is complex and not fully understood. The importance of addressing TMDs extends beyond their prevalence. By integrating advanced multivariate data analysis methods, researchers and clinicians can better characterise TMJ behaviour, identify dysfunction patterns, and develop personalised treatment plans. As noted by Mujakperuo et al. (2010), a comprehensive understanding of the skeletal and muscular interactions in TMD is critical to improving clinical outcomes

Biomechanical models have significantly enhanced our understanding of muscle function during various jaw movements, shedding light on the complex interplay of active and passive forces involved. Understanding the activity of muscles that are being used in jaw motions is essential for diagnosing and addressing challenges in everyday functions such as mastication, speaking, swallowing, and breathing. Surface electromyography (sEMG) has emerged as a valuable tool for investigating these muscle activities, particularly during specific jaw movements like opening, closing, and lateral deviations (protrusion and retrusion).

As highlighted by Wojnicz et al. (2019), sEMG provides a non-invasive method to measure the electrical activity of muscles, offering insights into their performance and coordination. This technique is widely regarded as a cornerstone for detecting nerve or muscle dysfunctions and identifying issues in nerve-to-muscle signal transmission. Motor neurons are responsible for transmitting electrical impulses that cause muscle contractions, and disruptions in this pathway can lead to functional impairments, as noted by Mills (2005).

Furthermore, knowledge of superficial muscle activity gained through sEMG can be integrated into biomechanical models of the jaw. These models are valuable for simulating and understanding the forces and movements within the stomatognathic system. However, as Wojnicz et al. (2019) emphasised, a more comprehensive understanding of the processes occurring within the temporomandibular joint

during jaw movements requires additional investigative approaches. Advanced imaging techniques or direct measurements within the joint may be necessary to uncover the intricacies of TMJ mechanics and their role in overall jaw function.

Specific muscles that are responsible for distinct jaw movements:

- opening, primarily involves the suprahyoid and lateral pterygoid muscles;
- closing, relies on the temporalis, masseter, and medial pterygoid muscles;
- protrusion and retrusion, these movements, which often accompany opening and closing, are performed by the medial pterygoid, temporalis, and digastric muscles Tanteri et al. (2020).

Objectives

This study proposed the use of SOM, to analyse large multivariate datasets of surface electromyography signals from TMJ muscles during various jaw motions. The objective was to identify similar features within the datasets, and to compare the classifications generated by the network across different volunteers' sEMG signals. By employing SOM, the study aimed to visualise and compare data patterns, ultimately contributing to the extraction of hidden characteristics of the datasets, because it can simultaneously analyse sEMG signals from multiple muscles and map these large multidimensional inputs onto a 2D representation.

Due to the limitations of surface electromyography, which primarily captures the activity of superficial muscles, this study focused on analysing the masseter and temporalis muscles during jaw movements. These muscles are critical in the biomechanics of the temporomandibular joint, providing valuable insights into both normal function and potential disorders. At this point, it is important to note that analyses were performed on healthy patients who were not clinically diagnosed with any medical problem with TMJ, but some of them reported mild issues.

The final goal of this part of the research was to propose a tool that allows rapid identification and categorisation of patients with similar conditions, improving diagnostic efficiency and potentially leading to more targeted treatment strategies. The visualisation of large datasets through SOM offers new avenues for data analysis, making it a valuable method for exploring complex, multidimensional data in a clinical context.

Chapter 2

State of the Art

2.1 Biomechanics and Machine Learning

Following Stergiou (2020), biomechanics is a field dedicated to understanding the forces that act on the human body and the resulting effects. By studying motion, biomechanics aims to uncover the mechanisms that underlie various physical activities, contributing to a better grasp of how skills are acquired and regulated. This discipline is essential not only for understanding movement patterns but also for enhancing performance and preventing injuries across different stages of life.

Biomechanical research, especially in human development, evaluates fundamental movement patterns across the lifespan. Individuals of various ages are studied as they perform motor tasks, allowing researchers to examine the interaction between physiological mechanisms such as respiratory, cardiovascular, and metabolic functions, with the use of neuromuscular and skeletal systems (Potthast (2024)). These activities are then quantified, described, and analysed to improve both health outcomes and performance.

In recent decades, biomedical engineering and biomechanics have seen significant growth, driven by advancements in biomaterials, biomechanics, and bio-fabrication. These fields play crucial roles in interacting with biological systems, whether for medical, rehabilitation, or performance enhancement purposes. Notably, *in silico* modelling has emerged as a powerful tool, offering an efficient alternative to traditional *in vivo* investigations (Wu et al. (2024)).

Machine learning techniques are at the forefront of this expansion in biomedical engineering and biomechanics. By leveraging ML, researchers are developing innovative treatments and solutions to complex healthcare challenges. These

technologies are enabling breakthroughs in various areas, from personalised medicine to advancements in implants and prosthetics while providing aid in diagnosis, with every improvement promoting progress in healthcare and rehabilitation (Wu et al. (2024)).

2.1.1 Trends in Machine Learning Applications for Biomechanics

In recent years, Machine Learning, especially Deep Learning approaches, have attracted great attention in medical field. These algorithms have significantly advanced biomechanics by enabling the analysis of complex datasets, uncovering patterns, and enhancing predictive capabilities. Key trends in ML applications within biomechanics include:

1. Human Movement Analysis: ML techniques, particularly deep learning, have been employed to analyse human gait and movement patterns. For instance, Horst et al. (2019) utilised deep learning neural networks to identify unique gait patterns, enhancing the understanding of individual biomechanics.

2. Soft Tissue Characterisation: ML algorithms have been applied to estimate the mechanical properties of soft biological tissues. A comprehensive review by Donmazov et al. (2024) highlights the use of ML in analysing stress-strain curves and pressure-volume loops, particularly in cardiovascular engineering.

3. Spine Biomechanics: ML deep learning models have been integrated with musculoskeletal modelling to assess spinal biomechanics during complex activities. This approach facilitates evaluations in scenarios such as workplace lifting and sports biomechanics (Ghezelbash et al. (2024)).

4. Running Biomechanics: Systematic reviews have explored ML approaches in running biomechanics using wearable sensors, emphasising the role of ML in enhancing performance and injury prevention strategies (Xiang et al. (2022)).

5. Gait Analysis for Injury Monitoring: ML-based analytics have been utilised in gait analysis to monitor and enhance fracture recoveries. Rezapour et al. (2024) demonstrated the potential of supervised ML models in predicting complications through gait data analysis.

6. Human Activity Recognition: ML techniques have been applied to recognise human activities based on biomechanical data. Nazari et al. (2021) investigated the use of knee motion data to classify human activities, highlighting the applicability of ML in activity recognition.

These trends illustrate the growing integration of machine learning in biomechanics, facilitating more precise analyses, personalised interventions, and the development of advanced assistive technologies.

2.2 Applications of Machine Learning models to issues of Human Abdominal wall

Abdominal wall reconstruction is a complex procedure and clinicians often face challenges in predicting rare outcomes or complications. Recent research has focused on improving predictions outcomes in abdominal wall reconstruction, such as Ayuso et al. (2023). The Authors compared conventional deep learning models with generative adversarial network anomaly deep learning models and showed improved performance on imbalanced data sets, increasing model sensitivity. Another comprehensive review was conducted by Hassan et al. (2022), where the Authors compared nine supervised ML algorithms that were developed to preoperatively predict hernia recurrences. In which ML was used to characterise 4 unique significant predictors of hernia recurrences. Algorithms trained on readily available preoperative clinical data accurately predicted complications of abdominal wall reconstruction. Whereas Lima et al. (2024) reviewed 13 articles that confirmed the use of ML for abdominal wall reconstruction to be a promising tool to predict outcomes and identify factors that could lead to postoperative complications. Finally, Elhage et al. (2021) proposed an image-based deep learning model routine to use preoperative computed tomography images and predict surgical complexity itself. They found it to be even more accurate than an expert surgeon's judgment. Other notable reviews on the use of deep learning to advance surgical procedures, especially to predict the complexity of abdominal wall reconstruction and postoperative outcomes in hernia surgeries, include: Taha et al. (2022) and Mayol (2023), while Vogel and Mück (2024) provide a comprehensive review of deep learning applications in surgical settings.

Deep learning can also be applied to segment medical images for various purposes. For example, work by Micomyiza et al. (2022) to use an automated

convolutional neural network to segment abdominal adipose tissue from radiology images. Identification, segmentation and quantification of abdominal fat images. The proposed approach outperformed state-of-the-art other deep learning networks in accuracy. In other work, Kim et al. (2021) assessed the diagnostic performance of artificial neural networks to detect pneumoperitoneum in abdominal radiographs for the first time. The diagnostic performance of their approach obtained a sensitivity of 88.6% and predictive value of the negative tests of 91.3%. Recently, Sadikine et al. (2024) proposed novel semi-over complete convolutional auto-encoder to generate shape priors from public datasets focusing on the segmentation of abdominal organs and vessels. Results show that this approach outperformed the U-Net model, both with and without shape priors derived from a standard auto-encoder.

2.3 Applications of Machine Learning models to issues of Temporomandibular Joint

Similarly to the research on abdominal wall, ML algorithms can be successfully applied to studies conducted on the temporomandibular joint and medical conditions associated with it. In this section, recent advancement in the studies of TMJ and machine learning models are presented.

Since the temporomandibular joints consist of a complex formation of bones, muscles, and tendons, pain in the jaw area often results from disorders or injury to these structures. Recognising this complexity, Sharma et al. (2019) embarked on research aimed at predicting TMJ syndrome. Unlike the more straightforward load joints, such as the knee or hip, the TMJ presents unique challenges due to its intricate biomechanics and functional demands. Sharma et al. (2019) proposed an artificial intelligence model based on neural network theory designed to assist in detecting whether a patient is suffering from TMJ disorder. Their model automatically predicts the presence of a TMD by analysing risk factors and symptoms provided by patients. This AI-based approach offers a significant advancement in the early detection and diagnosis of TMJ syndrome, potentially improving patient outcomes through more timely and personalised interventions.

Ozsari et al. (2023b) proposed a deep learning-based approach in order to automatically diagnose Temporomandibular Disorder on Magnetic Resonance (MR) images. In this study, 2576 magnetic resonance (MR) images from 200 patients diagnosed with and without temporomandibular disorders were collected and

classified into 8 different groups. Initially, a basic Convolutional Neural Network (CNN) was employed to address the classification problem. Following this, six different fine-tuned pre-trained convolutional neural network models were applied to the dataset, including Xception, ResNet-101, MobileNetV2, InceptionV3, DenseNet-121, and ConvNeXt. The results from these deep learning-based architectures demonstrated their effectiveness in diagnosing TMD. The application of these advanced models can contribute to more accurate and automated diagnostic processes, supporting clinicians in detecting and analysing temporomandibular disorders with greater precision.

Later, the same Authors reviewed studies that apply AI-based algorithms and computer-aided programs for investigating TMJ and TMJ-related diseases Ozsari et al. (2023a). A comprehensive survey of the literature led to the assessment of 66 articles within the defined scope of temporomandibular joint studies. These articles were distributed across several key research areas as follows: 11 focused on segmentation techniques, 10 on TMJ Osteoarthritis, 21 on Temporomandibular Joint Disorders, and 6 on decision support systems.

The analysis revealed a growing trend in the use of artificial intelligence algorithms in TMJ-related research. Although there are still gaps in the research to be filled. This trend suggests that the number of studies utilising AI for TMJ diagnosis, treatment planning, and analysis will likely increase, as AI-driven methodologies show promising potential for enhancing clinical decision-making, improving diagnostic accuracy, and advancing the understanding of TMJ pathologies.

Kreiner and Viloria (2022) argued that temporomandibular disorders and orofacial pain are highly prevalent, with rates comparable to leading non-communicable diseases. Many patients face treatment delays, missed diagnoses, and unnecessary therapies. While artificial intelligence has been successfully applied to the diagnosis of numerous conditions, no studies had specifically focused on its use for diagnosing TMD and orofacial pain. In line with Sharma et al. (2019), Kreiner and Viloria (2022) developed and tested the performance of a novel neural network, specifically a multilayer perceptron, aimed at diagnosing orofacial pain and TMD. Their model included the capability to diagnose certain types of referred pain, offering a promising new approach to addressing the diagnostic challenges faced by clinicians in this field.

Next, the study by Lee et al. (2024) explored the effectiveness of deep learning-based models for automatically detecting temporomandibular joint effusion using

magnetic resonance imaging in patients with temporomandibular disorders. The researchers sought to determine whether the model's diagnostic accuracy improved when clinical information about the patients was provided in addition to the MRI images. Their findings suggested that combining patient clinical data with imaging enhanced the model's ability to accurately detect TMJ effusion, indicating the potential for more comprehensive diagnostic tools using AI in clinical practice.

Taşkıran and Çunkaş (2021) developed a decision support system using deep learning and neural network algorithms to aid in the diagnosis of Temporomandibular Joint disorders. Their approach involved creating a non-invasive device to record TMJ sounds, with an interface designed to assist dentists in analysing the data. This data included the sounds from both the left and right TMJ, ambient noise, the patient's clinical information, the dentist's observations, diagnosis, and treatment plan. By applying signal processing techniques and machine learning algorithms, the system classified the recorded sounds and helped to generate a decision protocol regarding the patient's condition. This tool provided valuable feedback to clinicians, helping them evaluate the effectiveness of treatments for joint sounds, which are critical symptoms in the diagnosis of TMJ disorders.

Chapter 3

Unsupervised Machine Learning

The following chapter introduces a type of machine learning algorithms called *unsupervised*. Previously, in Chapter 2 only supervised learning models were discussed, where the networks are trained to produce the correct outputs. Unsupervised ML models differ from them in that there is no feedback information into whether the network learned correctly or not. The learning goal is not defined, training data is also the test data. This feature brings with it certain advantages and disadvantages. This dissertation focused on clustering feature of the unsupervised ML model called Self-Organising Maps, thus application and challenges on clustering are presented in this chapter.

3.1 Clustering Algorithms and Their Applications

A useful technique for identifying grouping patterns in data is clustering. Numerous clustering techniques and algorithms have been introduced in the literature (Ezugwu et al. (2022)). There are partitioning and hierarchical ones that can be used to broadly categorise the clustering methods. The principles of partitioning involve the optimisation or minimisation of a numerical function. Then clustering is performed by using the ideas of homogeneity and separation (Everitt et al. (2011)), i.e. objects in a group have cohesive structures, are well-separated from those in other clusters, and are located closely together (intra-cluster compactness; inter-cluster separation) (Batool (2019)). Some significant obstacles must be overcome when performing cluster analysis. The number of clusters in the data and the best clustering algorithm to maintain the clustering structure for the particular data application are the two main challenges. The number of clusters must be

given as a parameter to many clustering algorithms. Both choosing the clustering algorithm and deciding how many clusters to create are difficult processes. Another vital aspect is validation of clustering results. Many clustering indices have been proposed over the years (Arbelaitz et al. (2013)). These indices are typically determined by some clustering criterion, such as the distance between clusters or the density of the clusters. One of which is average silhouette width score proposed by Kaufman and Rousseeuw (1990).

3.1.1 A few clustering applications

Nowadays clustering algorithms can have various applications. From field of medicine, financial sector, aviation sector, marketing and sales sector, industries and manufacturing context, urban development, privacy protection, to robotics and artificial intelligence itself (Ezugwu et al. (2022)). Since, it was proven that clustering can be used with fair results in terms of bioinformatics and medicine this is approach behind this dissertation and the use of these groupings will be applied for retrieving new information from medical and mechanical point of view.

3.1.2 Challenges in cluster analysis

Cluster analysis presents several challenges, particularly when applied to complex datasets. These challenges include:

1. Determining the Optimal Number of Clusters - one of the most significant challenges is deciding the ideal number of clusters, as most algorithms (e.g., K-means) require this input.

2. High-Dimensional Data - as the number of features increases, the distance metrics used to group data become less effective.

3. Interpreting Clusters - after clusters are formed, understanding what they represent and validating their significance in the context of the problem can be difficult.

4. No Ground Truth for Evaluation - unlike supervised learning, clustering lacks labelled data for validation. Metrics such as silhouette score, Davies-Bouldin index, or manual inspection are often used.

5. Scalability - for large datasets, clustering algorithms like hierarchical clustering may become computationally expensive.

6. Overlapping Clusters - some data points might belong to multiple clusters.

Defining clear boundaries becomes a challenge in such cases.

7. Handling Noisy and Outlier Data - outliers and noise can distort the clustering results. Algorithms need to be robust against such anomalies.

8. Choice of Distance Metric - the effectiveness of clustering depends on the choice of a distance or similarity metric.

9. Feature Selection and Scaling - selecting relevant features and scaling the data (e.g., standardisation or normalisation) is critical for meaningful clusters.

10. Interpretability and Actionability - if clusters are mathematically valid, they must provide actionable insights or interpretable results for real-world applications.

Addressing these challenges often requires combining domain expertise, exploratory data analysis, and the use of multiple clustering approaches to validate results (Batool (2019); Gao et al. (2023a)).

3.1.2.1 Selection of the neighbourhood measure

A solution for a clustering problem always starts with a definition of a suitable distance measure. All methods are sensitive to the one being used. Another aspect to be considered is how to assign weights to data and what we define as a similarity between objects. To answer such questions one can use a perfect literature position on the matter, namely Deza and Deza (2016). Couple of most used distance measures are Euclidean, Mahalanobis, Minkowski, Chebyshev, Manhattan, Canberra, cosine, dot product or Chord distance (Gao et al. (2023a)). Detailed description of some of these for binary, categorical, continuous and mixed data types can be found as well in Everitt et al. (2011). To select the proximity measure depends on the type of application and the data, what types of clusters are meant to be discovered, whether the data space is Euclidean or not, what kind of clustering method is to be used. Additionally, with hierarchical clustering methods the linkage method which influences the shape of the clusters needs to be chosen.

3.1.2.2 Optimal number of clusters

The appropriate number of clusters for the data set is one of the most vital task. It will define the results of the analysis and groupings of the data objects. As there is not a generally accepted definition of a cluster in the literature (Hennig et al. (2015)). The relationship between the variables will influence the suitable number of clusters. Therefore, it is important to be aware of features and what data represents before the clustering analyses.

3.1.2.3 Quality and Validation measures

To validate clustering results firstly we need to know what we are trying to discover. There is no universal "the best clustering", different aims will have different measuring criterion or indices. Alas, in the literature, a gold standard what specific situation an index is good for and how they differ to each other, to guide the user with the final choice of a technique is yet to be developed (Batool (2019)). Fortunately a good start with choosing the right evaluation measure is provided in tables 5-6 in the work made by Gao et al. (2023a). One can employ many methods available to validate the "correct" number of clusters via e.g. indexes named Gap, SDbw, Davies–Bouldin, Calinski and Harabasz's, Dunn's, Fowlkes and Mallows, or tools like average silhouette width, Hartigan's rule, and Bayesian information criterion (Batool (2019); Gao et al. (2023a)).

3.2 Theoretical foundations of Self-Organising Maps

Following the name of this chapter, Self-Organising Map is an unsupervised machine learning model, which was first introduced by Teuevo Kohonen in the 80s' (Kohonen (1982)). The concept was inspired by working principle of a human brain (Kohonen (2013)). Nowadays, it is a powerful ML tool used for visualisation, classification and clustering of multivariate high dimensional data (Kohonen (2013)). The main idea behind SOM is to transform high-dimensional data into a lower-dimensional (typically two-dimensional) representation while preserving the topological relationships of the data, which can be further analysed for new pieces of information. This representation of a dataset is done with set number of nodes (processing units) that are constructed by a learning method in an iterative manner. Each data point in the dataset is associated with a node by means of a metric function calculated by the algorithm. This generates a two-dimensional distribution of the entire data that are grouped by a similarity measure. The similarity between data points of an input is visualised by the nodes that represent them and are placed in the topology close to each other. Respectively, data points which are dissimilar are placed further away.

SOM unlike standard Artificial Neural Networks (which often are supervised ML models) works via a principle of competitive learning, the neurons of the output network compete among themselves to represent input data, with the result that only one output neuron is activated at a time. The output neuron that wins the

competition is called a winning neuron (Haykin (2009)). It is worth mentioning, that the SOM represents input data by models, which are local averages of the data. Only in some special cases the relation of input items with their projection images is one-to-one in the SOM. More often, especially in industrial and scientific applications, the mapping is many-to-one: i.e., the projection images on the SOM are local averages of the input-data distribution. The SOM models are also called "codebook vectors". So, when an input vector is mapped into a particular node on the SOM array by comparing it with all of the models, then the winner, better called the best-matching unit (BMU), is identified. The most essential difference with respect to e.g. the k-means clustering, is that the models of the SOM also reflect topographic relations between the projection images which are similar to those of the input data. So the SOM is actually a data compression method, which represents the topographic relations of the data space by a finite set of models on a topographic map, in an orderly fashion.

The algorithm starts when all initial values of the codebook vectors are determined. In Kohonen (1997) Kohonen demonstrated that initial values can be selected as random vectors, whereas much faster ordering and convergence will be obtained if the initial values are selected as a regular, two-dimensional sequence of vectors taken along a hyperplane spanned by the two largest principal components of x (i.e., principal components associated with the two highest eigenvalues). Which was called by him linear initialisation. As for learning algorithms, there are two, mathematically proven in Kohonen (2013), the original sequential algorithm and a faster converging the batch algorithm. The map size can be initialised and determined by utilising a heuristic formula of total number of nodes: $M = 5\sqrt{N}$ (Vesanto and Alhoniemi (2000)), where M is the number of samples in the dataset. And the ratio of the side lengths of a given map is determined according to the ratio between the two largest eigenvalues of the input data matrix. Further, the important parameter for a SOM model is the map shape. The usual SOM models, after learning, exhibit border effects i.e. the spacing of the neighbouring model nodes are not as regular near the borders as in the middle of the SOM. To avoid this problem a continuous shape of maps can be used for analyses i.e. the toroidal setting.

3.2.1 SOM algorithm

To better describe the learning and self-organisation process let us assume: the $\boldsymbol{x} \in \mathbb{R}^n$ be the n-dimensional input vector which is selected from the input space, $\boldsymbol{x} = [x_1, x_2, \ldots, x_n]$. Each neuron is a n-dimensional weight vector where n is equal to the dimension of the input vectors. Thus the weight vector of neuron j is described as $\boldsymbol{w}_j = [w_{j1}, w_{j2}, \ldots, w_{jn}]$.

The SOM training algorithm moves the weight vectors so that they span across the data cloud and the map of neurons is organised so that the neighbouring neurons on the grid get similar weight vectors (Kohonen (2014); Vesanto et al. (1999)). The training process is based on a criterion of minimising Euclidean distance and leads to finding the best matching unit (BMU), the wining neuron in the output map for an input vector.

Thus, BMU here denoted as c is the node which minimises the Euclidean distance to the input vector x according to the following equation (3.1):

$$||\boldsymbol{x} - \boldsymbol{w_c}|| = \min_j(||\boldsymbol{x} - \boldsymbol{w}_j||). \tag{3.1}$$

The weights of neighbouring nodes that are topographically close to one another in the grid are then updated according to the formula (3.2) (Yin (2008)), when using sequential algorithm:

$$\boldsymbol{w}_j(t+1) = \boldsymbol{w}_j(t) + h_{cj}(t)[\boldsymbol{x}(t) - \boldsymbol{w}_j(t)], \tag{3.2}$$

distributing similar data locally around the BMU where t is the iteration number, $\boldsymbol{w}_j(t)$ is the weight vector, $\boldsymbol{w}_j(t+1)$ is updated weight vector and $h_{cj}(t)$ is a neighbourhood function, which governs how the neurons surrounding the winning neuron (BMU) are updated during the learning process. It ensures that not only the BMU but also its neighbouring neurons in the grid adjust their weights to better represent the input data, preserving the topological structure of the data. While when using batch training algorithm, which was used throughout this dissertation due to its better performance (Kohonen (2013)), the whole data set is presented to the map before any adjustments and then the new weight vectors are calculated as:

$$\boldsymbol{w}_j(t+1) = \frac{\sum_{i=1}^{n} h_{cj}(t)\boldsymbol{x}_i}{\sum_{i=1}^{n} h_{cj}(t)}. \tag{3.3}$$

Within the SOM analysis, an input data item $\boldsymbol{x}_i$ is presented to a set of nodes,

of which the BMU, marked yellow in Fig. 3.1, matches best with $\boldsymbol{x}_i$. All nodes that lie in the neighbourhood of a BMU in the map will be updated during training iterations and finally match better with $\boldsymbol{x}_i$.

Generally, SOM pseudo-algorithm can be summarised as shown below (Yin (2008); Haykin (2009)):

- initialisation of weigh vectors $\boldsymbol{w}_j$ for all units $j = 1, 2..., N$ where N is the number of units on the grid;
- selection of a sample $\boldsymbol{x}$ from the input to be presented to the grid;
- finding the best matching unit (BMU), which most closely resembles the input pattern – using a distance measure;
- updating the weights of the winning unit;
- updating the weights of other units – reducing the neighbourhood function;
- decreasing the learning rate;
- repeat until convergence of the map is achieved.

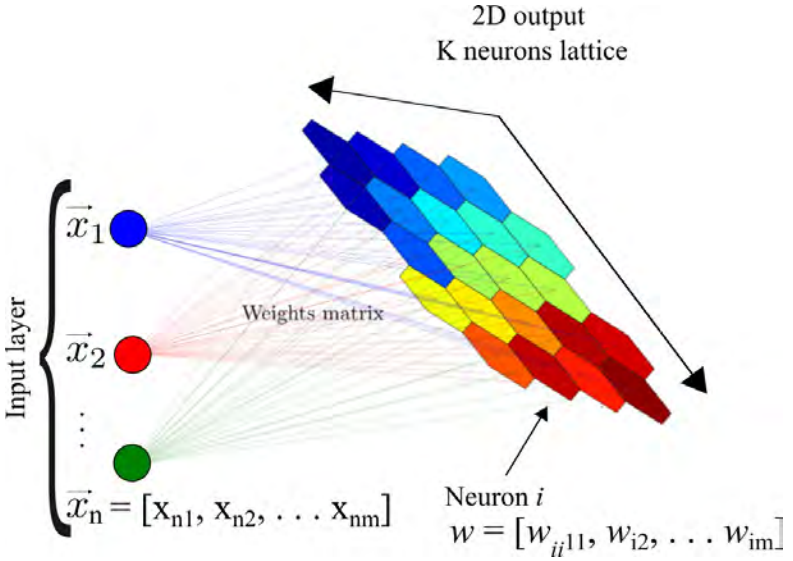

Figure 3.1: A schematic representation of an architecture of Self-Organising Maps with projections on a U-matrix map, figure modified from (Kind and Brunner (2013)).

3.2.2 SOM modelling, visualisation and clustering, the implementation of MATLAB Toolbox

The powerful feature of SOM modelling lies in its ability to visualise the output maps and possibilities of further computation it enables. Such visualisation is possible with the use of the U-matrix (unified distance) map a visualisation technique for SOM that depicts the distance between the neurons on the map. It shows the organised structure of the calculated output. The similar outputs are grouped in clusters marked by uniform areas of low values (dark colours). The high values (bright colours) on the map indicate a cluster borders. A classic example of a U-matrix visualisation of the SOM analysis is of Fisher's Iris dataset (Fig. 3.2). The analysis involved using SOM to visualise and explore the structure of this well-known flowers dataset. The Iris dataset contains 150 samples of four features of (sepal length, sepal width, petal length, petal width) for three species of Iris flowers: Iris setosa, Iris versicolor, and Iris virginica.

The results of SOM analysis can also be visualised through individual component planes, which represent arrays of scalar values corresponding to the i^{th} components of all the weight vectors w_j. Essentially, these planes (Fig. 3.3) show the dimensionless weighted average values for one variable of the input data (each value in each map unit), offering a detailed visualisation of how each variable contributes to the final SOM output.

By plotting the component planes for all dimensions, we can display the entire dataset's information, providing a clear view of how each variable affects the neurons on the map. The colour-coded component planes help to identify the relative influence of specific variables on the overall clustering and classification process.

For purposes of this dissertation SOM Toolbox was applied to the analysis of two different datasets listed in Chapters 5 and 6. In both cases, the main goal was to identify groups of data that are similar to each other by a measure of the selected distance calculation and SOM algorithm. On the contrary, motivation for these two datasets were distinct. More on this topic is presented in respective Chapters. Nevertheless, the core of implementation of the SOM Toolbox for MATLAB (Vesanto et al. (2000, 1999)) stayed the same and is presented in this section. Codes written were original and self developed with the use of SOM functions from the mentioned above Toolbox.

Therefore, firstly the input for SOM has to be prepared. The structures of the

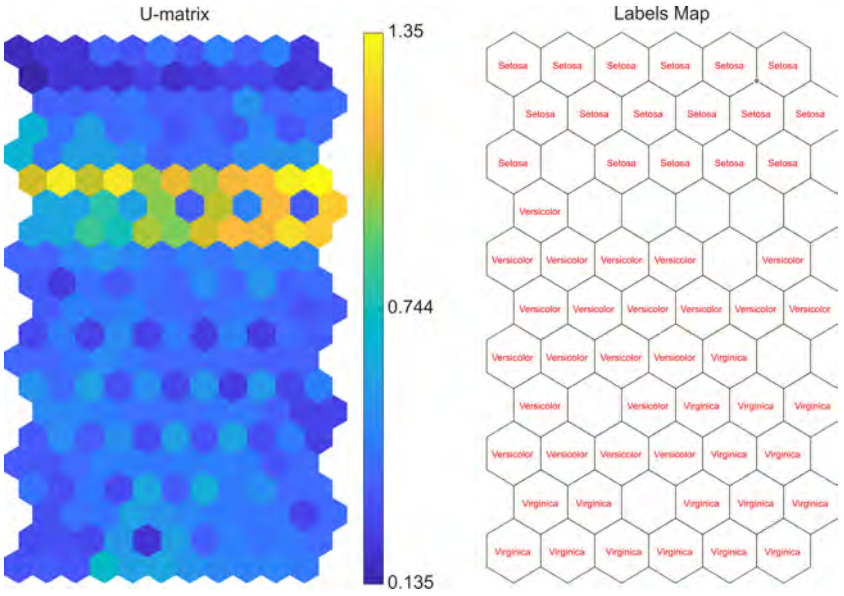

Figure 3.2: On the left Self-Organisation shown on U-matrix map of Fisher's Iris dataset and on the right labelled map of types of irises grouped in clusters by SOM.

inputs of studied cases are shown in the respective Tables 5.1.5 and 6.2. Further steps of the functions and code implemented for the calculation with SOM is presented in the form of list below:

- A data structure (a collection of data values) is constructed;
- data is normalised linearly from 0 to 1;
- map is initialised linearly along its greatest eigenvectors (function **linint**)
- the map size is calculated with the use of a heuristic formula of total number of nodes $M = 5\sqrt{N}$, where N is number of data samples;
- the SOM is set with batch algorithm and gaussian neighbourhood and is trained in two phases: rough training and then fine-tuning (using function **som_make**);
- for a given data vector from a given output map BMUs are found (using function **bmus**), additionally the indexes of these vectors in the output map that best matched to the vectors in the input data are returned;

Optionally:

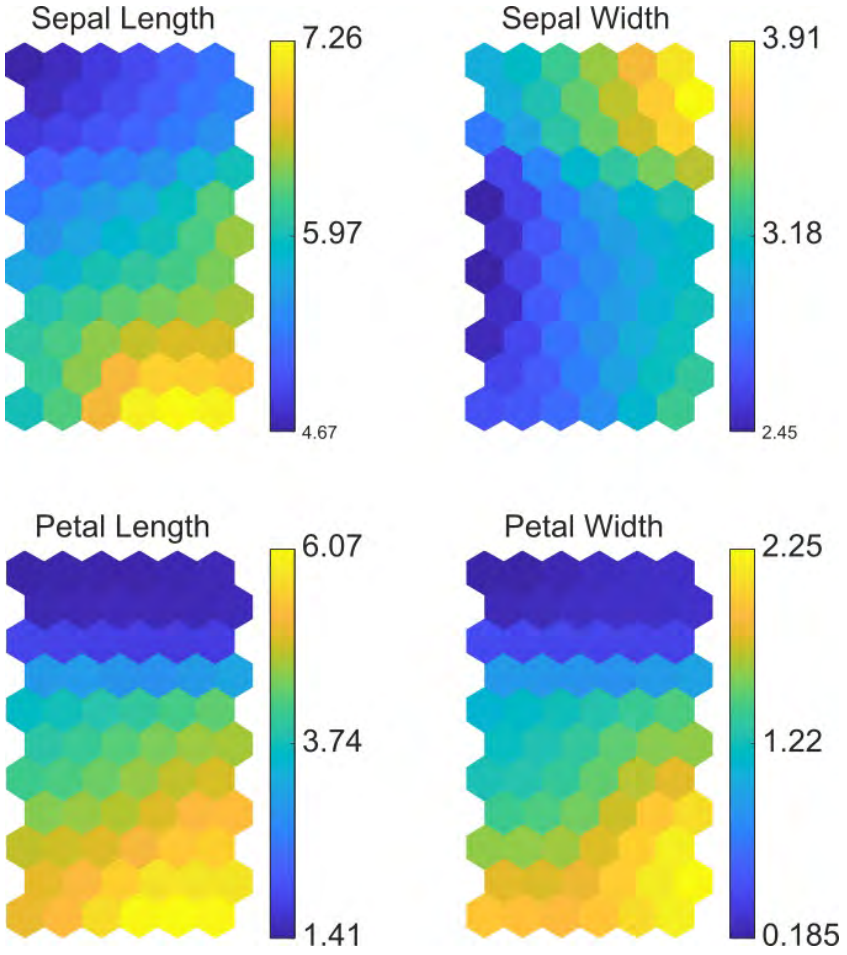

Figure 3.3: Component planes of Fisher's Iris dataset, show the dimensionless weighted average values for one variable of the input data.

- automatically labels are given to the map structure based on an labelled input data (using function **autolabel**); the BMU of each vector in the output is found from among the vectors in the input, and the vectors in are added to the corresponding vector;

- quantisation and topographic error is calculated to give the quality of the output SOM, it is a first steps to evaluate the results (function **som_quality**).

- clusters are found based on local minima of U-matrix (using function **dmat-clusters**); the minimum neighbourhood is found for each map unit to which it belongs relative to every other map unit; the best results of clustering was provided with the use of clusters forming method where a centroid was used (centre of the group of cases) to determine the average distance between clusters of units.

3.3 Quality Assesment of SOM Output

Data mining techniques focus on searching for and identifying similarities within encoded information, it is essential to assess the outcomes provided by clustering algorithms to prevent incorrect data assignment to clusters. One commonly used metric for visually evaluating clustering performance is the silhouette value, introduced by Kaufman and Rousseeuw (1990). The one that was selected to assess results for analyses presented.

The silhouette value s_i for the i^{th} data point is calculated using the following formula:

$$s_i = \frac{b_i - a_i}{\max(a_i, b_i)}, \tag{3.4}$$

where a_i represents the average distance from the i^{th} data point to all other points within the same cluster, and b_i denotes the minimum average distance from the i^{th} data point to points in other clusters. The silhouette value can range from -1 to 1, with higher values suggesting that the data point has been accurately assigned to its cluster. Typically, silhouette values above 0.5 indicate well-classified data points, while an average width below 0.2 signals poorly classified objects Everitt et al. (2011).

Chapter 4

Deformation Definition and Measures

4.1 Concept of Stress

Original idea of a relation of a force acting upon a body, was formulated by Robert Hooke as simply *as the force, so the extension* (Humphrey and Delange (2015)). Alas it is rarely applicable to any real world material. There are many more variables that govern the behaviour of any body when force is applied to it. Then it was Euler that described *stress* as intensity of a force acting normal to an area (Humphrey and Delange (2015)). Thus, e.g. if we want to determine the strength of a soft tissue, the force relative to the size is important (Fung (1993)). Hence, the stress that is related to the strength of the material can be described as:

Let the cross-sectional area be A, and let the force that acts be F.

$$\boldsymbol{\sigma = F/A} \tag{4.1}$$

Thus in mechanics, stress (4.1) represents the internal forces per unit area within a material that arise from external loads, internal body forces, or temperature changes. It quantifies how material parts interact with and exert forces on one another, effectively describing the intensity of the internal forces. Stress plays a crucial role in understanding material behaviour under various conditions, serving as a foundational concept in continuum mechanics for analysing structural and biomechanical systems.

Mathematically, stress is a tensor, which is defined independent of a coordinate system. To address practical issues, it is essential to calculate stress components in

relation to a specific coordinate system. Since coordinate systems can vary—being defined by different origins and sets of base vectors—there can be numerous sets of stress components at the same point within a material under a single set of applied forces (Humphrey and Delange (2015)). E.g. for three Cartesian coordinate systems a point may take three different sets of components of the same stress $\sigma_{(\text{face})(\text{direction})}$:

$$\begin{bmatrix} \sigma_{xx} & \sigma_{xy} & \sigma_{xz} \\ \sigma_{yx} & \sigma_{yy} & \sigma_{yz} \\ \sigma_{zx} & \sigma_{zy} & \sigma_{zz} \end{bmatrix}.$$

To describe stress components, consider a small cube within a material (Fig. 4.1). This cube has six faces. Define a set of rectangular Cartesian coordinates as $\mathbf{x}_1, \mathbf{x}_2, \mathbf{x}_3$. Let the face of the cube that is perpendicular to $\mathbf{x}_1$ be represented by ΔS_1. The stress vector acting on this face, denoted as τ, can be decomposed into three components along the coordinate axes, labelled $\tau_{11}, \tau_{12}, \tau_{13}$. These components, $\tau_{11}, \tau_{12}, \tau_{13}$, are the stress components on the cube. Likewise, we consider the faces ΔS_2 and ΔS_3, which are perpendicular to $\mathbf{x}_2$ and $\mathbf{x}_3$ respectively. The stress vectors acting on these faces and their respective components in the directions of $\mathbf{x}_1, \mathbf{x}_2, \mathbf{x}_3$ directions can be organised into a matrix.

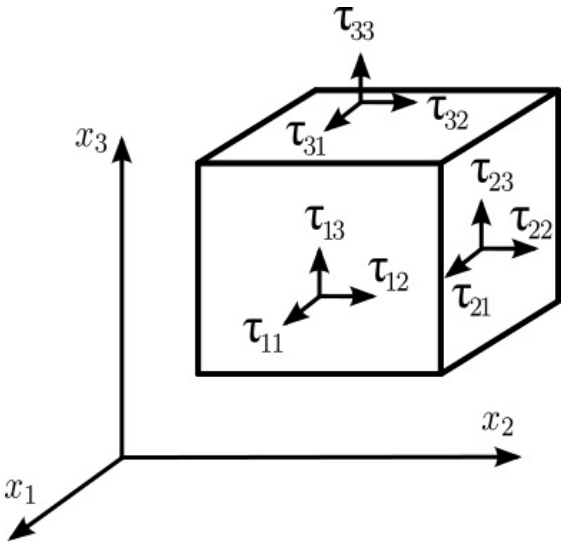

Figure 4.1: Notations of stress components.

This is illustrated in Fig. 4.1, the components $\tau_{11}, \tau_{22}, \tau_{33}$ are called normal stresses, and the remaining components τ_{12}, τ_{13}, etc., are called shearing stresses (Fung (1993)).

	Components of Stresses		
	1	2	3
Surface normal to $\mathbf{x}_1$	τ_{11}	τ_{12}	τ_{13}
Surface normal to $\mathbf{x}_2$	τ_{21}	τ_{22}	τ_{23}
Surface normal to $\mathbf{x}_3$	τ_{31}	τ_{32}	τ_{33}

The concept of stress is defined as the force per unit area exerted by the material on one side of a surface element on the material on the opposite side. This is understood in relation to the orientation of the outer normal of the surface. For example, if the outer normal surface of an element points in the positive direction of the $\mathbf{x}_2$ axis and the normal stress component τ_{22} is positive, then the corresponding stress vector will also point in the positive $\mathbf{x}_2$ direction. Conversely, if τ_{22} is positive but the outer normal points in the negative $\mathbf{x}_2$ direction, the stress vector will point in the negative $\mathbf{x}_2$ direction.

Similarly, for shear stresses, positive values of τ_{21} and τ_{23} indicate that the shear stress vectors will point in the positive directions of the $\mathbf{x}_1$ and $\mathbf{x}_3$ axes if the outer normal aligns with the positive $\mathbf{x}_2$ direction. If the outer normal points in the opposite direction, these shear stress vectors will instead point in the negative directions of the $\mathbf{x}_1$ and $\mathbf{x}_3$ axes.

4.2 Concept of Strain

Deformation in a solid that can be associated with stress is quantified by strain. For instance, consider a string with an initial length L_0. If the string is extended to a new length L, for small elongations, all measures converge, but differences become evident with larger elongations, demonstrating strain's sensitivity to deformation scale. The change in length can be expressed using dimensionless ratios such as, $\frac{L}{L_0}$, $\frac{(L-L_0)}{L_0}$, and $\frac{(L-L_0)}{L}$.

Using these ratios helps to remove the dependence on the absolute length. The ratio L/L_0 is known as the stretch ratio, denoted by λ.

The choice of strain measures is largely determined by the stress-strain relationship (i.e., the material's constitutive equation). Pulling a string causes it to elongate. Experimental data can be plotted as a curve of tensile stress σ versus the stretch ratio λ or strain e. An empirical formula can describe the relationship between σ and e. When the strain is infinitesimally small, the different strain measures coincide. It has been found that, for many engineering materials under

small uniaxial stretching, the relationship:

$$\sigma = Ee, \tag{4.2}$$

holds within a certain range of stresses, where E is a constant known as Young's modulus. This relationship is known as Hooke's law, and materials that follow it are called Hookean materials. For instance, steel behaves as a Hookean material up to specific yield stress limits. For small shear strains, the corresponding relationship is:

$$\tau = G \tan \alpha, \tag{4.3}$$

where G is the modulus of rigidity. The validity of this equation is also limited by yield stresses, which differ in tension, compression, and shear.

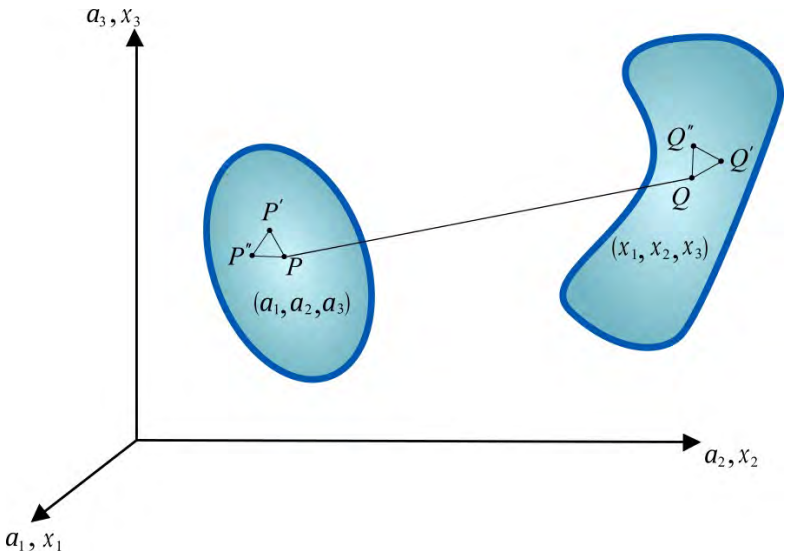

Figure 4.2: Deformation of a body.

In reality, deformations in most materials are more complex than these simple cases. Therefore, a general approach is needed. Let us consider a body occupying a space S (Fig. 4.2). In a rectangular Cartesian coordinate system, each particle in the body has coordinates. Upon deformation, each particle moves to a new position, described by new coordinates. For instance, a particle initially at coordinates (a_1, a_2, a_3) moves to (x_1, x_2, x_3) upon deformation. The vector **PQ**, or **u**, is called the displacement vector of the particle (Fig. 4.2). The displacement vector's components are:

$$u_1 = x_1 - a_1, \quad u_2 = x_2 - a_2, \quad u_3 = x_3 - a_3. \tag{4.4}$$

Knowing the displacement for every particle allows us to reconstruct the deformed body from its original shape. Thus, deformation can be described using the displacement field. The original position of a particle, given by (a_1, a_2, a_3), and its new position, given by (x_1, x_2, x_3), determine the deformation if x_1, x_2, x_3 are known functions of a_1, a_2, a_3:

$$x_i = x_i(a_1, a_2, a_3), \quad (i = 1, 2, 3). \tag{4.5}$$

This represents a mapping from (a_1, a_2, a_3) to (x_1, x_2, x_3). It is assumed that this transformation is unique, meaning the functions in the above equation are single-valued, continuous, and have a unique inverse:

$$a_i = a_i(x_1, x_2, x_3), \tag{4.6}$$

for each point in the body. A rigid-body motion does not induce stress, as displacement alone is not directly related to stress. To relate deformation with stress, it is necessary to consider the stretching and distortion of the body, particularly the change in distance between any two points (Fig. 4.3).

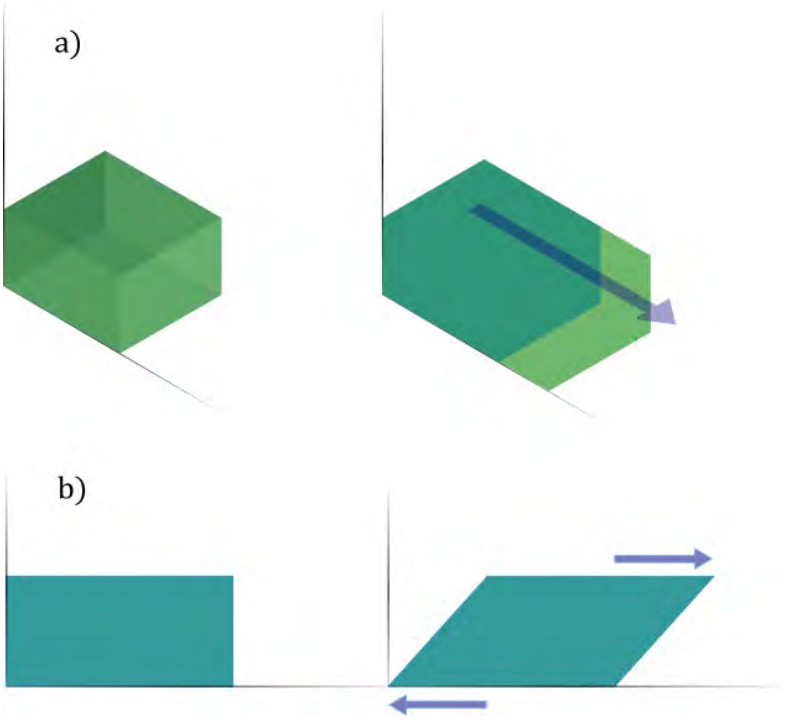

Figure 4.3: Patterns of deformation, a) elongation, b) simple shearing.

4.3 Measures Used

In this work, strain calculations were employed to analyse the mechanical behaviour of the human abdominal wall under pressure. Particular emphasis was given to the principal strains values a material undergoes when subjected to loading. As a measure of deformation, strain provides critical insights into how tissues respond to both internal and external forces. Principal strains may also be used to assess the compatibility of the abdominal wall and implant. This is particularly relevant when studying the abdominal wall's complex biomechanical properties.

To capture the localised deformations accurately, the Green-Lagrange strain tensor is utilised. This measure was used because such materials undergo large deformations, offering a robust representation of strain in non-linear material behaviour, which is characteristic of biological tissues. In this dissertation measures of strain that was used for analyses are the displacements and subsequent strains for which a local Green-Lagrange strain tensor was used and expressed as:

$$\mathbf{E} = \frac{1}{2}\left(\mathbf{F}^{\top}\mathbf{F} - \mathbf{I}\right), \tag{4.7}$$

where **F** is the deformation gradient. Based on the quantities of the eigenvalues and eigenvectors $\boldsymbol{\varepsilon}$ the analyses were performed for the principal strains (ε_1 and ε_2) and directions (α). The angle that separates the main direction from the transverse direction, x, is α. The directions of the local principal strain were obtained by using local strain tensors as shown in Szepietowska et al. (2023); Troka et al. (2024a). By focusing on local strain distributions, this approach helps to understand the mechanical behaviour of the abdominal wall and its spatial heterogeneity.

To elaborate, the local Green-Lagrange strain tensor is a mathematical representation used in the field of continuum mechanics to describe the deformation of a material. It quantifies the strain at a specific point within a material body as it undergoes deformation from its original (reference) configuration to its current (deformed) configuration. The tensor captures the change in length, angles, and volume elements, providing a comprehensive measure of deformation, where:

- **F** is the deformation gradient tensor, which describes how a small vector in the reference configuration transforms to the current configuration (Fig. 4.2);
- $\mathbf{F}^{\mathrm{T}}$ is the transpose of the deformation gradient tensor;
- **I** is the identity matrix.

The components of the Green-Lagrange strain tensor E_{ij} are given by:

$$E_{ij} = \frac{1}{2}\left(\frac{\partial u_i}{\partial X_j} + \frac{\partial u_j}{\partial X_i} + \sum_{k=1}^{3} \frac{\partial u_k}{\partial X_i}\frac{\partial u_k}{\partial X_j}\right), \tag{4.8}$$

where: u_i are the components of the displacement vector **u**, that describe the movement of points from the reference configuration; X_i are the coordinates in the reference configuration.

The tensor E_{ij} measures the strain by considering both the linear and non-linear contributions to the displacement field. This makes it particularly useful for analysis of finite deformations, where the changes in shape and size of a material body are not small. The Green-Lagrange strain tensor accounts for the fact that the length and angles between material elements can change significantly, providing a more accurate description of strain compared to simpler measures like the engineering strain tensor, which assumes small deformations.

Chapter 5

Human Abdominal Wall

In this Chapter (5) SOM was utilised to pinpoint regions of the living human abdominal wall that exhibit similar mechanical behaviour under intra-abdominal pressure, in order to grasp more information about the similar deformation properties of said regions. The research involved multiple human subjects, highlighting the diversity among the analysed patients. The Machine Learning driven methodology used full-field data gathered during experiments on patients undergoing peritoneal dialysis (Troka et al. (2024a)).

5.1 Experimental data acquisition

The study is based on experimental data collected *in vivo* on humans described also in Szepietowska et al. (2023). A total of 22 participants, comprising of 14 males and 8 females, consecutively labelled as D1–D22, diagnosed with end-stage renal insufficiency, were subjected to tests while undergoing peritoneal dialysis (PD), a procedure routinely performed on them in hospital. The investigation employed a Digital Image Correlation (DIC) system to capture the movements of their abdominal walls during PD, meaning during filling the abdominal cavity with dialysis fluid. The characteristics of these subjects are outlined in Table 5.1 with additional information on patient's hernia history listed below it. Despite not receiving formal physiotherapy or rehabilitation exercises prior to the study, patients were educated and motivated to engage in physical activity and sports. It is reasonable to infer that their level of physical activity was appropriate for their age and gender, aligning with the norms of the average individual in Poland. Four of them had a previous history of a hernia with or without operation. Therefore, the

experiments were carried out on subjects who had an abdominal wall insufficiency and on those who did not. Examining both unhealthy and healthy abdominal wall is important because it can be considered a reference for the desired repaired state, as noted in the research by Pachera et al. (2016).

No	sex	age	height [m]	weight [kg]	BMI [kg/m^2]	hernia
D1	M	78	1.63	80	30.1	no
D2	F	48	1.75	66	21.6	no
D3	F	73	1.60	68	26.6	no
D4	M	70	1.70	80.7	27.9	no
D5	M	74	1.67	84	30.1	no
D6	F	65	1.60	67	26.2	no
D7	M	88	1.72	89	30.1	no
D8	M	61	1.68	58	20.5	no
D9	M	46	1.76	85	27.4	no
D10	F	72	1.54	61	25.7	no
D11	M	36	1.76	86	27.8	no
D12	M	56	1.74	78	25.8	yes, details listed below the table
D13	M	55	1.75	97	31.6	yes, details listed below the table
D14	M	47	1.94	84	22.3	no
D15	M	61	1.84	94	27.9	yes, details listed below the table
D16	F	64	1.76	68	22.0	no
D17	M	62	1.68	65	23.0	no
D18	M	59	1.82	88	26.6	yes, details listed below the table
D19	F	68	1.70	75	26.0	no
D20	F	36	1.62	55	21.0	yes, details listed below the table
D21	M	81	1.75	81	26.4	no
D22	F	41	1.70	42	14.4	no

Table 5.1: Characteristics of the patients.

The following hernia problems reported by the tested subjects:

- D12 – an umbilical hernia repaired with an implant 2 years prior;
- D13 – a "dried" umbilical hernia without implants;
- D15 – an inguinal hernia;
- D18 – abdominal hernia due to an error during catheter insertion, additionally, in 2009, mesh implantation was performed to repair an inguinal hernia after overload during gym exercises, both sides;
- D20 – an umbilical hernia without surgery or any procedure.

5.1.1 Digital Image Correlation

Analysing biological tissues and organs, particularly in terms of their interaction with external forces, is made possible by measuring displacements and strains. This is a fundamental aspect of experimental biomechanics, as highlighted by Palanca et al. (2016). Given the anisotropic and inhomogeneous nature of biological samples, it is vital to obtain full-field measurements, ideally through non-contact techniques. Multivariate data analysis requires experimental input and validation through tests, but a fully monitored experiment at every point on a tested piece, such as with strain gauges, is not always feasible Palanca et al. (2016).

During mechanical testing, Digital Image Correlation (DIC) an optically based technique, can measure evolving 2D or 3D full-field coordinates on the surface of a test piece (as noted in Jones and Iadicola (2018)). The basic operation of a DIC system is straightforward: by capturing a sequence of images that track the movement of a marked point on the tested sample, the system can record the movement and deformation of the tested piece. For the full-field test it is necessary to track a large group of points, which is done by applying a special speckle pattern (a random granular, usually black and white, pattern) on the tested surface. Based on recorded sequence of images displacements, strains, and other relevant quantities can be calculated. For example, Fig. 5.1 illustrates prepared sample's surface and results of DIC measurement.

5.1.2 Data acquisition

The Dantec Q-400 four-digital-camera (VCXU-23M with a 2.3 Mpx matrix (resolution: 1920 x 1200 px)) DIC system with VS-1620HV lenses (16 mm f/2.0-16) was used (Fig. 5.2). In order to facilitate the correlation of images capturing the entire anterior abdominal wall, the stand was positioned above the area of interest as in Fig. 5.1. To apply a random granular like pattern of spots a flexible filament was prepared and used as a stamp. The pattern then was "printed" on the surface of the abdominal wall (top right in Fig. 5.1) with paint approved for skin colouring.

The process begins with spatial correlation calibration. The system was calibrated by recording the relative positions of the four cameras mounted on two tripods (Fig. 5.2) using a chequerboard-style calibration plate (35 mm, 9x9 marked white plastic), Szepietowska et al. (2023). After the images are divided into smaller sub-images (known as facets), a matching algorithm aligns the facets between the reference and deformed states. The displacement field is then computed, followed

Figure 5.1: Experiment: subject laid under the DIC setup (left), speckle pattern on the surface of the abdominal wall (top right), DIC grid (middle right), and the outcome map resulting from image correlation (bottom right), Szepietowska et al. (2023).

by the derivation of the strain field. Further details about the DIC methodology can be found in sources such as Sutton et al. (2009); Reu et al. (2018); Jones and Iadicola (2018).

Throughout the PD procedure, from emptying the abdominal cavity to filling it with two litres of dialysis fluid, the displacement of the abdomen under pressure was recorded by the DIC system. Next, as described in Pérez Díaz et al. (2017), intraperitoneal pressure was assessed during the medical procedure using a manometer attached to the dialysis bag. For ethical reasons the standard peritoneal dialysis protocol was adhered to. Throughout the testing, the same protocol was followed to ensure patient safety. In this study, each subject was examined just once, except for the subjects D8 and D17, who is the same patient, but testes interval was over a year. Inherently, it was worthwhile to examine the same person and see how body changes with regular dialysis procedures.

The experiments were fully non-invasive and the measurement was contactless. All participants consented to participate in the study under a protocol approved by the Independent Ethics Committee for Scientific Research at the Medical University of Gdańsk № NKBBN 314/2018.

Figure 5.2: Digital Image Correlation - experimental stand, Szepietowska et al. (2023).

Commercial image correlation software, Istra 4.7, was used to process the acquired images. The surface displacement of each tested abdominal wall in three dimensions was determined, please refer to the Table 5.2 for a selection of parameters used in image analysis. An approximate error radius found in DIC measurements is: (5.1)

$$Err = \sqrt{1/3(V(x) + V(y) + V(z))}, \tag{5.1}$$

which estimates the uncertainty of the 3D coordinates (x, y, z), where V is the variance.

No	faceted size [px]	grid size [px]	approx. grid spacing [mm]	frame rate [Hz]	calibration residuum [px]
D1	33	22	8	2	0.11
D2	25	19	8	5	0.09
D3	29	22	10	5	0.09
D4	25	19	8	5	0.08
D5	25	19	8	5	0.08
D6	29	22	9	5	0.09
D7	25	19	9	5	0.09
D8	25	19	8	5	0.09
D9	25	19	8	5	0.09
D10	25	19	8	5	0.08
D11	29	22	9	5	0.08
D12	29	22	9	5	0.08
D13	29	22	9	5	0.12
D14	25	19	8	5	0.11
D15	25	19	8	5	0.12
D16	25	19	8	5	0.11
D17	25	19	8	5	0.10
D18	25	19	8	5	0.10
D19	25	19	8	5	0.10
D20	25	19	8	5	0.10
D21	25	19	8	5	0.10
D22	25	19	8	5	0.09

Table 5.2: DIC test parameters.

5.1.3 Strain field of outer surface of abdominal wall

Analysis the mechanical behaviour of the abdominal wall in the context of its compatibility with implants used in hernia surgeries we focus on strain field. In particular on principal strains and their directions.

Strains along the surface object can be measured using the DIC method, which yields a normal vector **n** for each measurement point. This vector indicates the tangent plane in the area. The local x direction in the typical scenario is located where the xz plane and the z tangent plane intersect. **n** and x are perpendicular to the local y-direction. Every x, y value (strain, deformation) always refers to the coordinate system that was utilised for that particular measurement. The strain that was calculated for the analyses is referred to as Green-Lagrange strain (as in Chapter 4) because the deformation gradient and the "initial" strain is derived from it. The system created a grid of points on the recorded surface (see middle right in Fig. 5.1), and the displacements and strains at each grid point from formula (4.7) for a local Green-Lagrange strain tensor could be calculated. As a result, the abdominal wall's pressurisation variety throughout the entire surface was observed, shown in Fig. 5.3 for the patient labelled as D1.

Only half, along the *linea alba* (a midline structure), of the abdominal wall was taken into analysis (Fig. 5.1), because the catheter (delivering the dialysis fluid) covered part of the registration field and as was already demonstrated in (Lubowiecka et al. (2022)), the catheter's presence alters the abdominal wall's strain field.

In the early and final phases of the experiment, two pairs of time steps corresponding to breathing action were marked (Fig. 5.4). These four time steps represent four different deformation states of the abdominal wall and refer to different load levels. They were selected at exhalation and inhalation points at the initially empty abdominal cavity (around 20% of the experiment duration, time steps denoted T1 and T2 respectively) and abdominal cavity full of dialysis fluid (T3 on the exhale and T4 on the inhale) of the experiment (Fig. 5.4). Additionally an analysis considering all time steps was performed, although it is more computational costly and can introduce errors.

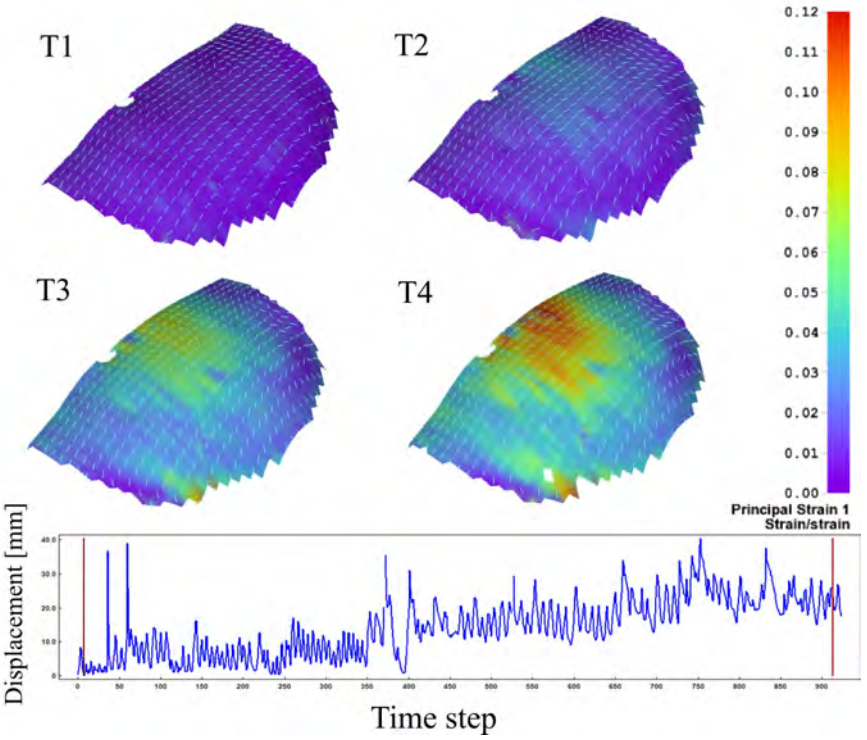

Figure 5.3: Map of the principal Lagrangian strain (shown by colour scale in [-]) and its direction in stages (a) T1 (b) T2 (c) T3 (d) T4 of subject D1. Displacement is shown for a single grid point in respect to the recorded time step.

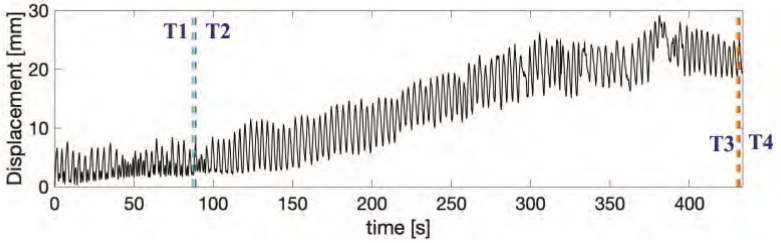

Figure 5.4: Graph of recorded displacement of a chosen point on the surface of the abdomen during PD procedure. Time steps (T1–T4) selected to the further analysis referring to different deformation states of the abdominal wall marked in the plot, Szepietowska et al. (2023).

5.1.4 Abdominal Wall Deformation

Before analysing any results it is a wise practice to understand the object/body which was being examined. Therefore since, the anterior abdominal wall features a complex, multilayered anatomical structure, divided into distinct regions that likely contribute to its diverse mechanical responses. The lateral parts consist of three primary muscles: the external oblique, internal oblique, and transversus abdominis, while the medial part comprises primarily the rectus abdominis muscle. This anatomical differentiation suggests that the abdominal wall may exhibit different mechanical behaviours between the side parts (lateral) and the middle (medial) region. Consistent with this hypothesis, Simón-Allué et al. (2017) observed similar mechanical division patterns using inverse analysis of *in vivo* data in rabbits, despite focusing solely on passive behaviours during inflation tests under anaesthesia, Podwojewski et al. (2014).

Previous studies highlight the significant influence of anatomical structures on mechanical behaviour. For instance:

- Podwojewski et al. (2014) noted that the strain pattern on the inner surface of the abdominal wall reflects its layered anatomical features more distinctly than the outer surface, where strains appear more homogeneous, Rath et al. (1997),
- variability in mechanical properties along the longitudinal direction can be expected due to:
    1. Differences in mechanical properties and structural changes of the rectus sheath along the arcuate line, Rath et al. (1997).
    2. Variations in the morphology and mechanical properties of the linea alba between the upper and lower abdominal wall, Gräßel et al. (2005).
    3. Variations in muscle thickness and fascicle orientation of the external oblique, internal oblique, and transversus abdominis muscles along the abdominal wall's longitudinal direction, Urquhart et al. (2005).

Furthermore, differences in fibre alignment contribute to mechanical response variations. Notably, the rectus sheath and linea alba show greater stiffness in the transverse direction, as observed by Astruc et al. (2018), emphasising their role in the passive mechanical response of the abdominal wall, Whitehead-Clarke et al. (2023).

If we take a look at Fig. 5.5 we could observe that the strain values in the tested abdominal wall exhibit noticeable changes with varying pressure levels. This behaviour is characteristic of elastic isotropic material structures, which deform proportionally to the applied load. However, it is intriguing to observe that the directions of the principal strains change during the experiment. This dynamic behaviour could be attributed to the active response of the abdominal wall, likely influenced by the cyclical forces generated during breathing. Such changes suggest that the abdominal wall's deformation is not purely passive but also reflects the mechanical interaction between its structural properties and the functional activity of the surrounding musculature. This phenomenon can likely be attributed to the anisotropy of the abdominal wall as a whole. Different tissue components, such as muscles, fascia, and connective tissues, may respond differently under load. When pressure increases, some components may become more dominant in bearing and distributing the load, altering the deformation patterns. This varying tissue behaviour under load highlights the complexity of the abdominal wall structure.

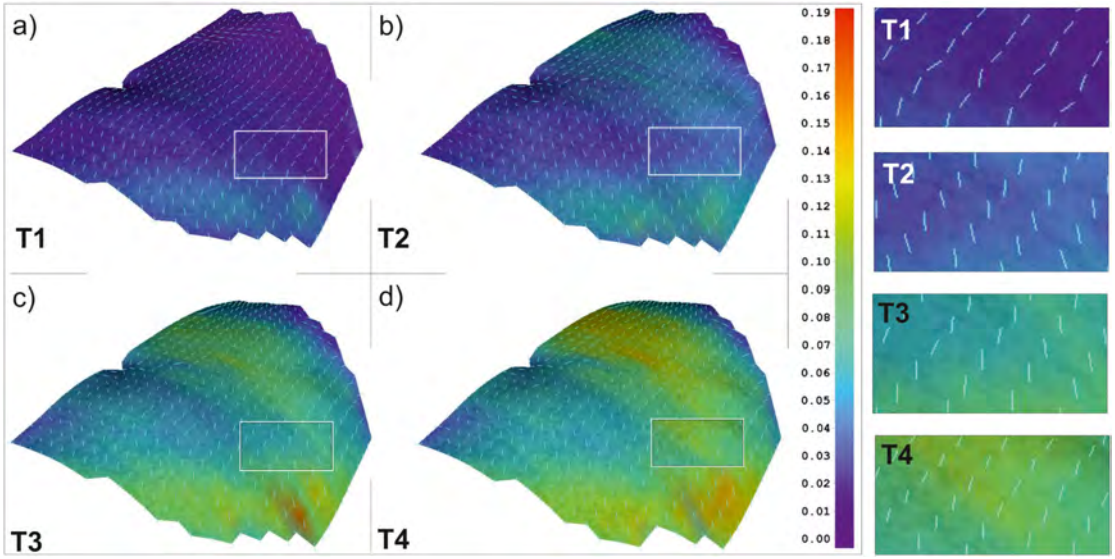

Figure 5.5: Map of the principal Lagrangian strain (shown by colour scale in [-]) and its direction in stages (a) T1 (b) T2 (c) T3 (d) T4 of subject D8; with zoomed marked parts of the abdominal surface with the directions of principal strains in T1–T4 on the right hand side (images of strain field adapted from Szepietowska et al. (2023)).

Moreover, the principal strain directions across the abdominal wall are not uniform. Certain regions exhibit a change in the dominant principal direction as the loading progresses through time steps T1, T2, T3, and T4. Conversely,

other regions maintain a consistent principal direction throughout the experiment. This variability highlights the complexity of the abdominal wall, as different areas respond uniquely to applied pressure, likely influenced by their structural and functional heterogeneity. Thus showing the anisotropic material behaviour of the abdominal wall and confirming the need of an analysis providing a holistic information.

5.1.5 Input datasets

When conducting any analysis with Machine Learning techniques, the challenge of constructing an appropriate input dataset is crucial. The input must be thoughtfully designed to ensure that the model captures relevant features for accurate predictions or classifications. Inadequate or improperly prepared inputs can lead to poor model performance.

In this section construction of input datasets for analyses with the use of Self-Organising Maps is presented.

In the research article Troka et al. (2024a) one variant of input dataset for analysis of the abdominal wall of patients was shown. Here, a broader spectrum of additional analyses was considered. The Table 5.3 below shows different variants for which analyses were conducted with the use of SOM and what kind of variables were used.

No	variables used	time steps used	analysis range
1	4 x ε_1	T1, T2, T3, T4	for each patient (D1-D12)
2	4 x ε_1	all time steps recorded	for each patient (D1-D12)
3	4 x (ε_1, α)	T1, T2, T3, T4	for each patient (D1-D22)
4	4 x (ε_1, ε_2, α)	T1, T2, T3, T4	for each patient (D1-D22)
5	4 x ε_1	T1, T2, T3, T4	one analysis, inter-patient

Table 5.3: Descriptors used for SOM analyses.

For visualised example of analysis no.1 the input dataset representing the entries in those four time points was structured and prepared as shown in Fig. 5.6. The vector length M refers to the number of grid points generated on the tested surface with the use of DIC system. The tested surface here is the surface of abdominal wall of a specific patient. Therefore, M can have different lengths. In this way, the analysed area of the abdominal wall is represented in the data set. The input vector constructed this way allows for simultaneous analysis of the abdominal wall

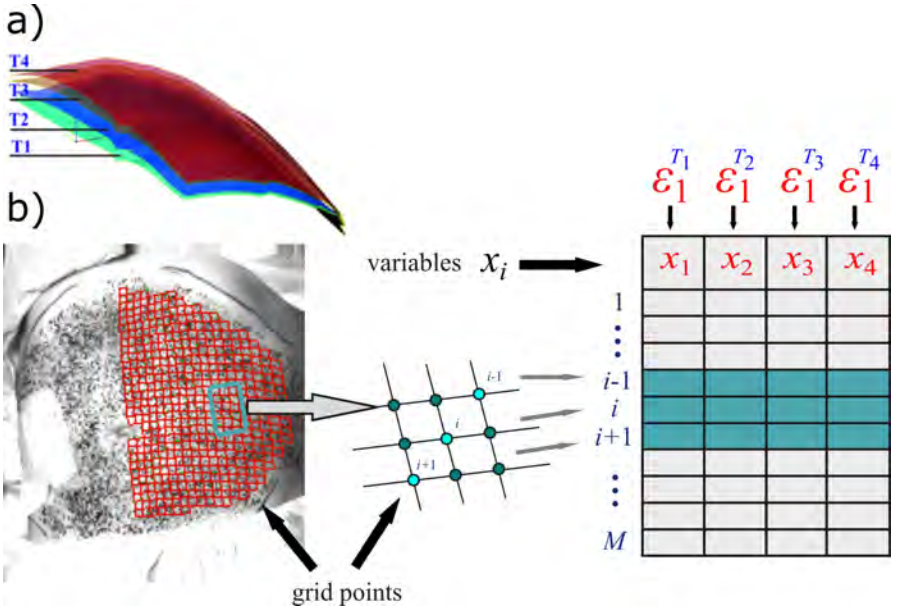

Figure 5.6: Input to Self-Organising Map: a) deformation states of the abdominal wall in the chosen steps (T1–T4); b) dataset and n-dimensional input vector to Self-Organising Map, example for the analysis no.1. Figure modified and adapted from Troka et al. (2024a).

mechanics on inhalation and exhalation and with filled and drained abdominal cavity.

The analyses no.1 and 2 are shown and discussed together to showcase the difference, advantages and disadvantages of using 4 chosen time steps and all recorded time steps of each patient. Finally, the number of variables refers to the strains measures for each grid point in each time step used for the specific analysis.

To further explain how the inputs were created please follow the list below:

1. 4–dimensional input vector $\boldsymbol{x}$= [$\varepsilon_1^{\mathrm{T1}}$, $\varepsilon_1^{\mathrm{T2}}$, $\varepsilon_1^{\mathrm{T3}}$,$\varepsilon_1^{\mathrm{T4}}$], where the superscript denotes the time step.

2. t–number of dimensions referring to the number of times steps recorded for the respective patient (Table 5.4) for $\boldsymbol{x}$= [$\varepsilon_1^{\mathbf{T1}}$, ... , $\varepsilon_1^{\mathrm{T}t}$], where the superscript denotes the time step.

3. 8–dimensional input vector $\boldsymbol{x}$= [$\varepsilon_1^{\mathrm{T1}}$, α^{T1}, $\varepsilon_1^{\mathrm{T2}}$, α^{T2}, $\varepsilon_1^{\mathrm{T3}}$, α^{T3}, $\varepsilon_1^{\mathrm{T4}}$, α^{T4}], where the superscript denotes the time step.

4. 12–dimensional input vector $\boldsymbol{x}$= [$\varepsilon_1^{\mathrm{T1}}$, $\varepsilon_2^{\mathrm{T1}}$, α^{T1},$\varepsilon_1^{\mathrm{T2}}$, $\varepsilon_2^{\mathrm{T2}}$,$\alpha^{\mathrm{T2}}$, $\varepsilon_1^{\mathrm{T3}}$, $\varepsilon_2^{\mathrm{T3}}$, α^{T3}, $\varepsilon_1^{\mathrm{T4}}$, $\varepsilon_2^{\mathrm{T4}}$, α^{T4}], where the superscript denotes the time step.

5. 4–dimensional input vector $\boldsymbol{x}$= [ε_1^{T1}, ε_1^{T2}, ε_1^{T3},ε_1^{T4}], where the superscript denotes the time step, but in this analysis data samples are taken for every patient, meaning the dataset consists of strains for respective time steps of all patients.

No.	Total grid points	t-number of total time steps
D1	744	920
D2	492	1901
D3	537	2174
D4	841	2039
D5	493	2048
D6	457	3105
D7	774	1987
D8	477	2171
D9	784	1799
D10	618	1968
D11	366	2491
D12	520	1931
D13	797	1818
D14	836	2086
D15	1012	1439
D16	753	3426
D17	945	1972
D18	833	2317
D19	480	1854
D20	619	1915
D21	798	2280
D22	504	2375

Table 5.4: DIC parameters of the experiment - number of grid points and t-number of time steps recorded for respective patient.

5.2 SOM Analysis and Results

Analyses mentioned in Section 5.1.5 are presented in here and one caveat worth noting is that the analysis no.1 from Table 5.3 is presented along analysis no.2 to show how selection of variables (meaning time steps of the same metric) impact final results.

For all analyses a guideline mentioned in Chapter 3.2 was followed (total number of nodes: $M = 5\sqrt{N}$ (Vesanto and Alhoniemi (2000)) to determine the size of map and number of neurons required for satisfactory results of the Self-Organising Maps. Training was conducted in batch mode, where the entire dataset is presented to the network simultaneously. This mode identifies the winning neurons for all samples before updating the weights, which influences all samples concurrently. The number of training epochs—defined as the number of iterations in which each sample is processed by the network until the SOM converges and was set 300 for the rough training and 100 for fine-tuning.

By plotting the component planes for all dimensions, the entire dataset's information can be displayed, providing a clear view of how each variable affects the organisation in the map. Fig. 5.7 shows the component planes for subject D1 from analysis no.4. The denormalised colour scale highlights the range of values for the neurons in each map. In this example it can be observed that majority of upper end of range organised in the bottom of the map. Worth nothing is that, the 2D representation of self-organisation is displayed on a rectangular grid, even though the U-matrices in this work were build on maps with the toroidal shape setting (unless stated otherwise), mitigating the borders effect Lötsch and Ultsch (2014).

5.2.1 Results

The results of multidimensional SOM analyses are presented in Figs 5.9–5.64. Identified clusters of grid points can be visualised on the abdominal wall surface of each patient in the 3D coordinate system (DIC coordinate system), see an explanatory workflow in Fig. 5.8.

The clusters that are mapped onto the abdominal wall geometry can be understood as zones of similar mechanical behaviour under load, as identified by the SOM analysis. These clusters are generated based on the input vector quantities depending on which analysis is considered (Table 5.3).

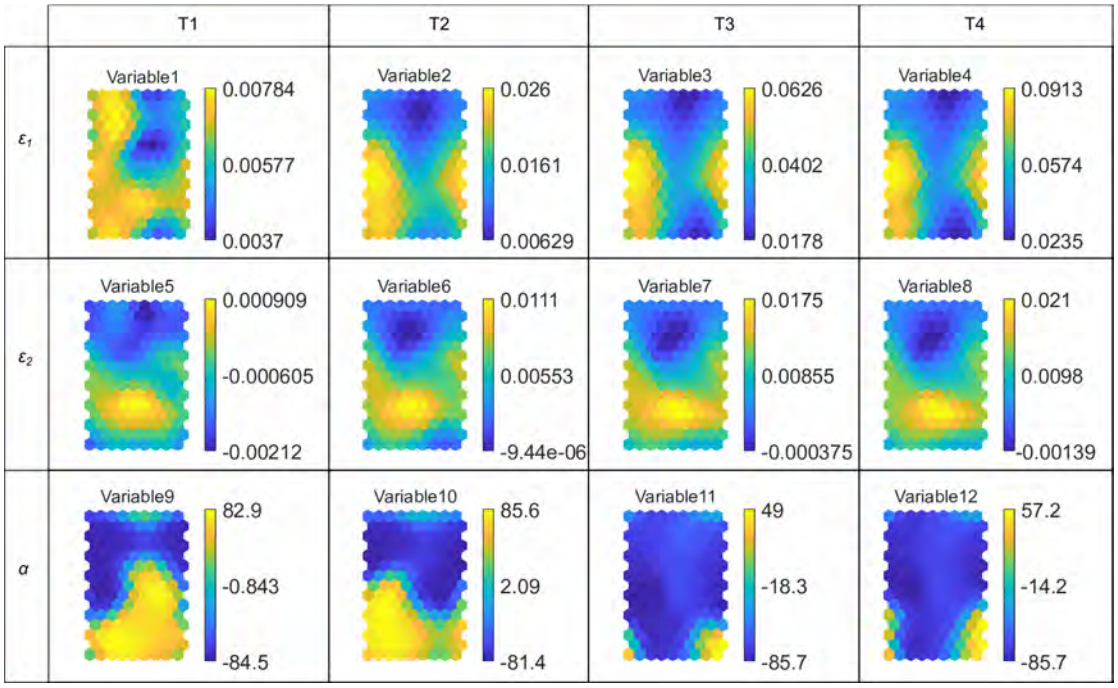

Figure 5.7: Component planes for subject D1 (analysis no.4). The following variables are the elements of input vector x. Figure adapted from Troka et al. (2024a).

Further to determine the best number of clusters averaged silhouette widths score are calculated (as presented in Section 3.3) for the entire dataset in respect to the number of clusters obtained with SOM (Figs 5.69, 5.70, 5.65 and 5.66). Next, based on that scores the best number of clusters is chosen and the silhouette values of each object of the dataset can be plotted in respect to their affiliation to the specific cluster (Figs 5.71, 5.72, 5.67 and 5.68). These plots here are treated as a quality measure, more in Section 3.3.

5.2.2 Analyses no.1 and 2: all steps vs. 4 steps of ε_1

In this section the analyses no.1 and 2 (from Table 5.3) are shown and discussed together to showcase the difference, advantages and disadvantages of using 4 chosen time steps and all recorded time steps of patients D1-D12 (Figs 5.9–5.20). Top part of the figures consists of analysis of all time steps and the bottom part the same patient but with analysis of only 4 time steps. Both analyses used principal strain (ε_1) as the variables. Along the U-matrix and clusters maps there are clusters mapped on the abdominal wall surface and below the quality assessment plots for this particular analysis. That is, an averaged silhouette score plot for varying

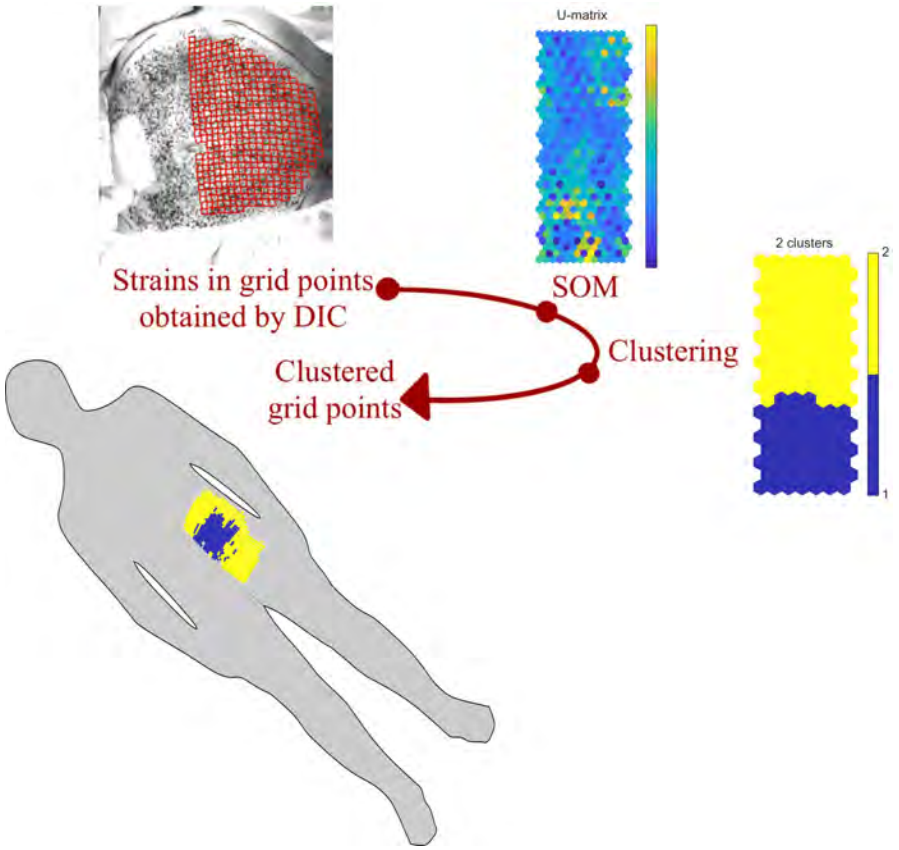

Figure 5.8: Workflow: strain in grid points obtained by DIC are the input to the SOM analysis. Then SOM neurons are clustered and mapped on the abdominal wall. Knowing which grid points are assigned to specific neuron, an assignment of the grid points to the cluster can be obtained. Figure adapted and modified from Troka et al. (2024a).

number of clusters and plotted next to it specific silhouettes values for the number of clusters which obtained better averaged score.

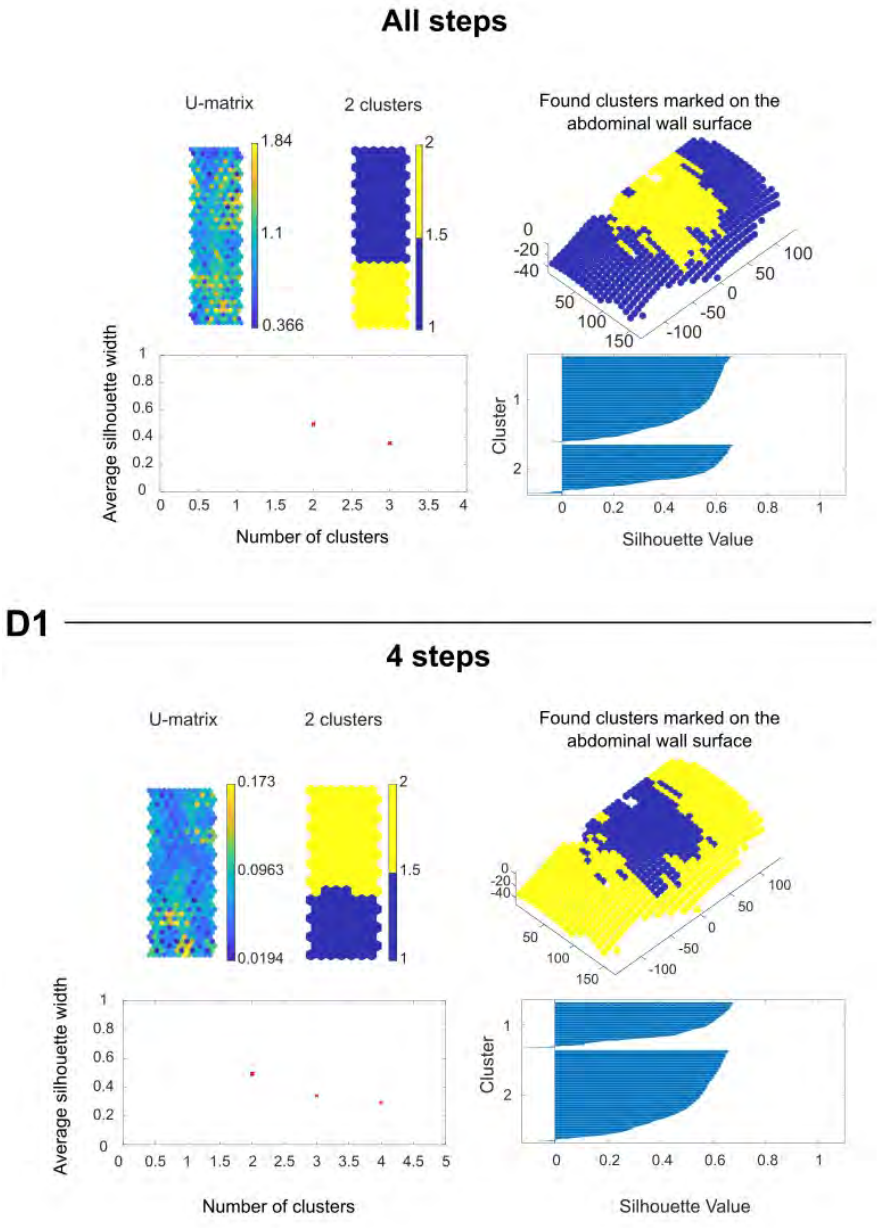

Figure 5.9: Results of D1 subject, analysis of ε_1 variable, for all steps and with cluster score = 0.49. Analysis for 4 steps with cluster score = 0.49. Both analyses resulted in 2 separate clusters.

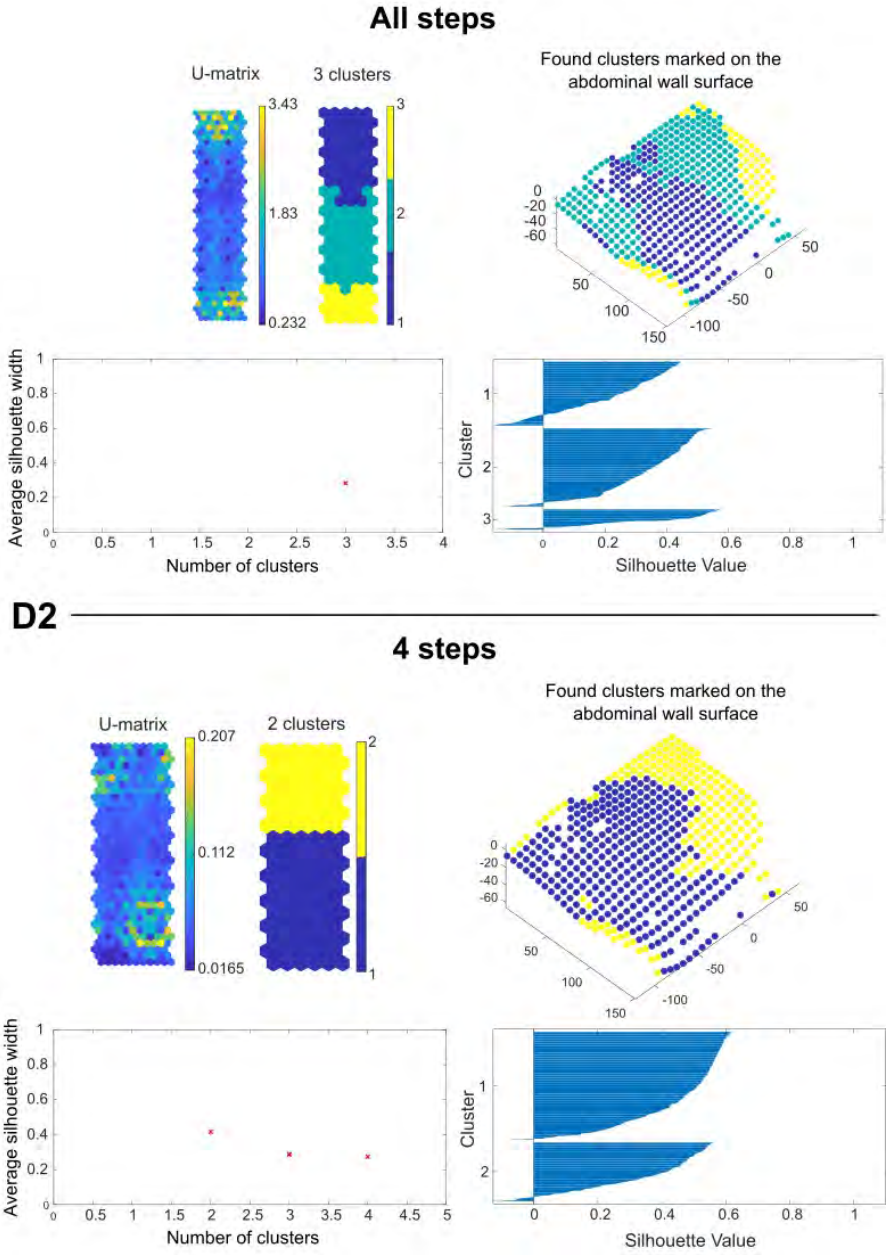

Figure 5.10: Results of D2 subject, analysis of ε_1 variable, for all steps and with cluster score = 0.28 with 3 clusters. Analysis for 4 steps with cluster score = 0.42 with 2 clusters.

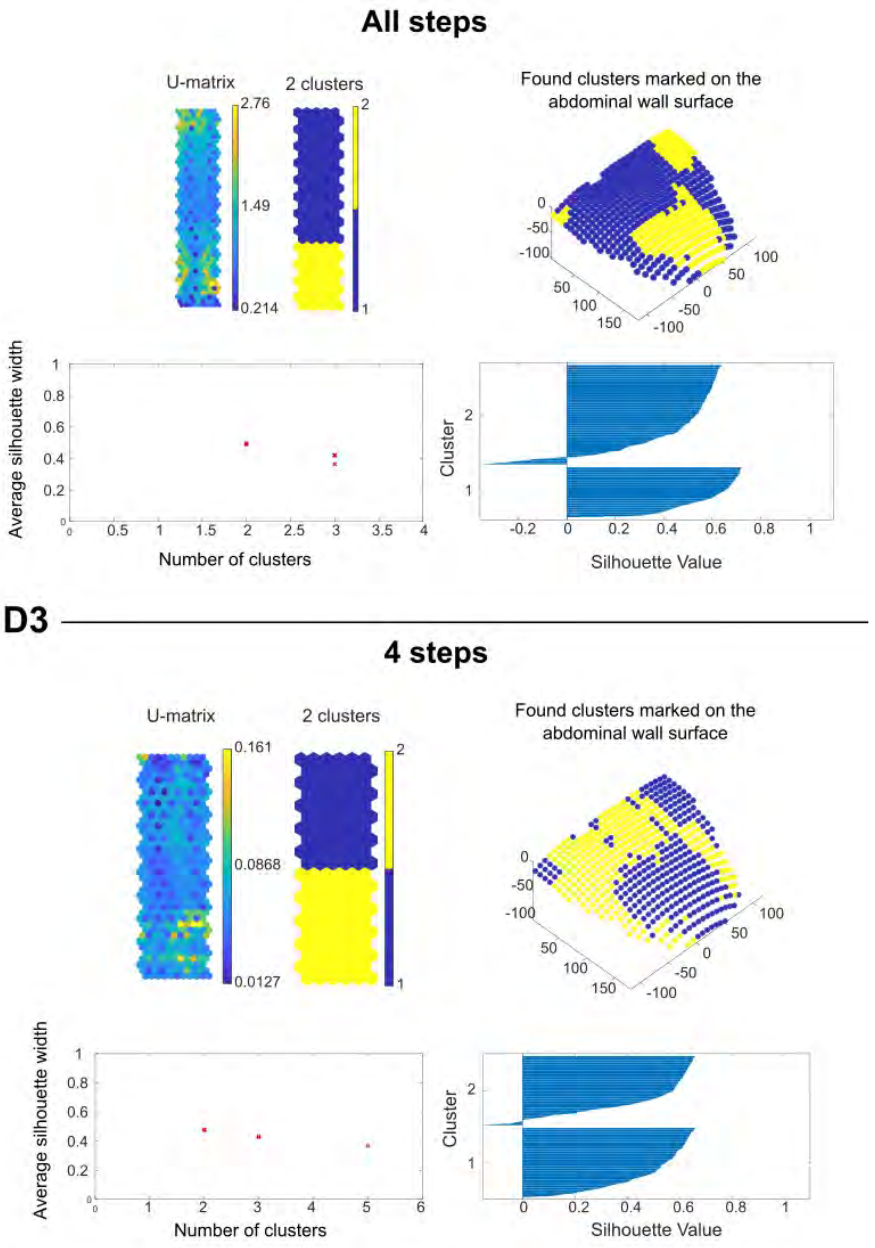

Figure 5.11: Results of D3 subject, analysis of ε_1 variable, for all steps and with cluster score = 0.49. Analysis for 4 steps with cluster score = 0.48. Both analyses resulted in 2 separate clusters.

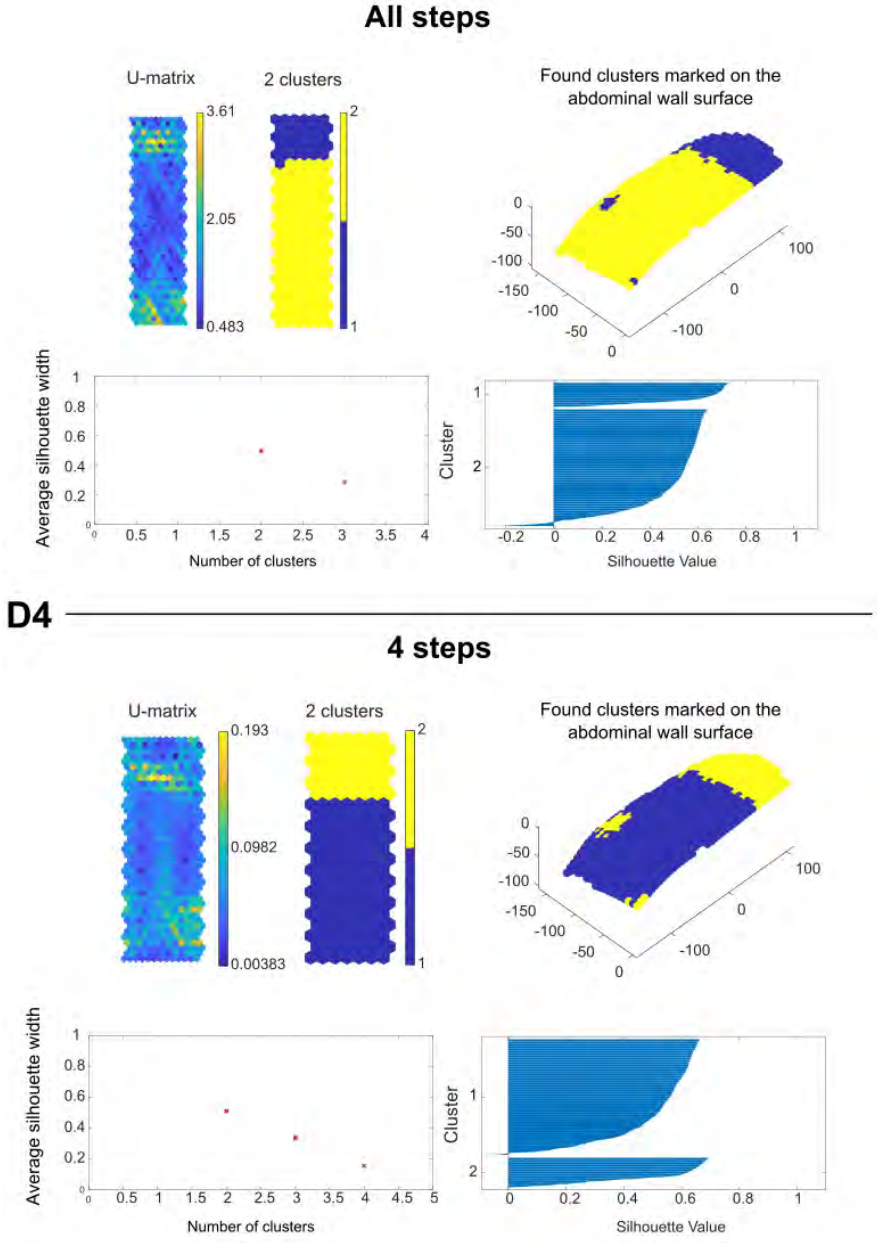

Figure 5.12: Results of D4 subject, analysis of ε_1 variable, for all steps and with cluster score = 0.50. Analysis for 4 steps with cluster score = 0.51. Both analyses resulted in 2 separate clusters.

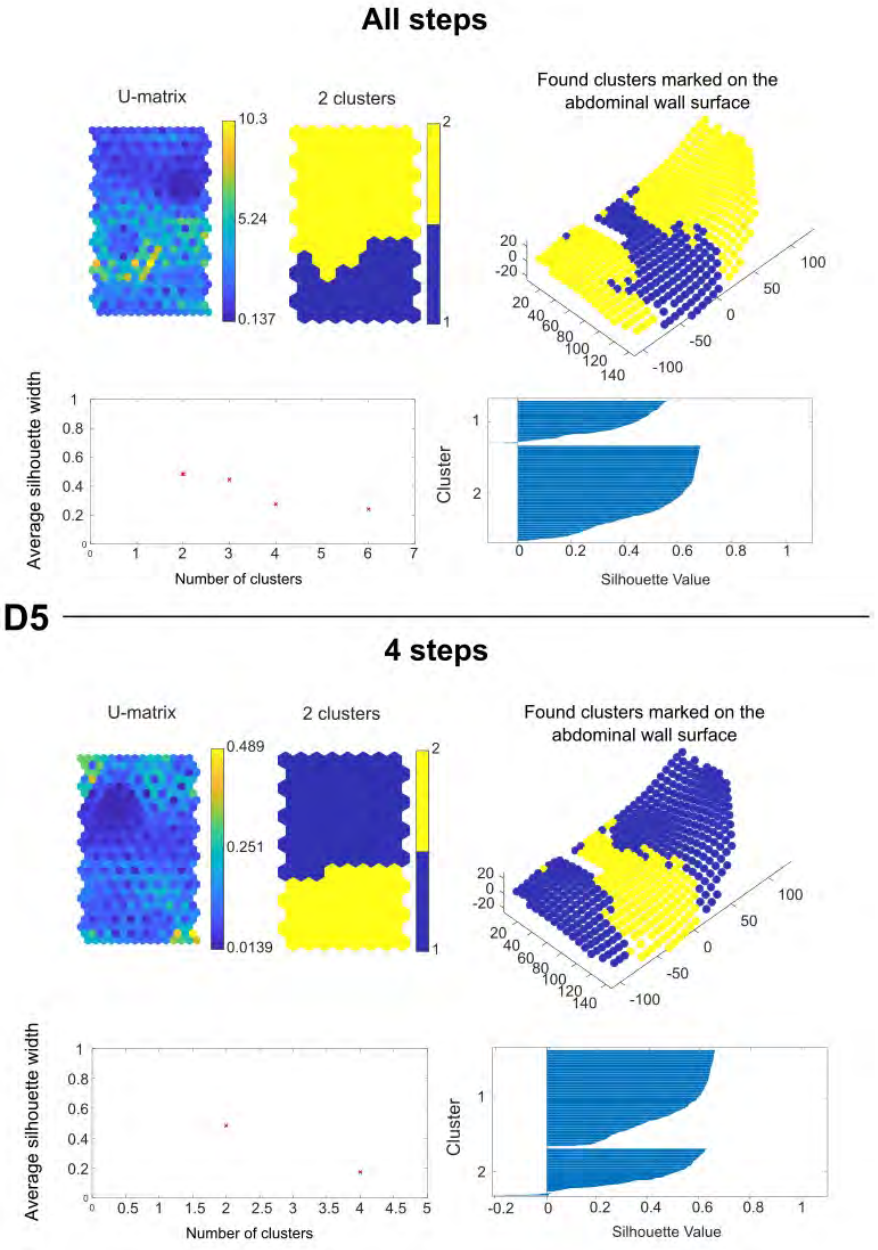

Figure 5.13: Results of D5 subject, analysis of ε_1 variable, for all steps and with cluster score = 0.48. Analysis for 4 steps with cluster score = 0.48. Both analyses resulted in 2 separate clusters.

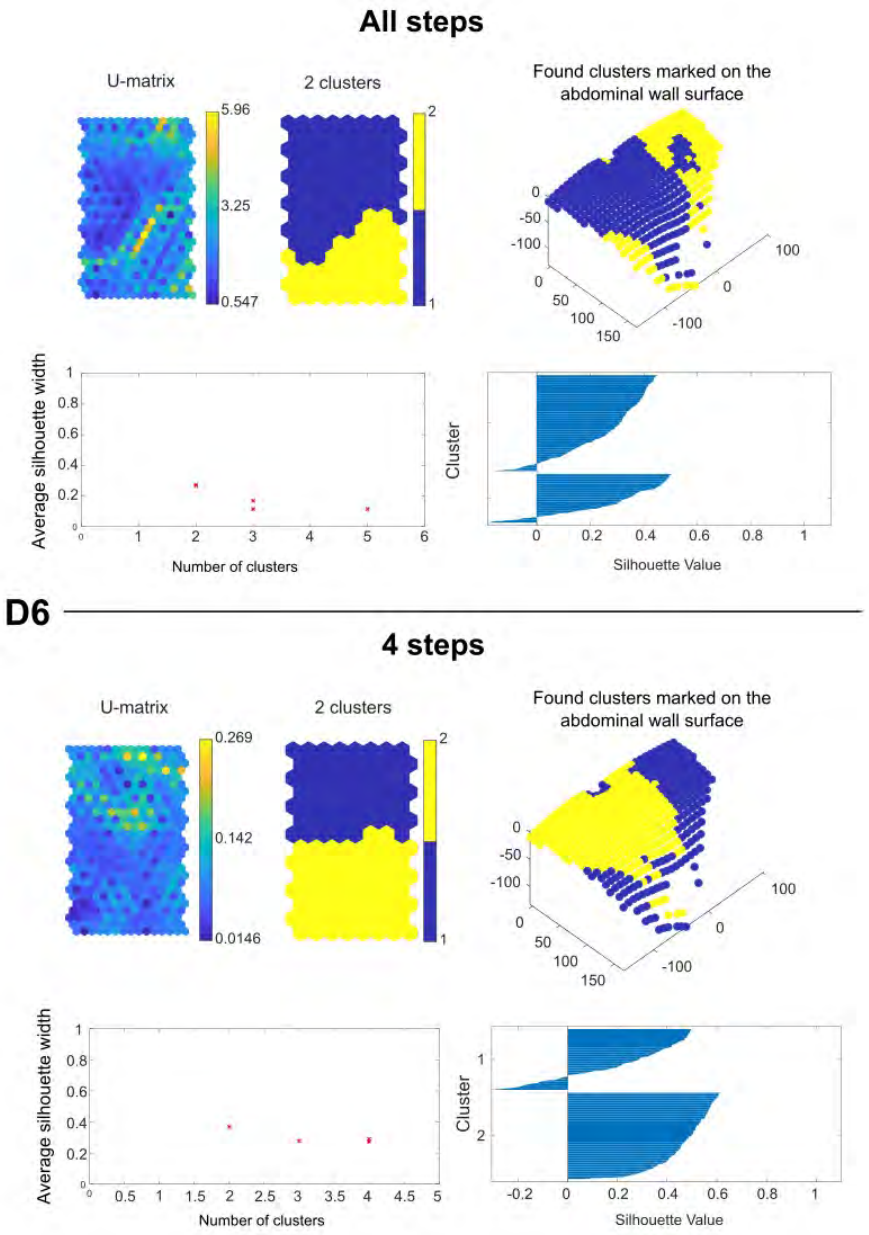

Figure 5.14: Results of D6 subject, analysis of ε_1 variable, for all steps and with cluster score = 0.27. Analysis for 4 steps with cluster score = 0.37. Both analyses resulted in 2 separate clusters.

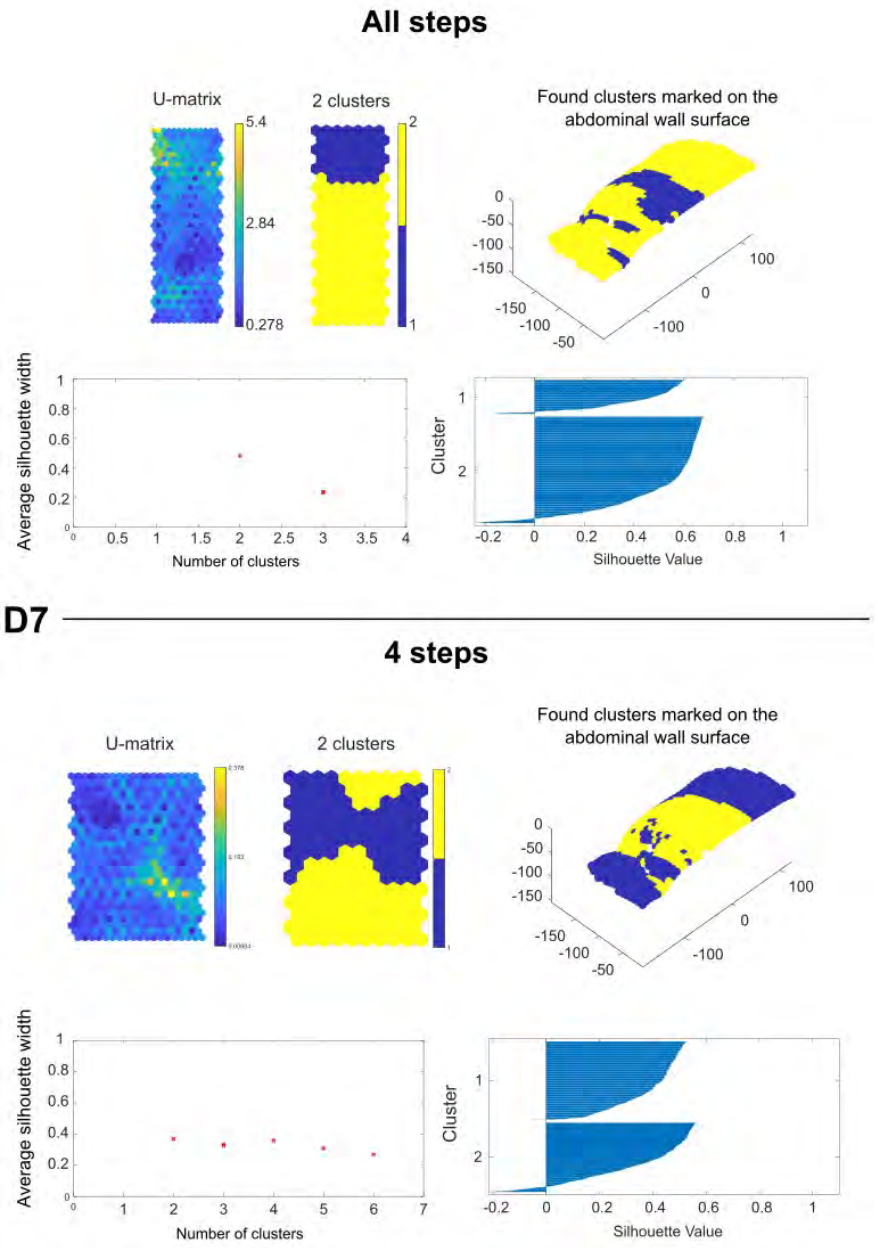

Figure 5.15: Results of D7 subject, analysis of ε_1 variable, for all steps and with cluster score = 0.48. Analysis for 4 steps with cluster score = 0.37. Both analyses resulted in 2 separate clusters.

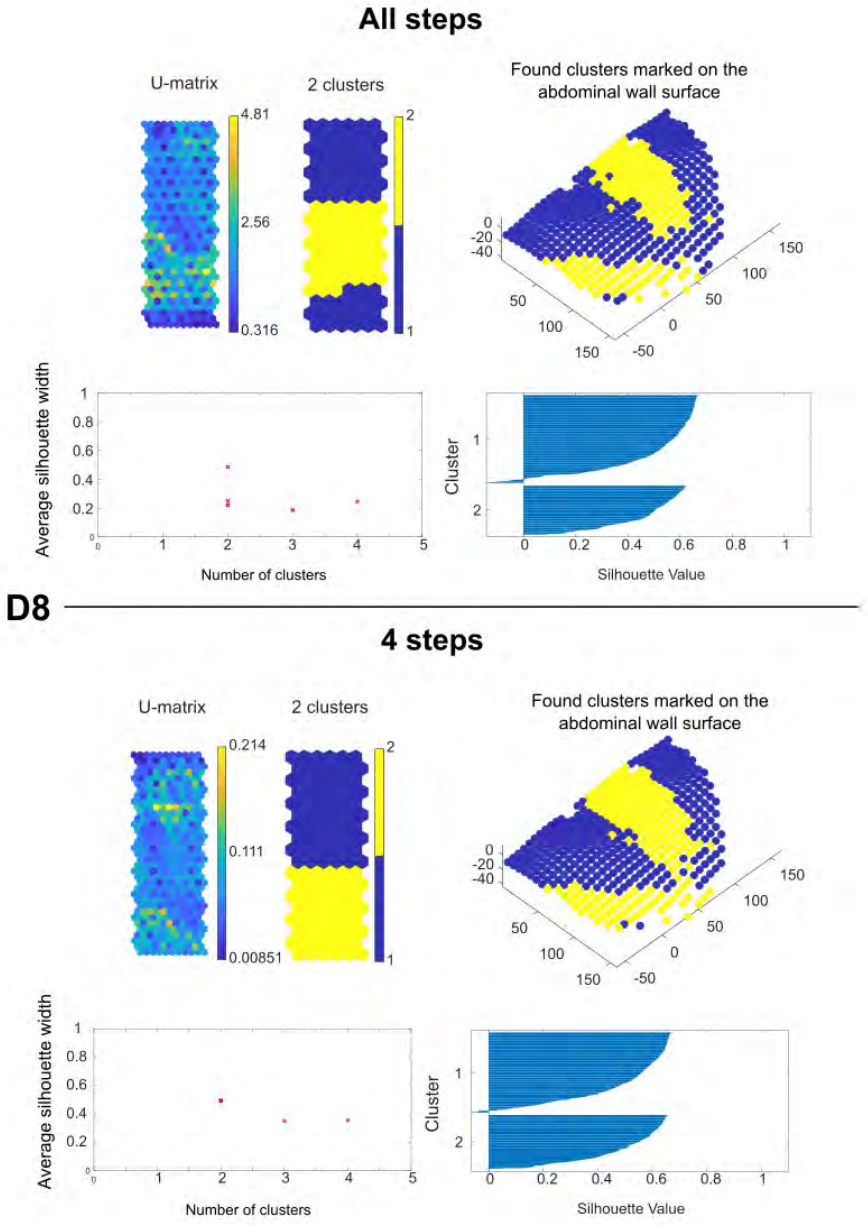

Figure 5.16: Results of D8 subject, analysis of ε_1 variable, for all steps and with cluster score = 0.49. Analysis for 4 steps with cluster score = 0.49. Both analyses resulted in 2 separate clusters.

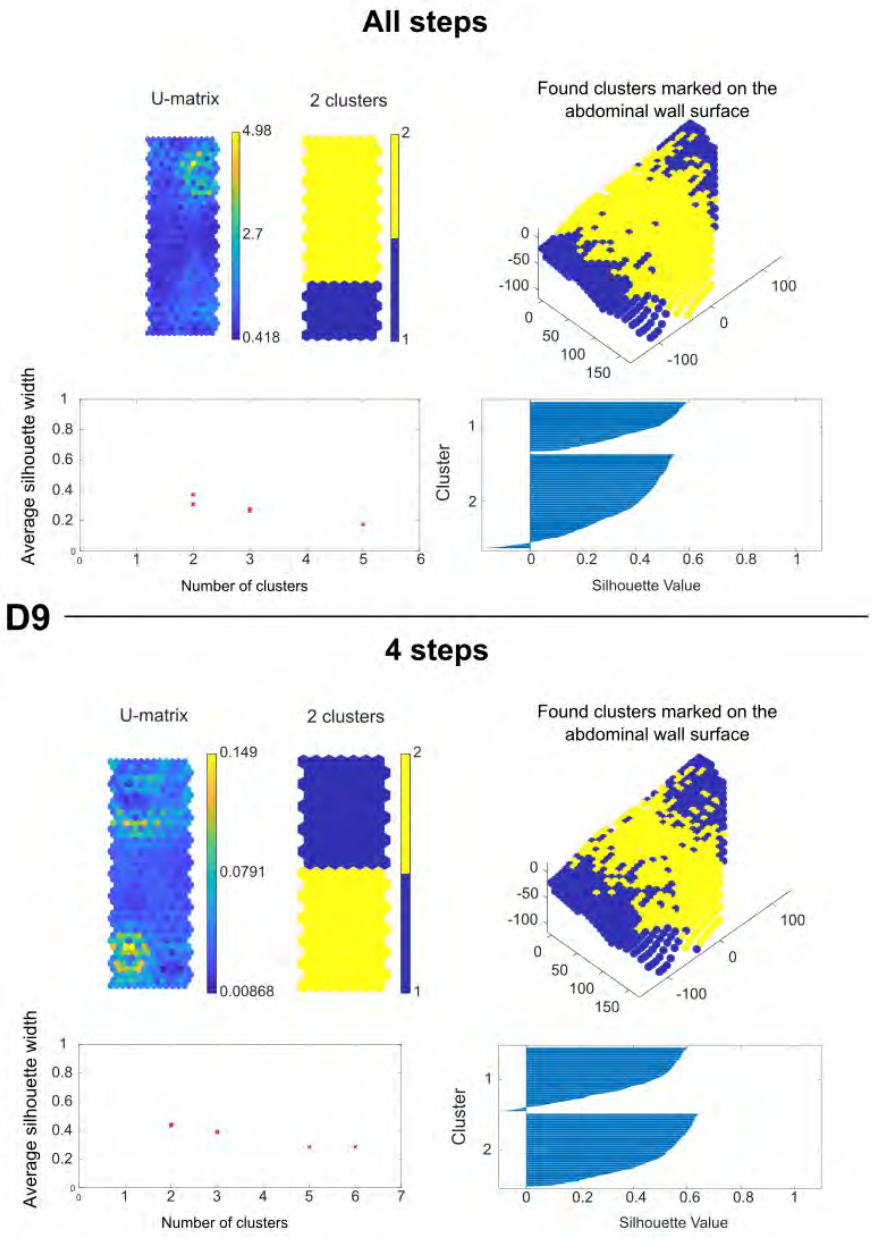

Figure 5.17: Results of D9 subject, analysis of ε_1 variable, for all steps and with cluster score = 0.37. Analysis for 4 steps with cluster score = 0.44. Both analyses resulted in 2 separate clusters.

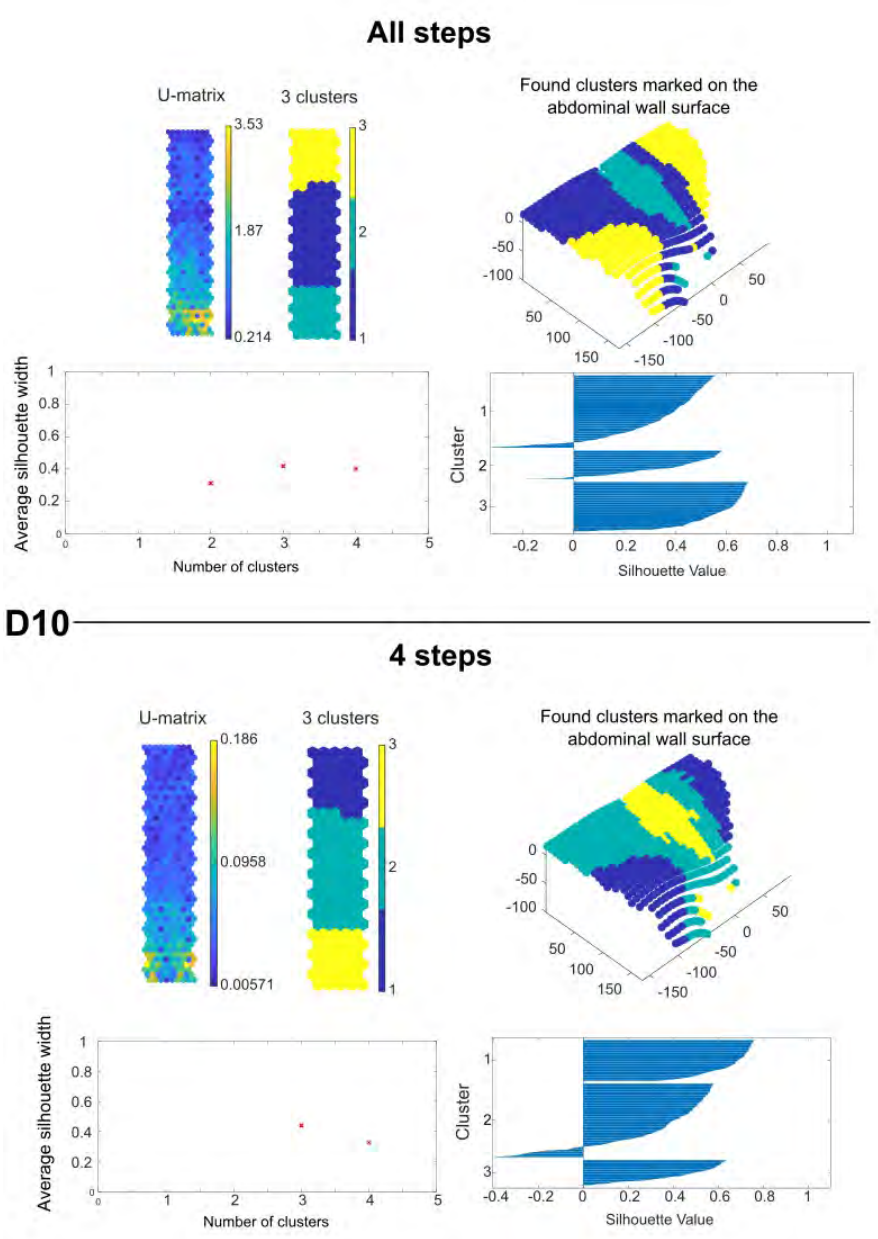

Figure 5.18: Results of D10 subject, analysis of ε_1 variable, for all steps and with cluster score = 0.42. Analysis for 4 steps with cluster score = 0.44. Both 3 clusters.

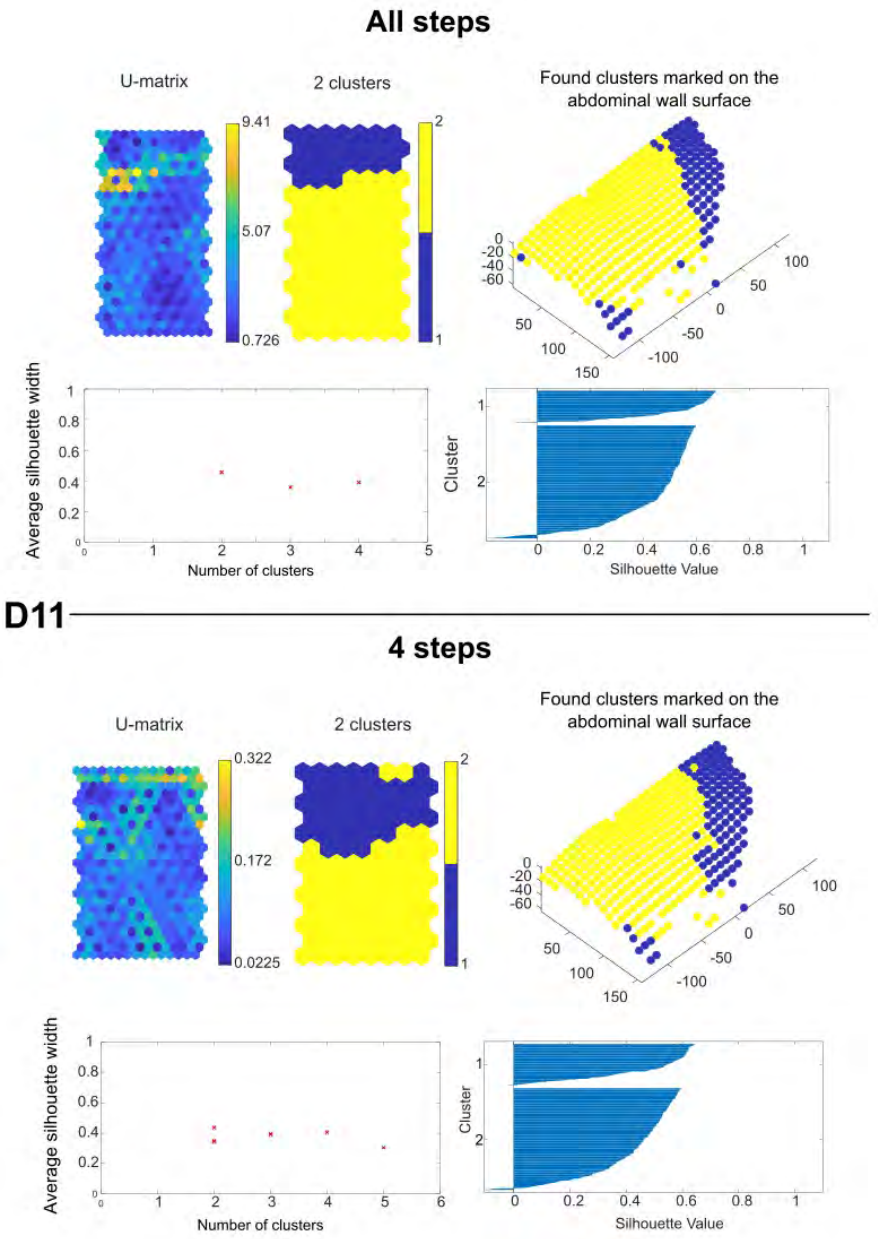

Figure 5.19: Results of D11 subject, analysis of ε_1 variable, for all steps and with cluster score = 0.46. Analysis for 4 steps with cluster score = 0.44. Both analyses resulted in 2 separate clusters.

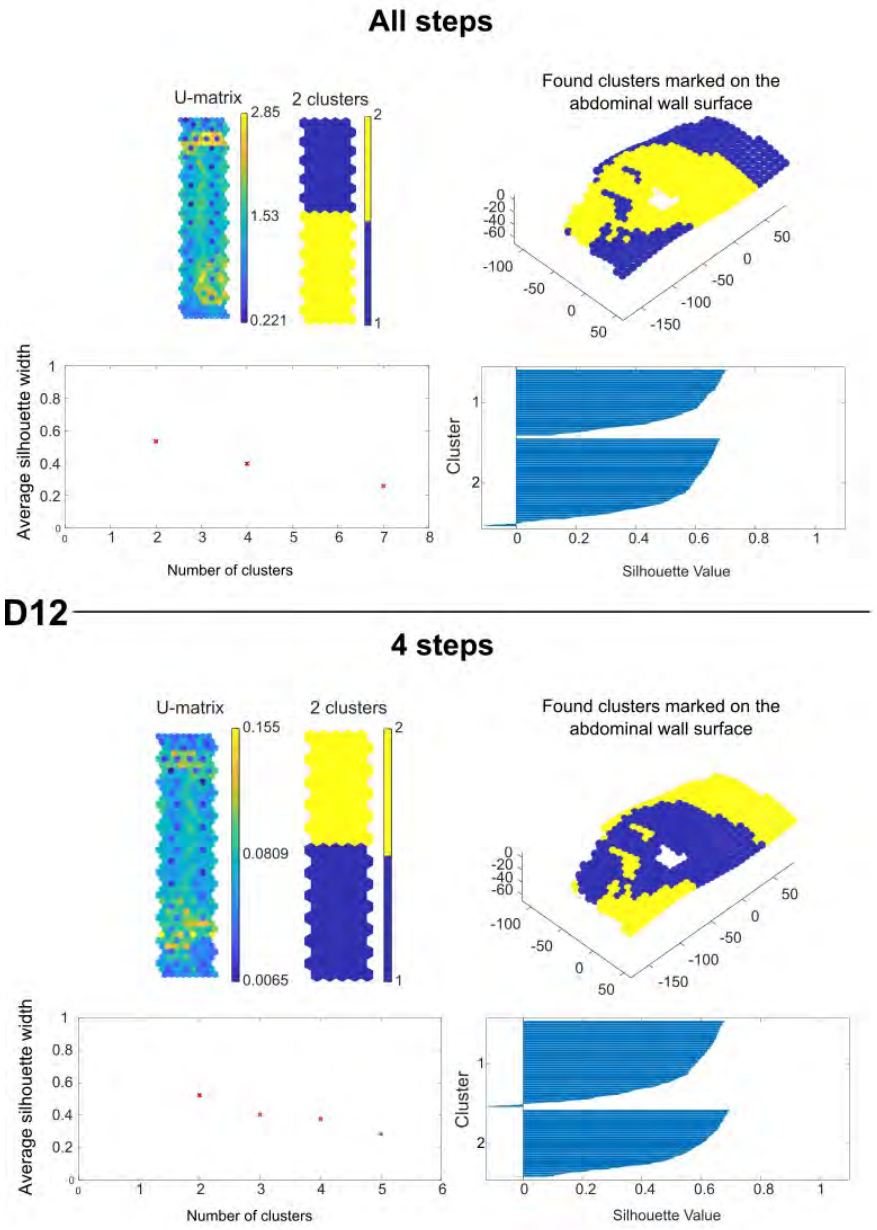

Figure 5.20: Results of D12 subject, analysis of ε_1 variable, for all steps and with cluster score = 0.53. Analysis for 4 steps with cluster score = 0.52. Both analyses resulted in 2 separate clusters.

Generally, the better silhouette scores when analysing 4 steps were obtained, taking into account strains ε_1 as variables. The distribution of clusters on the surface of the abdomen did not change much either. What is more, for subject D2 for all steps analysis 3 clusters were identified and the silhouette score was 0.28, whereas for 4 steps analysis it was higher at 0.42. For other subjects the differences were not that apparent. Then although, an outlier was found in subject D7, where all steps analysis resulted in the silhouette score of 0.48 and 4 steps analysis score of 0.37, the general outcome was clear. Meaning 4 steps analysis resulted in overall better silhouette scores.

Considering the above, it was concluded that using the data from 4 time steps as representative variables of the whole process of deformation during experiment is justified. Nevertheless, an analysis of all steps is important as well to verify any disruption in the data therefore potential pathologies in the behaviour of the abdomen under load. Thus, in the following analyses, meaning no. 3, 4 and 5 only 4 steps were considered as the representative samples to get an overview of how grid points on the abdominal wall with their appropriate strain values can be grouped in regions due to their similar mechanical performance.

5.2.3 Analysis no.3, 4 time steps ε_1 and α variables

In this section the results of SOM analysis applied to principal strain (ε_1) and its direction (α) variables in 4 time steps, thus making it a 8 variable dataset, for each subject are presented in Figs 5.21–5.42 and discussed below.

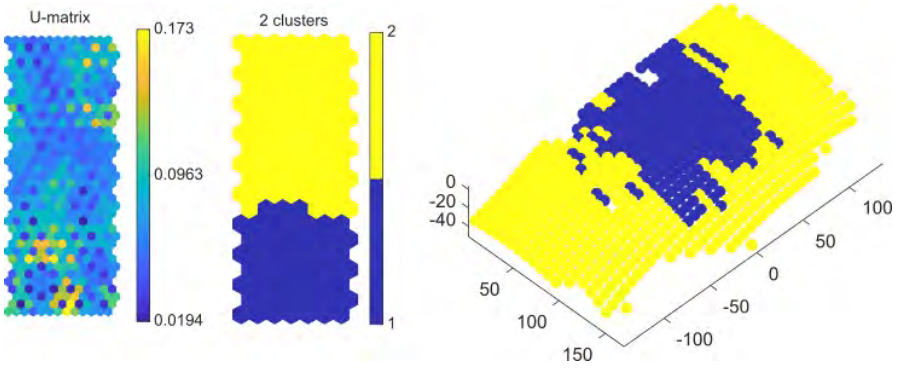

Figure 5.21: Results of D1 subject, analysis for 4 steps, ε_1 and α variables. Respectively from the left: a U-matrix map, a clusters map and the abdominal wall surface of the patient with marked clusters.

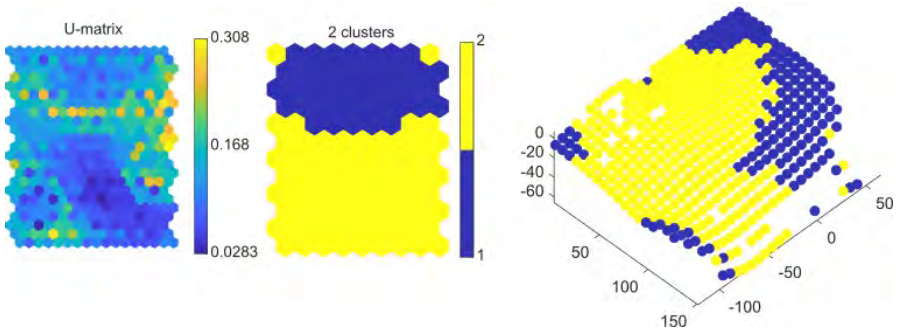

Figure 5.22: Results of D2 subject, analysis for 4 steps, ε_1 and α variables. Respectively from the left: a U-matrix map, a clusters map and the abdominal wall surface of the patient with marked clusters.

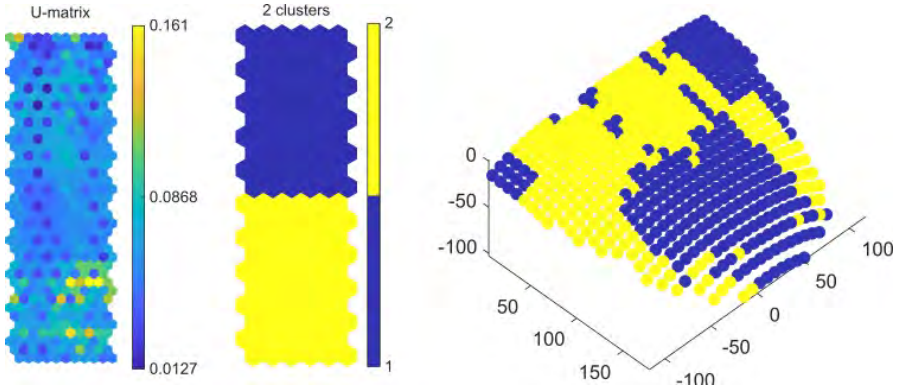

Figure 5.23: Results of D3 subject, analysis for 4 steps, ε_1 and α variables. Respectively from the left: a U-matrix map, a clusters map and the abdominal wall surface of the patient with marked clusters.

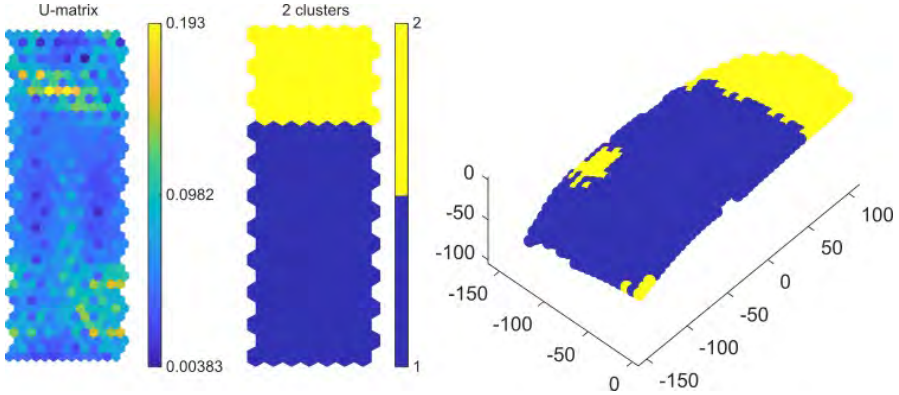

Figure 5.24: Results of D4 subject, analysis for 4 steps, ε_1 and α variables. Respectively from the left: a U-matrix map, a clusters map and the abdominal wall surface of the patient with marked clusters.

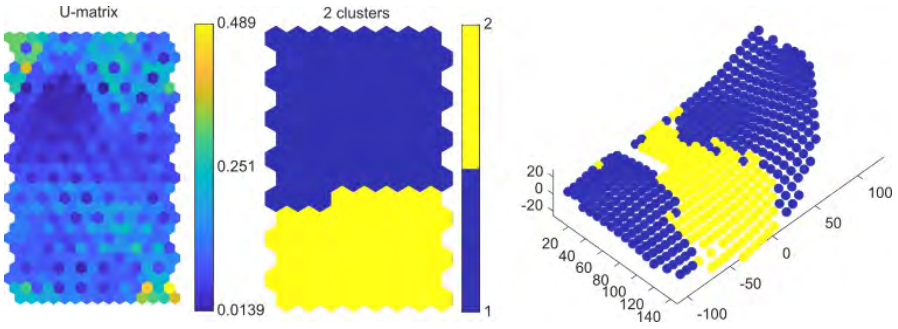

Figure 5.25: Results of D5 subject, analysis for 4 steps, ε_1 and α variables. Respectively from the left: a U-matrix map, a clusters map and the abdominal wall surface of the patient with marked clusters.

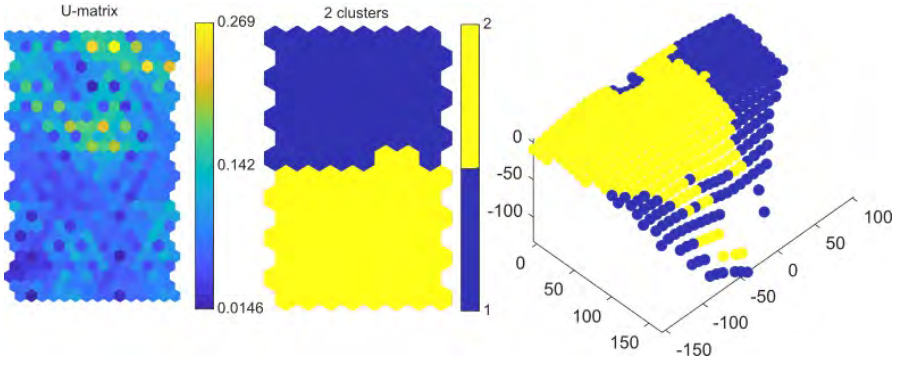

Figure 5.26: Results of D6 subject, analysis for 4 steps, ε_1 and α variables. Respectively from the left: a U-matrix map, a clusters map and the abdominal wall surface of the patient with marked clusters.

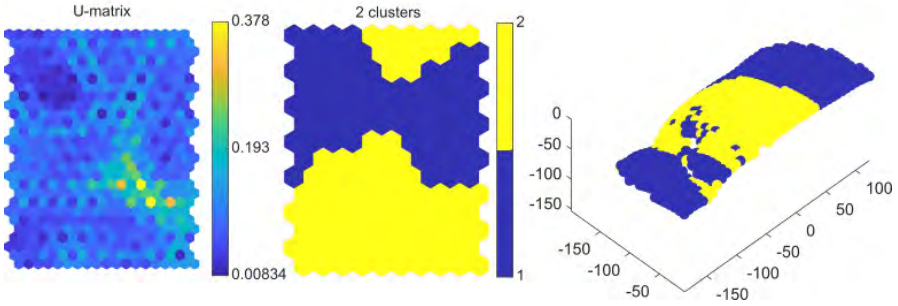

Figure 5.27: Results of D7 subject, analysis for 4 steps, ε_1 and α variables. Respectively from the left: a U-matrix map, a clusters map and the abdominal wall surface of the patient with marked clusters.

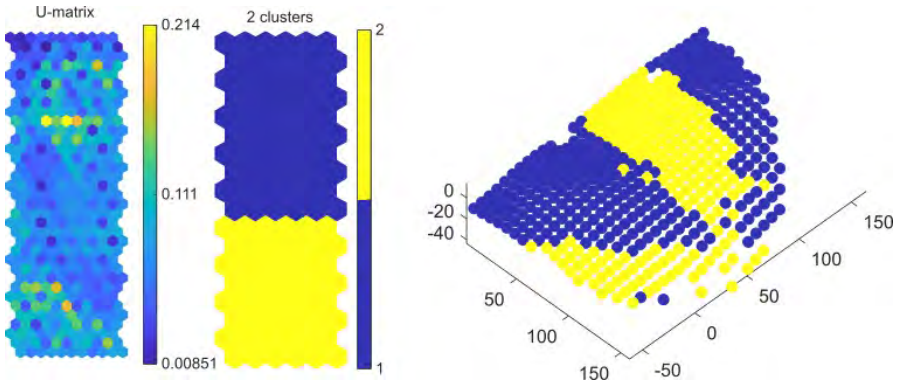

Figure 5.28: Results of D8 subject, analysis for 4 steps, ε_1 and α variables. Respectively from the left: a U-matrix map, a clusters map and the abdominal wall surface of the patient with marked clusters.

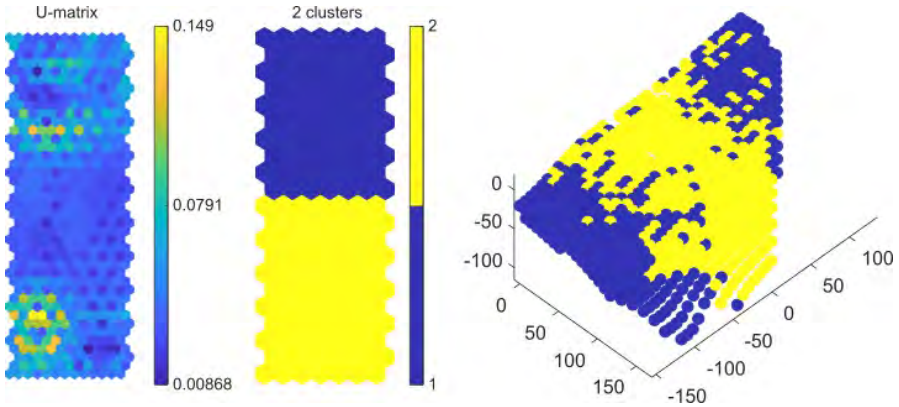

Figure 5.29: Results of D9 subject, analysis for 4 steps, ε_1 and α variables. Respectively from the left: a U-matrix map, a clusters map and the abdominal wall surface of the patient with marked clusters.

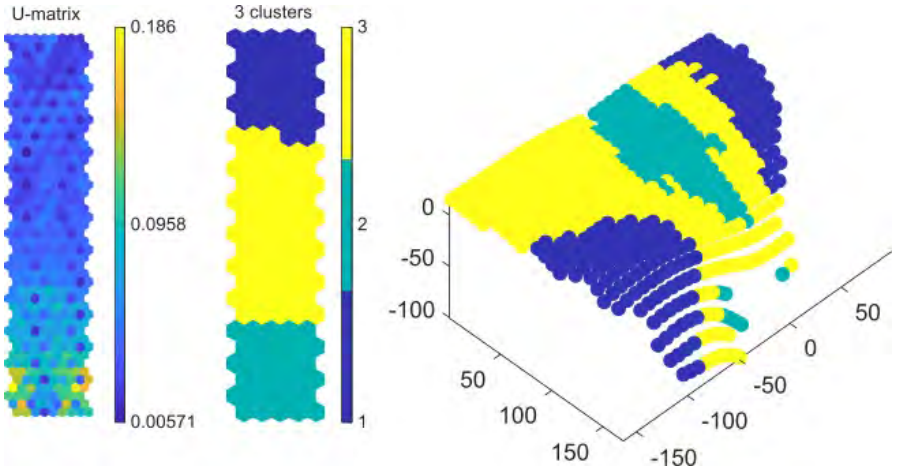

Figure 5.30: Results of D10 subject, analysis for 4 steps, ε_1 and α variables. Respectively from the left: a U-matrix map, a clusters map and the abdominal wall surface of the patient with marked clusters.

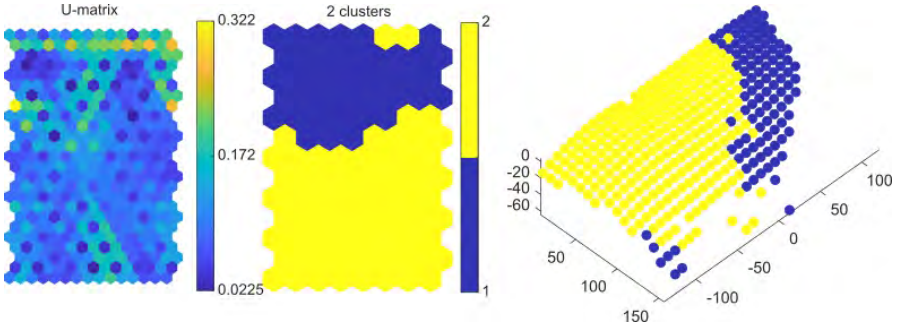

Figure 5.31: Results of D11 subject, analysis for 4 steps, ε_1 and α variables. Respectively from the left: a U-matrix map, a clusters map and the abdominal wall surface of the patient with marked clusters.

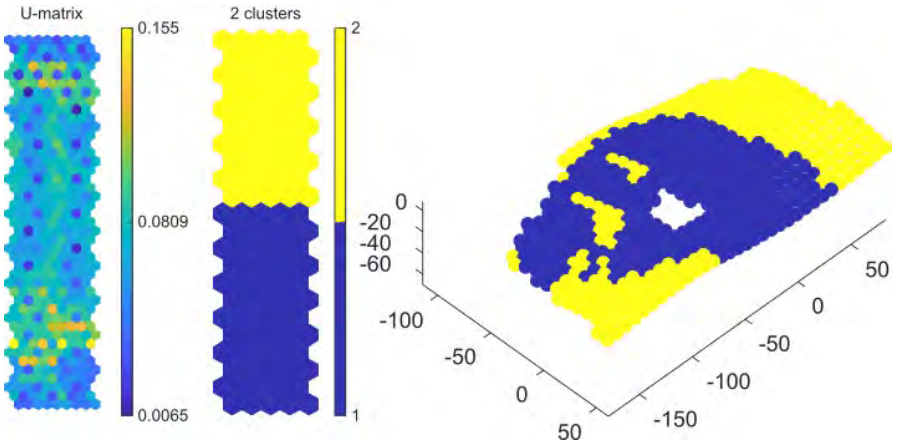

Figure 5.32: Results of D12 subject, analysis for 4 steps, ε_1 and α variables. Respectively from the left: a U-matrix map, a clusters map and the abdominal wall surface of the patient with marked clusters.

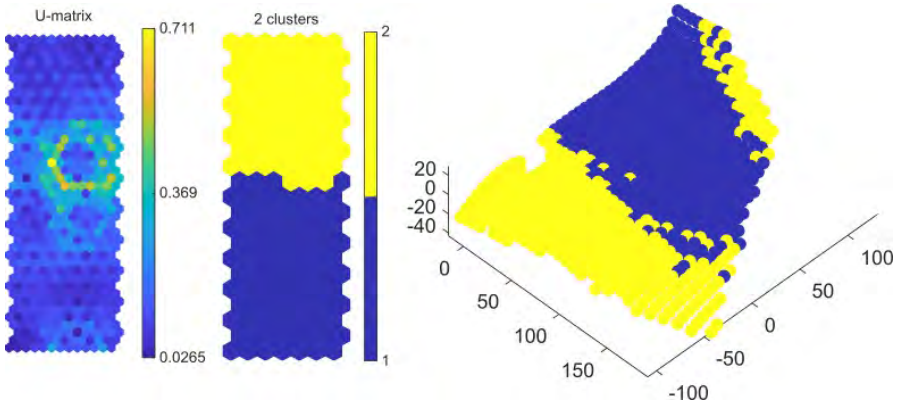

Figure 5.33: Results of D13 subject, analysis for 4 steps, ε_1 and α variables. Respectively from the left: a U-matrix map, a clusters map and the abdominal wall surface of the patient with marked clusters.

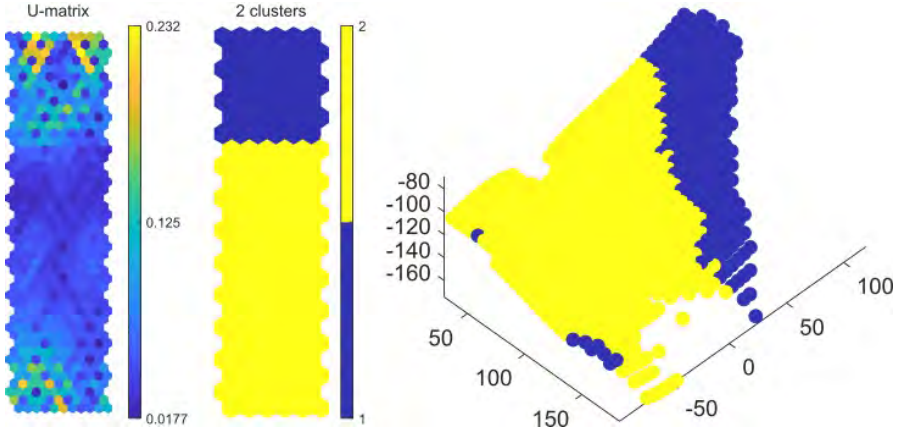

Figure 5.34: Results of D14 subject, analysis for 4 steps, ε_1 and α variables. Respectively from the left: a U-matrix map, a clusters map and the abdominal wall surface of the patient with marked clusters.

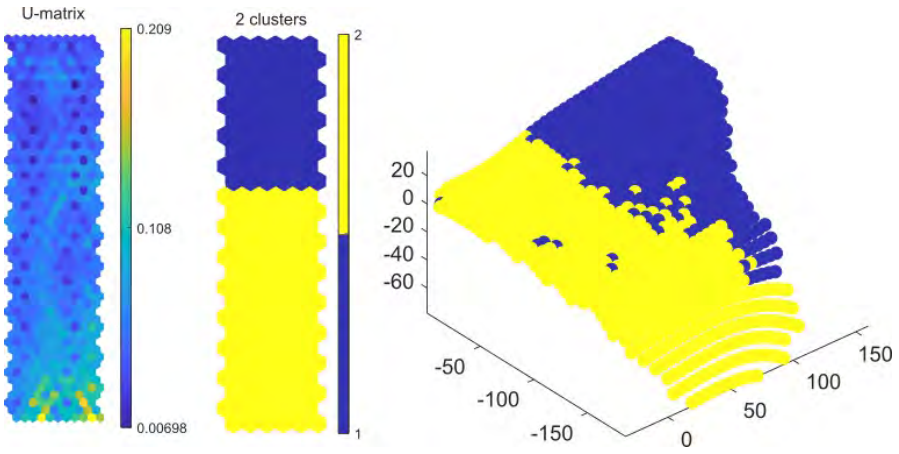

Figure 5.35: Results of D15 subject, analysis for 4 steps, ε_1 and α variables. Respectively from the left: a U-matrix map, a clusters map and the abdominal wall surface of the patient with marked clusters.

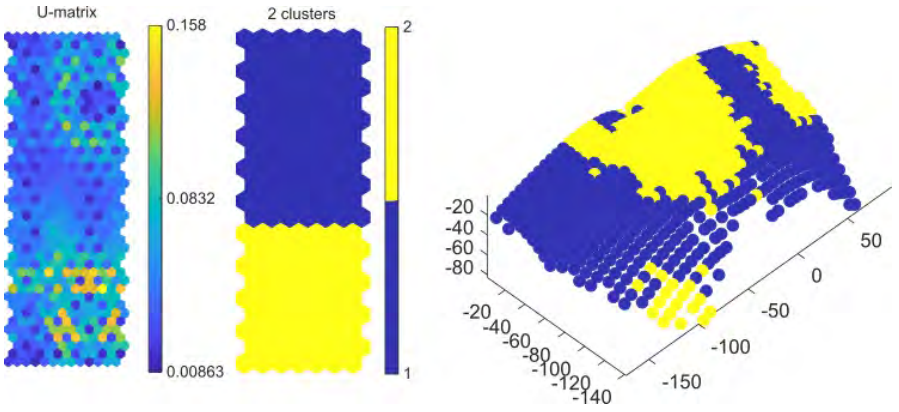

Figure 5.36: Results of D16 subject, analysis for 4 steps, ε_1 and α variables. Respectively from the left: a U-matrix map, a clusters map and the abdominal wall surface of the patient with marked clusters.

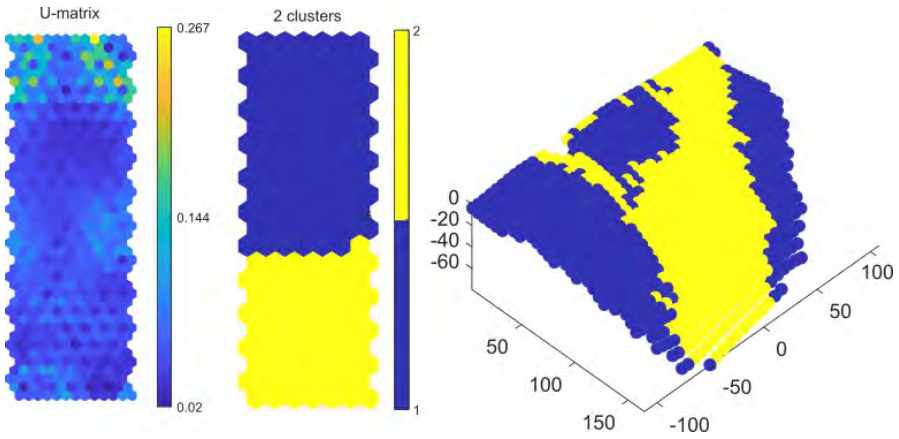

Figure 5.37: Results of D17 subject, analysis for 4 steps, ε_1 and α variables. Respectively from the left: a U-matrix map, a clusters map and the abdominal wall surface of the patient with marked clusters.

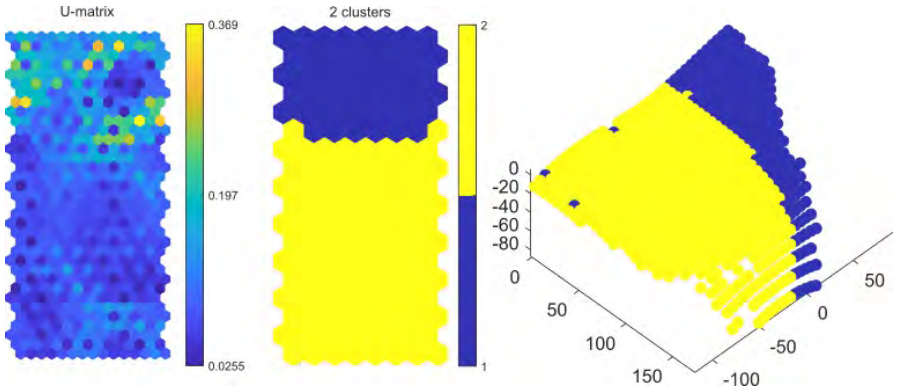

Figure 5.38: Results of D18 subject, analysis for 4 steps, ε_1 and α variables. Respectively from the left: a U-matrix map, a clusters map and the abdominal wall surface of the patient with marked clusters.

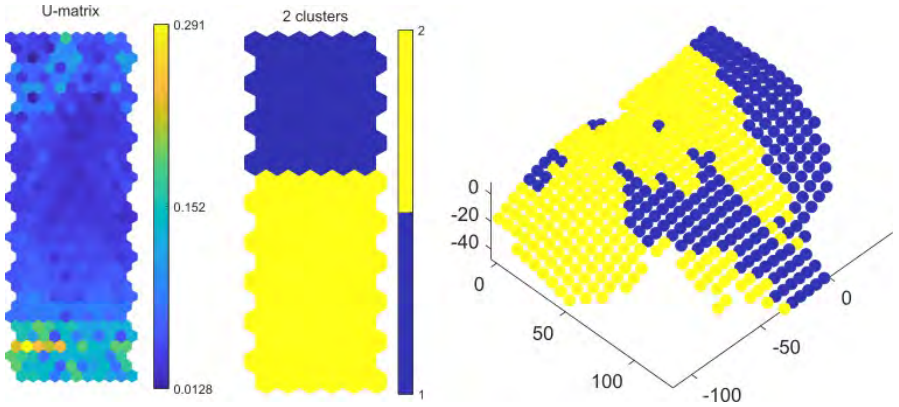

Figure 5.39: Results of D19 subject, analysis for 4 steps, ε_1 and α variables. Respectively from the left: a U-matrix map, a clusters map and the abdominal wall surface of the patient with marked clusters.

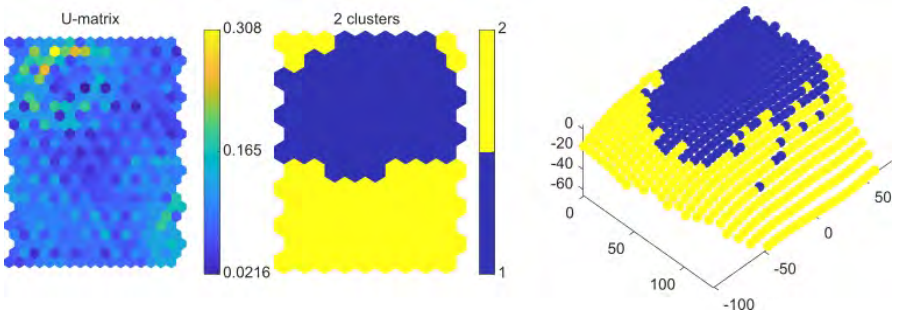

Figure 5.40: Results of D20 subject, analysis for 4 steps, ε_1 and α variables. Respectively from the left: a U-matrix map, a clusters map and the abdominal wall surface of the patient with marked clusters.

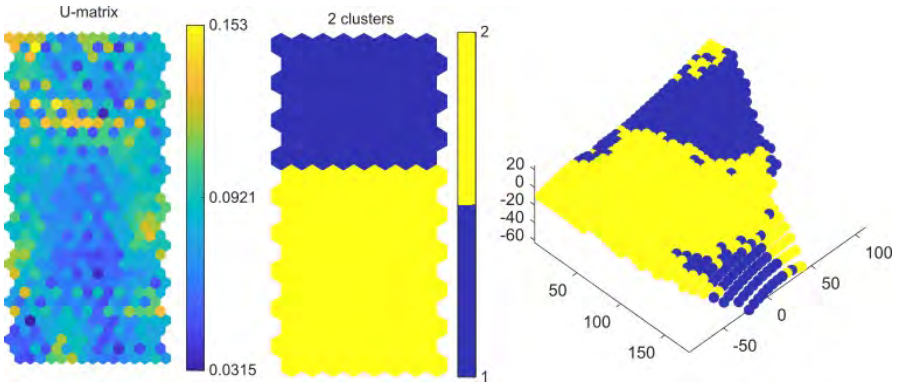

Figure 5.41: Results of D21 subject, analysis for 4 steps, ε_1 and α variables. Respectively from the left: a U-matrix map, a clusters map and the abdominal wall surface of the patient with marked clusters.

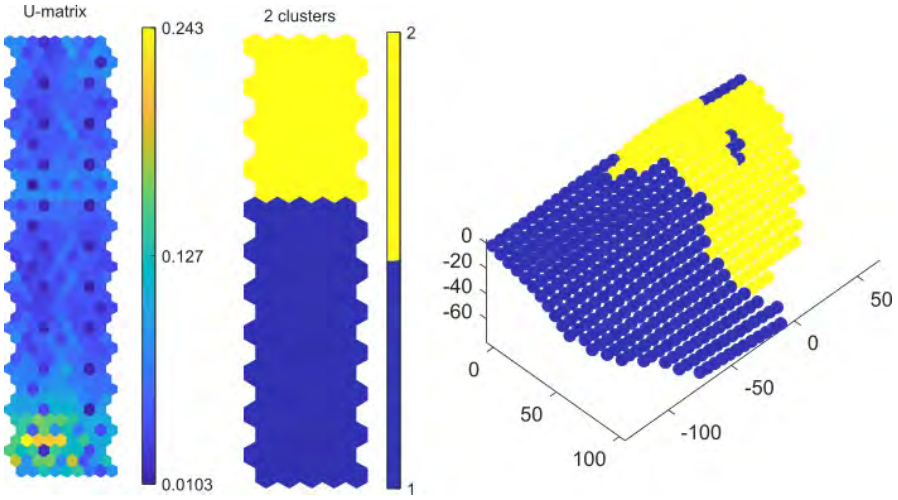

Figure 5.42: Results of D22 subject, analysis for 4 steps, ε_1 and α variables. Respectively from the left: a U-matrix map, a clusters map and the abdominal wall surface of the patient with marked clusters.

Apart from patient D10, every analysis resulted in groupings of just two separate clusters. The majority of clusters division schemes can be classified into a group described as *Divided clusters by mediolateral axis with separation by anatomical features* in Table 5.6. There we have subjects markes as D2, D3, D8, D9, D11, D14, D15, D18, D19 and D21. Another big group is clusters formed by encompassing the navel with D1, D10, D12, D16, D17 and D20. Both of which may suggest that such a division into two areas behaving similarly is a good first refinement into the research of dividing the abdomen into zones of different mechanical behaviour. Potentially, mechanically different implants can be assigned to these zones in planning hernia repair surgeries.

5.2.4 Analysis no.4, 4 time steps ε_1, ε_2 and α variables

In this section results of SOM analysis of the three variables, principal strains ε_1, ε_2, and α in 4 time steps, thus making it a 12 variable dataset, for each subject are presented and discussed.

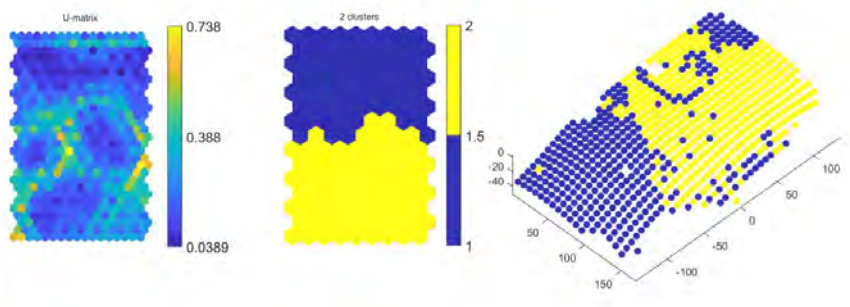

Figure 5.43: Results of D1 subject, analysis for 4 steps, ε_1, ε_2 and α variables. Respectively from the left: a U-matrix map, a clusters map and the abdominal wall surface of the patient with marked clusters.

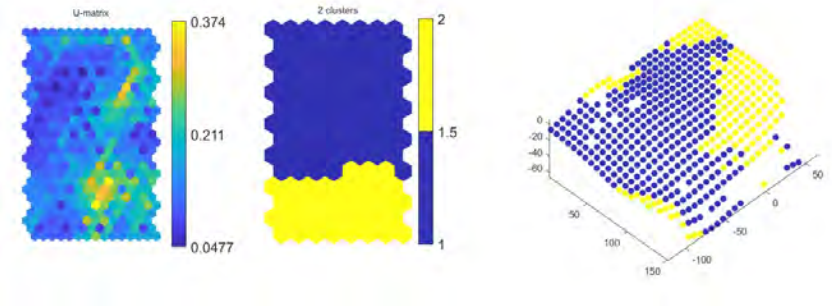

Figure 5.44: Results of D2 subject, analysis for 4 steps, ε_1, ε_2 and α variables. Respectively from the left: a U-matrix map, a clusters map and the abdominal wall surface of the patient with marked clusters.

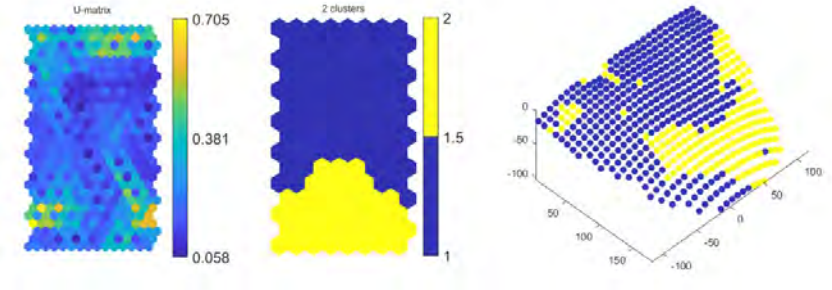

Figure 5.45: Results of D3 subject, analysis for 4 steps, ε_1, ε_2 and α variables. Respectively from the left: a U-matrix map, a clusters map and the abdominal wall surface of the patient with marked clusters.

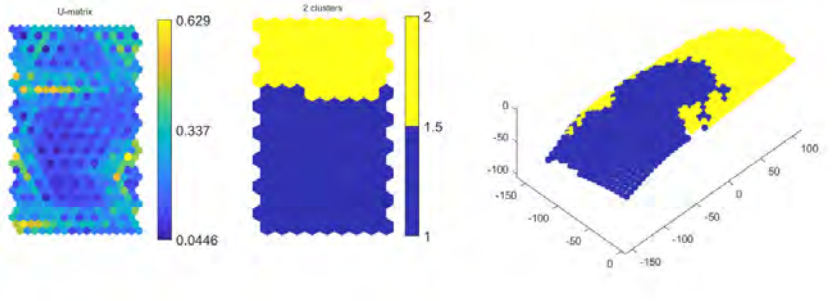

Figure 5.46: Results of D4 subject, analysis for 4 steps, ε_1, ε_2 and α variables. Respectively from the left: a U-matrix map, a clusters map and the abdominal wall surface of the patient with marked clusters.

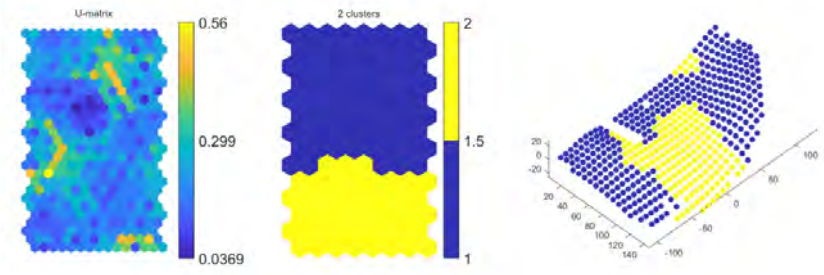

Figure 5.47: Results of D5 subject, analysis for 4 steps, ε_1, ε_2 and α variables. Respectively from the left: a U-matrix map, a clusters map and the abdominal wall surface of the patient with marked clusters.

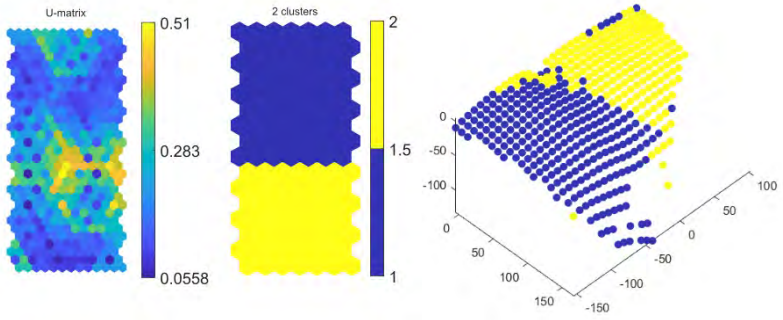

Figure 5.48: Results of D6 subject, analysis for 4 steps, ε_1, ε_2 and α variables. Respectively from the left: a U-matrix map, a clusters map and the abdominal wall surface of the patient with marked clusters.

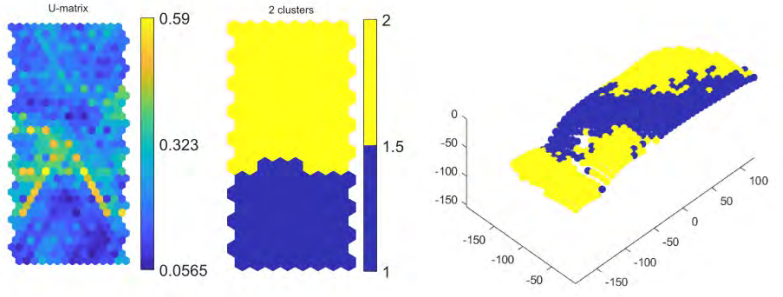

Figure 5.49: Results of D7 subject, analysis for 4 steps, ε_1, ε_2 and α variables. Respectively from the left: a U-matrix map, a clusters map and the abdominal wall surface of the patient with marked clusters.

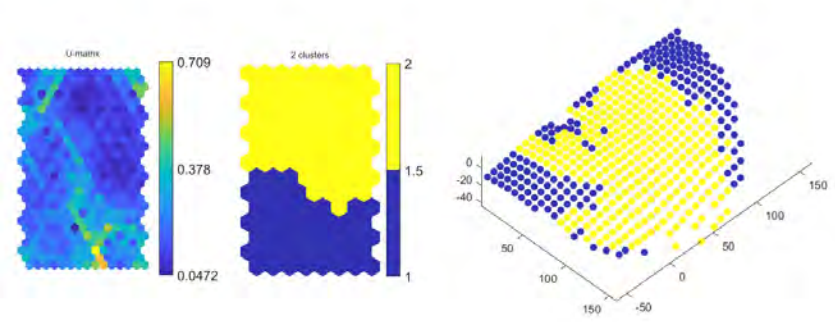

Figure 5.50: Results of D8 subject, analysis for 4 steps, ε_1, ε_2 and α variables. Respectively from the left: a U-matrix map, a clusters map and the abdominal wall surface of the patient with marked clusters.

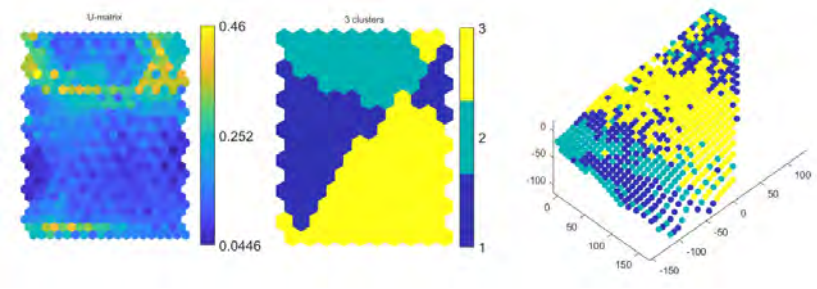

Figure 5.51: Results of D9 subject, analysis for 4 steps, ε_1, ε_2 and α variables. Respectively from the left: a U-matrix map, a clusters map and the abdominal wall surface of the patient with marked clusters.

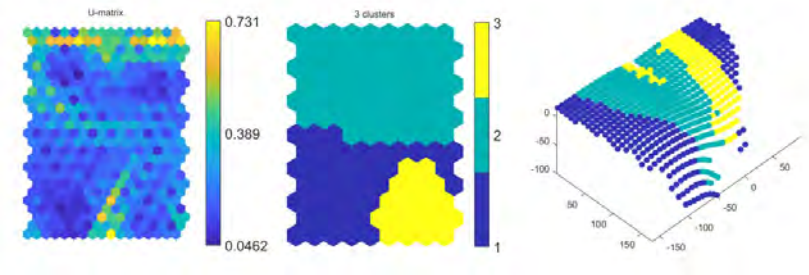

Figure 5.52: Results of D10 subject, analysis for 4 steps, ε_1, ε_2 and α variables. Respectively from the left: a U-matrix map, a clusters map and the abdominal wall surface of the patient with marked clusters.

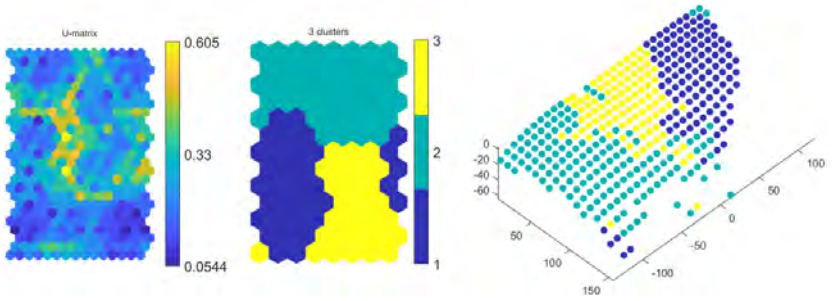

Figure 5.53: Results of D11 subject, analysis for 4 steps, ε_1, ε_2 and α variables. Respectively from the left: a U-matrix map, a clusters map and the abdominal wall surface of the patient with marked clusters.

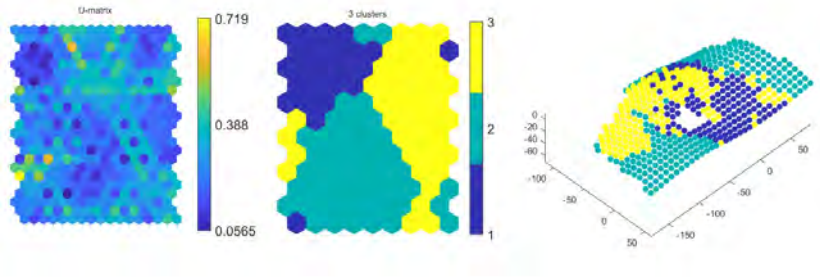

Figure 5.54: Results of D12 subject, analysis for 4 steps, ε_1, ε_2 and α variables. Respectively from the left: a U-matrix map, a clusters map and the abdominal wall surface of the patient with marked clusters.

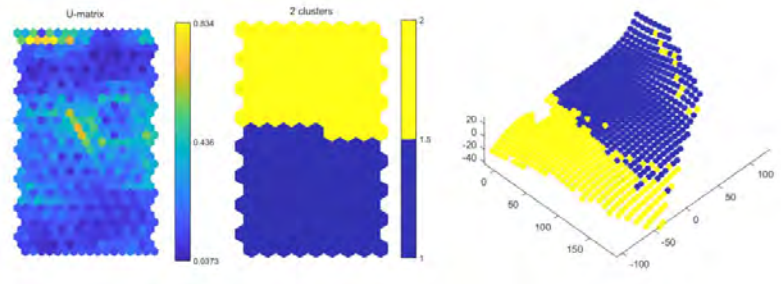

Figure 5.55: Results of D13 subject, analysis for 4 steps, ε_1, ε_2 and α variables. Respectively from the left: a U-matrix map, a clusters map and the abdominal wall surface of the patient with marked clusters.

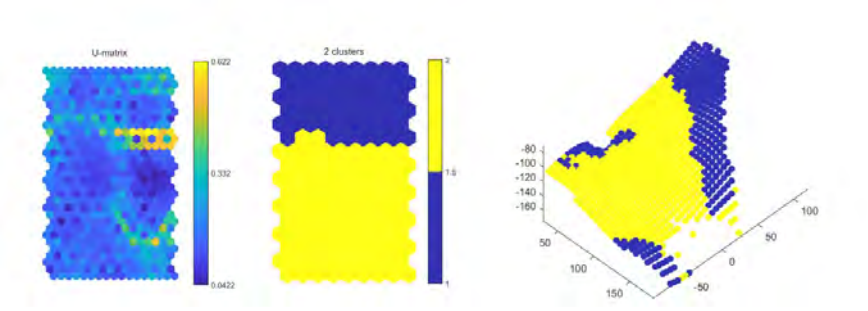

Figure 5.56: Results of D14 subject, analysis for 4 steps, ε_1, ε_2 and α variables. Respectively from the left: a U-matrix map, a clusters map and the abdominal wall surface of the patient with marked clusters.

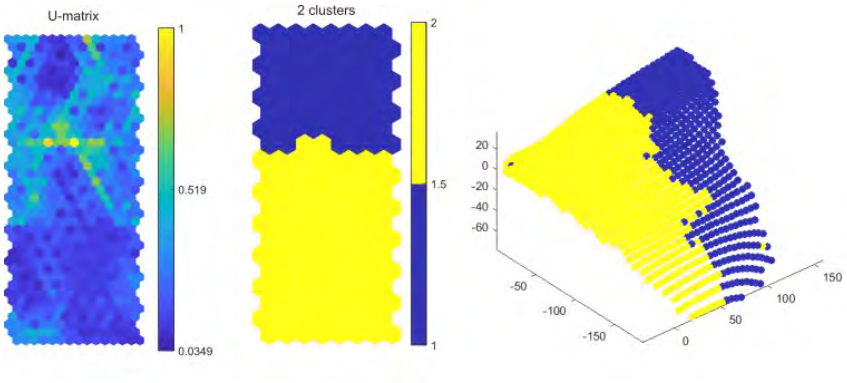

Figure 5.57: Results of D15 subject, analysis for 4 steps, ε_1, ε_2 and α variables. Respectively from the left: a U-matrix map, a clusters map and the abdominal wall surface of the patient with marked clusters.

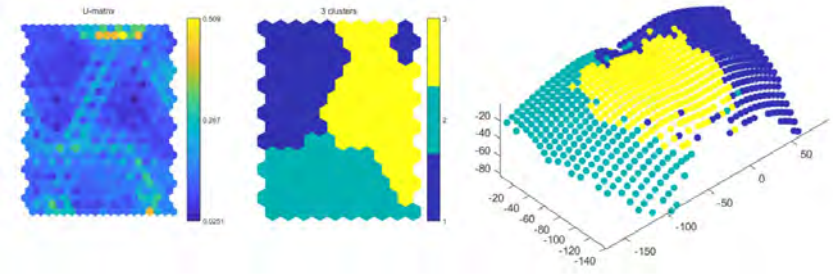

Figure 5.58: Results of D16 subject, analysis for 4 steps, ε_1, ε_2 and α variables. Respectively from the left: a U-matrix map, a clusters map and the abdominal wall surface of the patient with marked clusters.

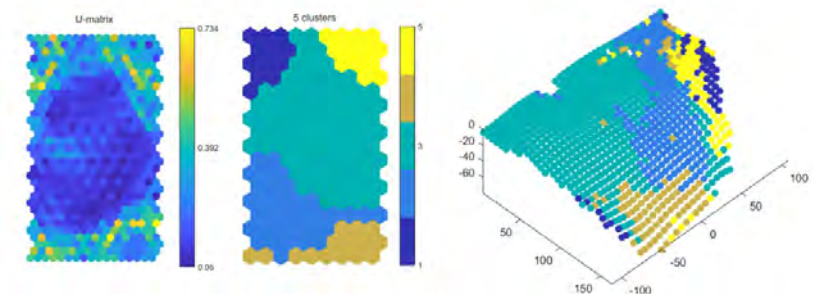

Figure 5.59: Results of D17 subject, analysis for 4 steps, ε_1, ε_2 and α variables. Respectively from the left: a U-matrix map, a clusters map and the abdominal wall surface of the patient with marked clusters.

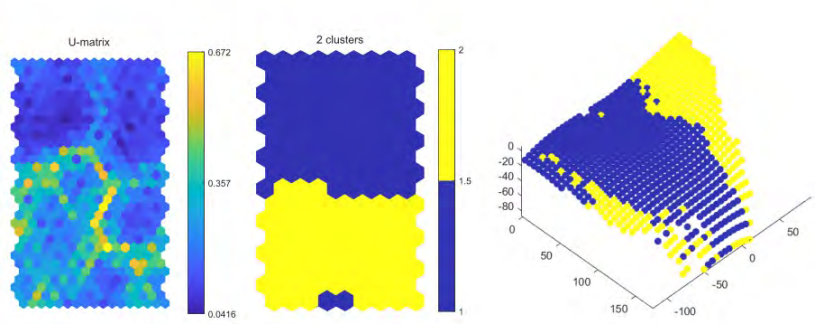

Figure 5.60: Results of D18 subject, analysis for 4 steps, ε_1, ε_2 and α variables. Respectively from the left: a U-matrix map, a clusters map and the abdominal wall surface of the patient with marked clusters.

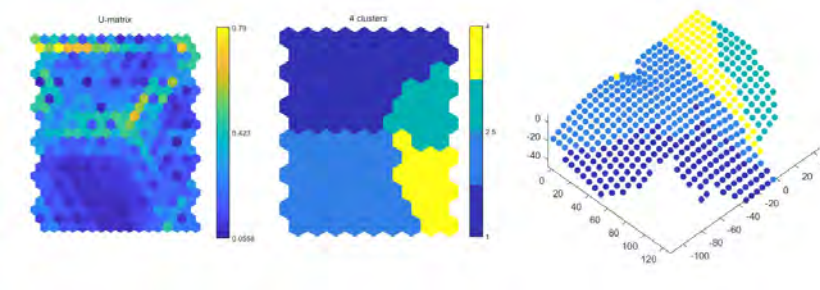

Figure 5.61: Results of D19 subject, analysis for 4 steps, ε_1, ε_2 and α variables. Respectively from the left: a U-matrix map, a clusters map and the abdominal wall surface of the patient with marked clusters.

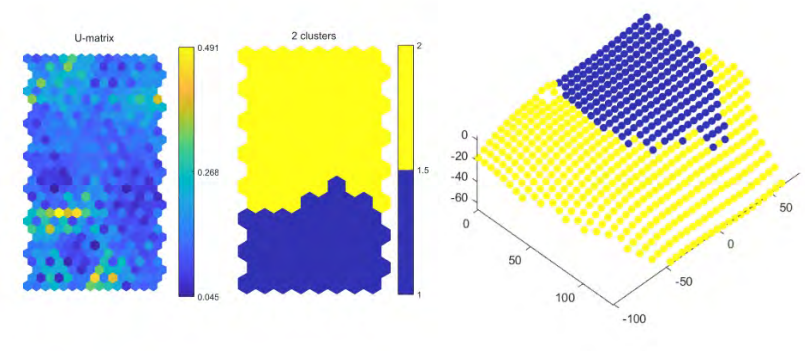

Figure 5.62: Results of D20 subject, analysis for 4 steps, ε_1, ε_2 and α variables. Respectively from the left: a U-matrix map, a clusters map and the abdominal wall surface of the patient with marked clusters.

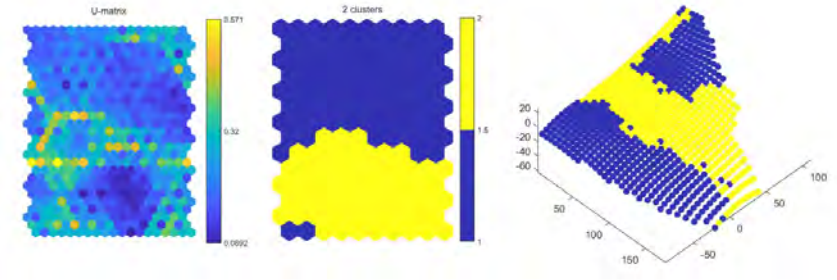

Figure 5.63: Results of D21 subject, analysis for 4 steps, ε_1, ε_2 and α variables. Respectively from the left: a U-matrix map, a clusters map and the abdominal wall surface of the patient with marked clusters.

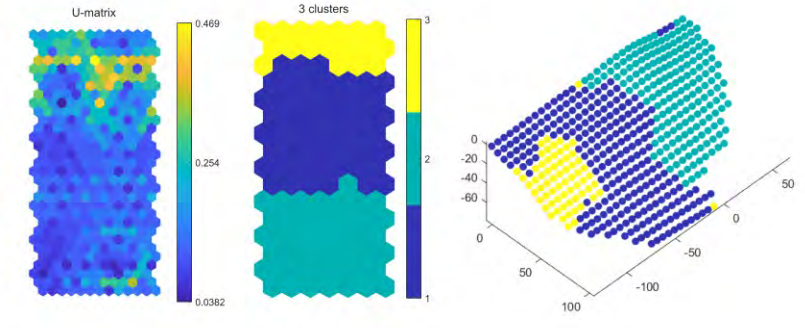

Figure 5.64: Results of D22 subject, analysis for 4 steps, ε_1, ε_2 and α variables. Respectively from the left: a U-matrix map, a clusters map and the abdominal wall surface of the patient with marked clusters.

Introducing additional variable (ε_2) resulted in more diverse display of bright borders between clusters on U-matrix maps than in previous analysis. Which in turn caused more subjects to have their abdomens divided into 3 clusters. It was observed in subjects D9–D12 (Figs 5.51–5.54) and D16 (Fig. 5.58), D17 (Fig. 5.59), D19 (Fig. 5.61), D22 (Fig. 5.64). Unfortunately, what manifests, as more diverse often results in worse quality than uniformity of 2 clusters distribution (Table 5.5). In this analysis more subjects were classified to have their clusters encompassing the navel, thus it may suggest that ε_2 influences the behaviour around the linea alba.

5.2.5 Assessment of the quality of the results obtained from SOM analysis

As introduced in Section 3.3, silhouette plots can be used to evaluate the classification of analysed data into clusters. Silhouette scores represent the averaged sum of silhouette values for all data points classified into clusters. However, to determine the best number of clusters for each case the silhouette scores for varying numbers of clusters were plotted.

Cluster score and silhouette widths plots for the analysis of the 4 time steps vs. all the time steps, can be found alongside SOM plots in respective Figs 5.9–5.20. Analysis of the inter-patients organisation of similarity between all patients for one variable, ε_1, with 4 time steps is shown in Fig. 5.73. For both mentioned analyses their quality discussion is presented alongside the results discussion in previous sections.

The averaged silhouette widths are collectively presented in the Table 5.5 below. The plots themselves are shown in respective succeeding Figs (5.67, 5.68, 5.71, 5.72). General outcome is that introducing another variables, namely ε_2, leads to more disruption in the data and therefore lower quality silhouette scores. Here are two exceptions in subjects D6 and D19. The best overall classification into clusters had patients D1–D7 and D10. Among those, the D6 had the best average silhouette score of 0.5.

In the analysis with ε_1 and α as input variables for all the patients (except for D10) the best silhouette scores were obtained when data were classified into just 2 separate clusters (Figure 5.65–5.66).

In the analysis with ε_1, ε_2 and α, 2 clusters were the best for D1–D8 and D13, D17, D18, D20–D21 subjects. In the same analysis, patients D9-D12 patients

D9–D12 and D16, D22 the best grouping was for 3 clusters. An outlier, subject D19, achieved the best silhouette score with 4 clusters. Considering the best number of clusters, the precise silhouette plots are shown for each patients (Figure 5.71).

No	Best no of clusters [ε_1 and α ; ε_1, ε_2 and α]	Averaged silhouette widths [ε_1 and α ; ε_1, ε_2 and α]	Total number of observations
D1	2 ; 2	0.50 ; 0.35	744
D2	2 ; 2	0.35 ; 0.31	492
D3	2 ; 2	0.48 ; 0.38	537
D4	2 ; 2	0.51 ; 0.36	841
D5	2 ; 2	0.48 ; 0.35	493
D6	2 ; 2	0.37 ; 0.47	457
D7	2 ; 2	0.37 ; 0.38	774
D8	2 ; 2	0.52 ; 0.30	477
D9	2 ; 3	0.44 ; 0.23	784
D10	3 ; 3	0.44 ; 0.42	618
D11	2 ; 3	0.44 ; 0.22	366
D12	2 ; 3	0.52 ; 0.34	520
D13	2 ; 2	0.56 ; 0.50	797
D14	2 ; 2	0.42 ; 0.34	836
D15	2 ; 2	0.49 ; 0.47	1012
D16	2 ; 3	0.46 ; 0.34	753
D17	2 ; 2	0.50 ; 0.22	945
D18	2 ; 2	0.53 ; 0.39	833
D19	2 ; 4	0.27 ; 0.42	480
D20	2 ; 2	0.29 ; 0.30	619
D21	2 ; 2	0.43 ; 0.34	798
D22	2 ; 3	0.50 ; 0.37	504

Table 5.5: Averaged silhouette widths with respect to the best number of clusters obtained with SOM for analysis of 4 time steps with two variables (ε_1 and α) and three variables (ε_1, ε_2 and α).

Clusters plots of analysis with 4 time steps ε_1 and α variables

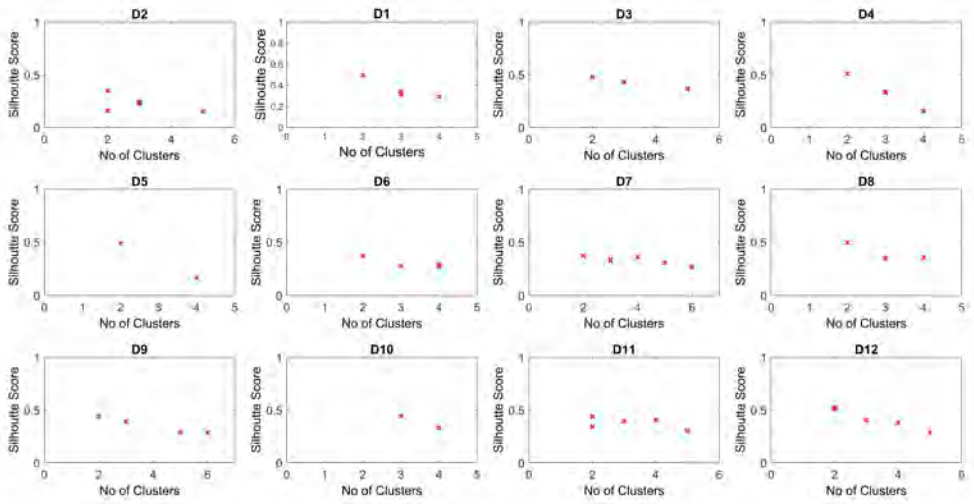

Figure 5.65: Averaged silhouette width for the entire dataset in respect to the number of clusters obtained. Plot for patients datasets D1 to D12 with 4 time steps, ε_1 and α as variables. Detailed results are in Table 5.5.

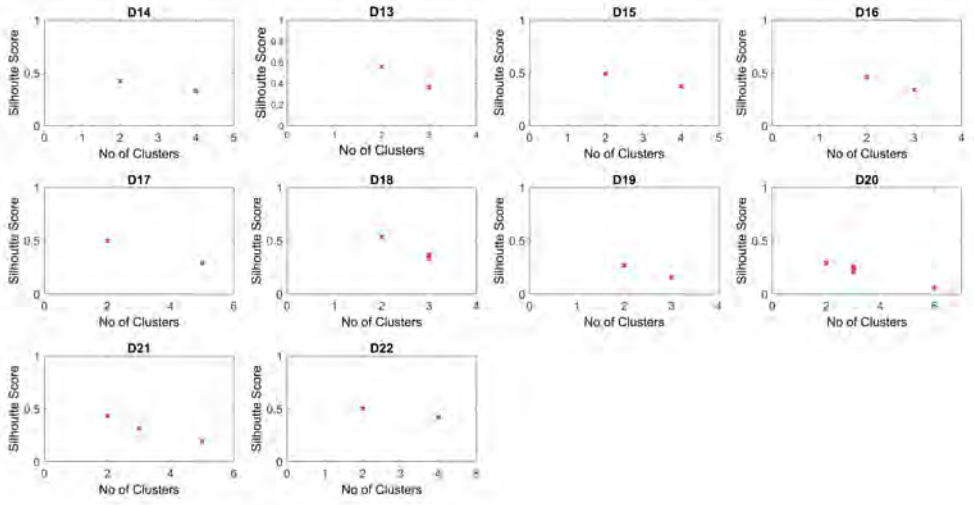

Figure 5.66: Averaged silhouette width for the entire dataset in respect to the number of clusters obtained. Plot for patients datasets D13 to D22 with 4 time steps, ε_1 and α as variables. Detailed results are in Table 5.5.

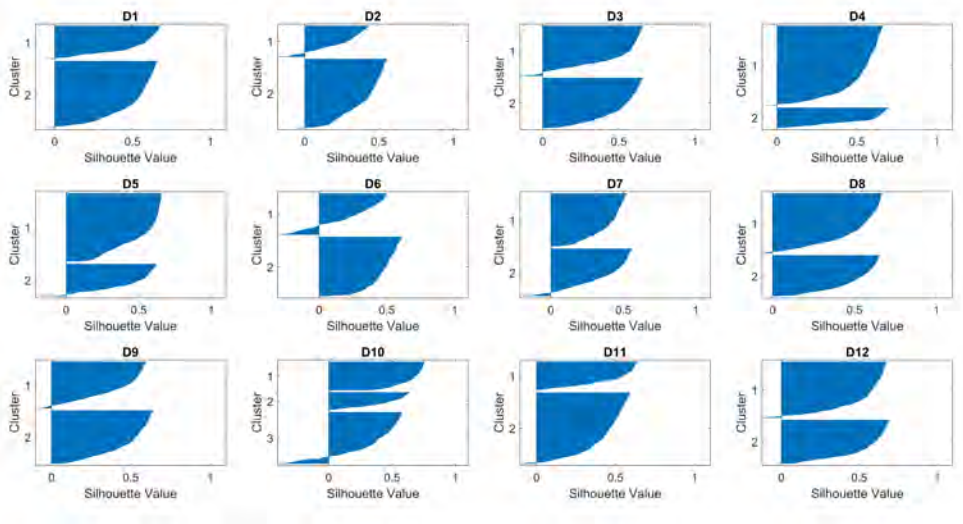

Figure 5.67: Silhouette plots of clusters obtained for patients datasets D1 to D12 with 4 time steps, ε_1 and α as variables. Detailed results are in Table 5.5.

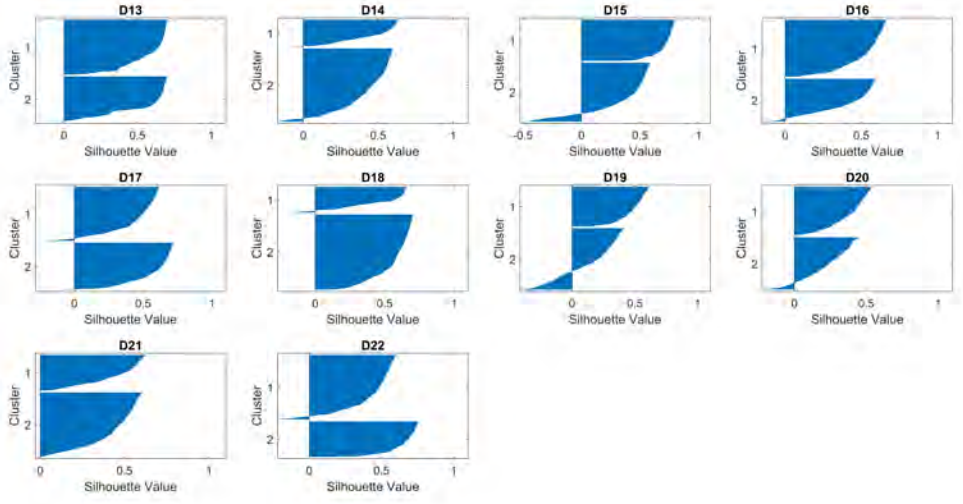

Figure 5.68: Silhouette plots of clusters obtained for patients datasets D13 to D22 with 4 time steps, ε_1 and α as variables. Detailed results are in Table 5.5.

Clusters plots of analysis with 4 time steps ε_1, ε_2 and α variables

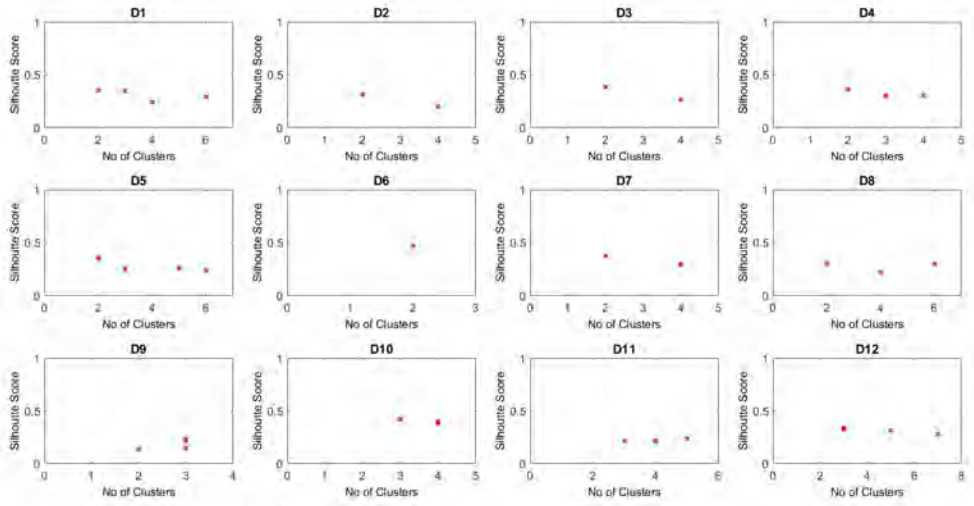

Figure 5.69: Averaged silhouette width for the entire dataset in respect to the number of clusters obtained. Plot for patients datasets D1 to D12 with 4 time steps, ε_1, ε_2 and α as variables.

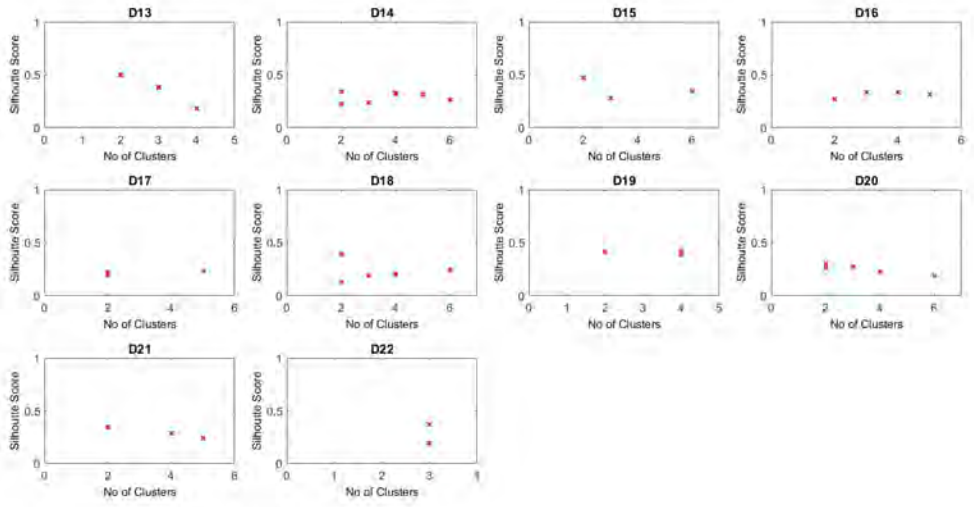

Figure 5.70: Averaged silhouette width for the entire dataset in respect to the number of clusters obtained. Plot for patients datasets D13 to D22 with 4 time steps, ε_1, ε_2 and α as variables.

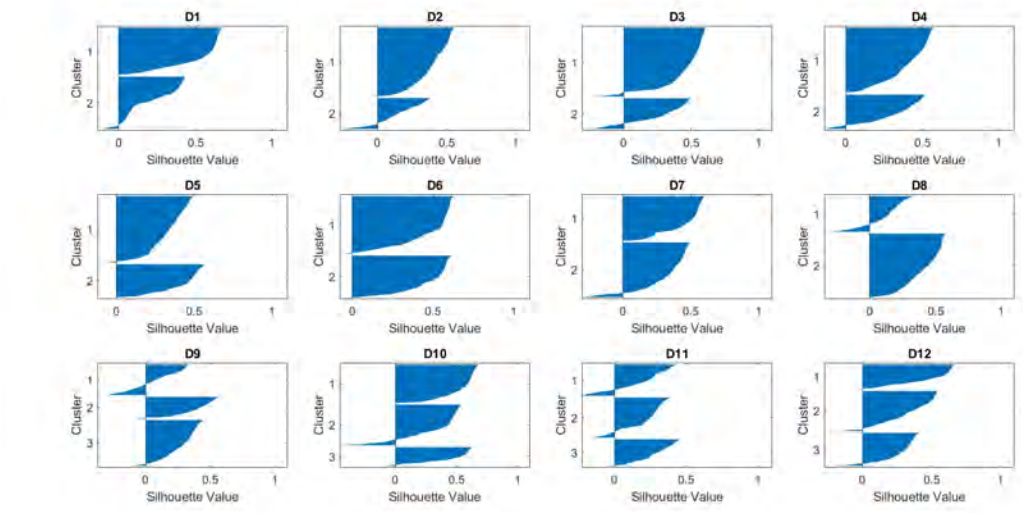

Figure 5.71: Silhouette plots of clusters obtained for patients datasets D1 to D12 with 4 time steps, ε_1, ε_2 and α as variables. Detailed results are in Table 5.5.

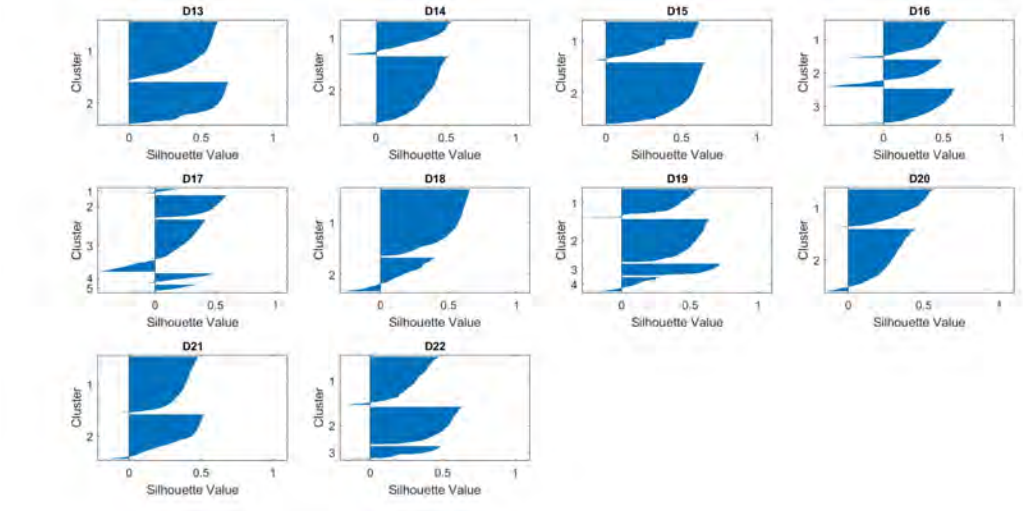

Figure 5.72: Silhouette plots of clusters obtained for patients datasets D13 to D22 with 4 time steps, ε_1, ε_2 and α as variables. Detailed results are in Table 5.5.

5.2.6 Analysis no.5, inter-patients analysis

Since significant differences between patients were observed in the strain field of the tested group of subjects, an inter-patients analysis was also performed. Determining similarity in patterns between subjects can be essential for guiding the design of implants tailored to groups with similar abdominal wall behaviour. Such approach can ensure that implants are optimised for mechanical compatibility, improving outcomes and reducing complications. In this section, an analysis is presented where principle to use clustering feature of SOM to identify subjects with similar deformation responses is applied.

SOM modelled the data and divided it into two separate clusters, which quality is shown via silhouette width and score in the Fig. 5.73 below. Both, according to Everitt et al. (2011), show not well classified data into clusters with average silhouette score of only 0.25. Nevertheless, the findings that come from this analysis are as follows. Cluster denoted with number 2 is homogeneous, meaning the data objects grouped there are similar. Therefore, subjects D1, D6, D9, D17, D19, D20 in this analysis are believed to be similar in terms of this dataset. This type of results could potentially lead to pinpointing similarities between these subjects. On the other hand, it can be the first step to classify them together and analyse them further within a smaller group. The same applies to subjects D13, D14, D17, D21 and D22, although they were grouped in less homogeneous cluster number 1, which resulted in a not favourable silhouette score.

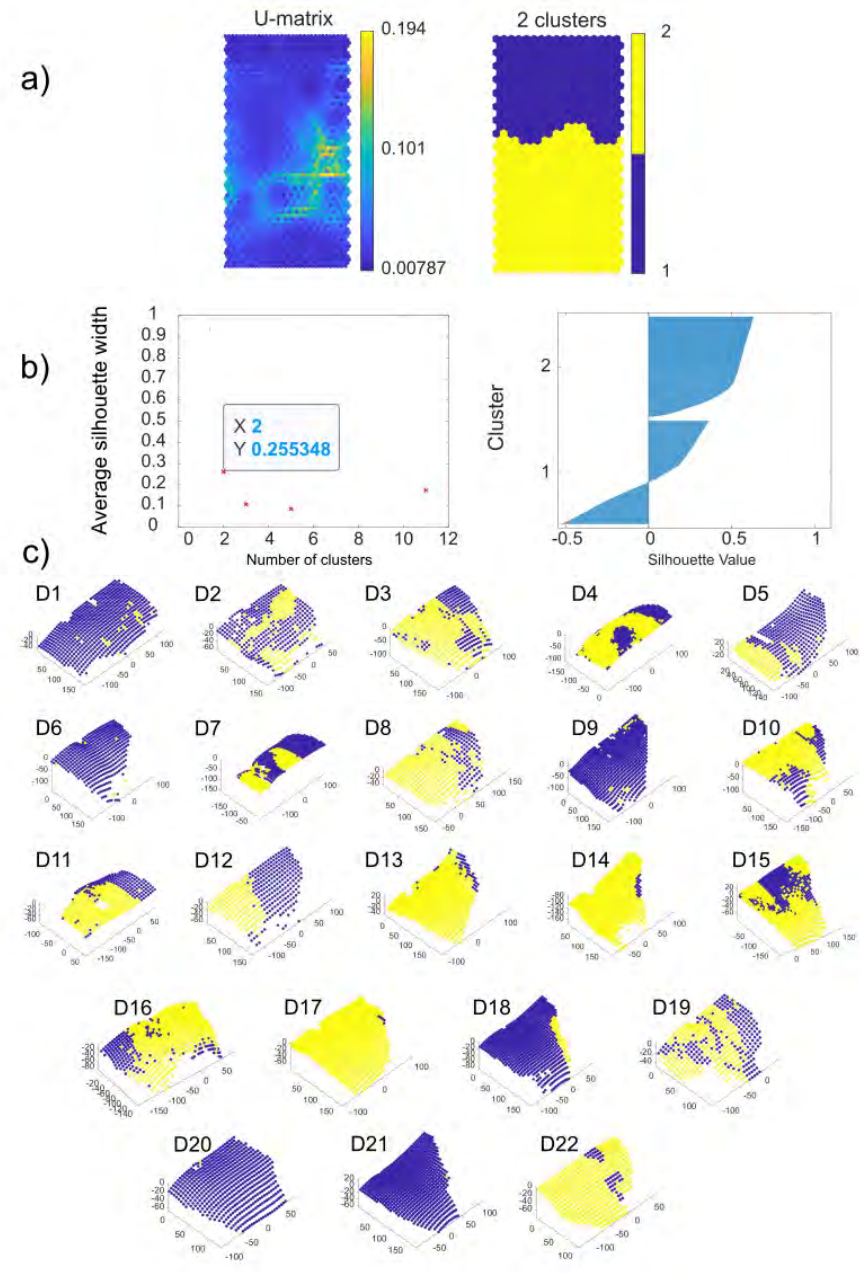

Figure 5.73: D1-D22 Patient similarity ε_1 variable for 4 steps combined figures. a) U-matrix map and identified clusters map; b) averaged clusters score plot and silhouette values plot; c) abdominal walls of all subjects with mapped clusters of respective subjects.

5.2.7 Discussion of the SOM results

The instances of the way that the clusters were formed in the presented analyses can be found in the Table 5.6 below. Worth noting, analysis no. 5 due to the fact that it is an analysis that focused on finding similarities between subjects was not encapsulated into the table and was discussed in previous section.

Subject classification due to the formed clusters				
Analysis no.	Divided clusters by mediolateral axis with separation by anatomical features	Separated clusters by the linea alba	Clusters encompassing the navel	Clusters that divided the abdomen transversely
1) 4steps x ε_1	D2, D3, D8, D9, D11, D12	D5	D1, D5, D7, D10	D4, D6
2) All steps x ε_1	D3, D8, D9, D11, D12	D5	D1, D5, D10	D2, D4, D6, D7
3) 4steps x (ε_1, α)	D2, D3, D8, D9, D11, D14, D15, D18, D19, D21	D5, D13, D22	D1, D10, D12, D16, D17, D20	D4, D6, D7
4) 4steps x (ε_1, ε_2, α)	D2, D6, D14, D21	D1, D6, D9, D13, D15, D22	D3, D5, D7, D10, D11, D12, D16, D17, D20	D4, D18, D19

Table 5.6: Distribution of formed clusters in respect to chosen analysis.

In presented SOM analyses, the mapped clusters on the surface of the patients' abdomens often align with the mediolateral axis of the body. The clustering patterns reflect anatomical features and, in some instances, respond to external boundaries like the rib cage and hip bones, where strain behaviours skew the cluster shapes (notably at the top and bottom of the abdominal wall). These clusters form around those features showcasing distinction between subjects.

For some subjects, the SOM identified distinct clusters separated by a linea alba – a transverse line intersecting the navel. This line divides one cluster above the navel and another below it.

For other subjects the SOM detected a cluster around the navel, distinguishing it from surrounding areas. In such cases clusters forming around the midline but

separated by the navel, or encompassing the area around the navel, reinforcing the role of the navel area in distinguishing distinct mechanical zones.

In some subjects the SOM clusters tended to divide the abdominal wall transversely, suggesting distinct mechanical properties along the longitudinal direction. However, the transverse division may also result from the influence of boundary conditions, which can be challenging to determine precisely.

The key finding from the above results is that, despite using different variables, distinct characteristics of specific subjects consistently emerged and were clearly identifiable. While there were variations in how the clusters were formed, the overall patterns remained and can be recognised.

5.2.7.1 Spatial distribution of strains values on the abdominal wall

In strain analysis, contour maps are graphical representations that show spatial distributions of strain values over a structure or material. Each contour line or region on the map represents points with the same strain magnitude, allowing visualisation of how strain varies under specific loading conditions. These maps provide insights into regions of high or low strain and are useful for identifying patterns. In other words, contour maps provide detailed spatial distributions of individual variables. This approach can enrich the understanding of abdominal wall mechanics under pressure and highlight the nuanced interplay between different mechanical quantities.

In Figs 5.74–5.75 the ranges of the principal Lagrangian strain ε_1 on the abdominal walls of subjects (D3–D12) in T1–T4 are shown in the form of contour maps. The maps contain isolines on the x-y plane of half of the abdominal wall surface, showing the range of values observed in different areas of the abdominal wall for each subject. On the y axis, different ranges of principal strains (ε_1) are shown in colours, on the horizontal x axis on the left side, grid points of the half the abdomen are shown. Next to them respective halves of their abdomens with mapped clusters identified by SOM analysis are presented.

In work by Szepietowska et al. (2023) detailed explanations, along with comparable results for other patients, as well not only principal Lagrangian strain ε_1, but also ε_2 values and the direction of their α angle on the abdominal walls are shown.

SOM analysis can synthesise these distributions (analysing a greater number of load steps) to reveal deeper patterns and correlations. Thus, in conjunction with contour maps SOM can be a comprehensive approach to such data. What, in

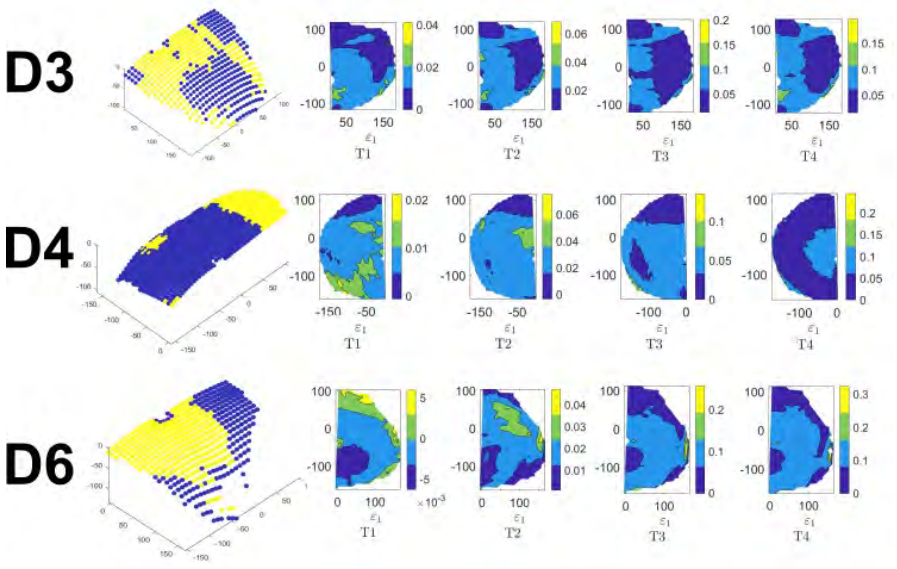

Figure 5.74: Contour maps and respective halves of abdomens of patients (D3–D6) with mapped clusters. On the y axis, different ranges of principal strains (ε_1) are shown in colours, on the horizontal x axis on the left side, grid points of the half the abdomen are shown. Contour maps adapted from Szepietowska et al. (2023).

turn, can raise important questions regarding the contribution and variability of individual variables in the identified clusters. Whether any single variable could adequately represent the deformation behaviour and provide a multidimensional view of the mechanical behaviour of the abdominal wall under pressure.

Comparing contour maps of ε_1 variable and SOM analysis (Fig. 5.74 and Fig. 5.75) of all steps for the same respective strain variable one can observe the following:

- In subject D3, in range of T2–T4 load steps and cluster no. 2 (yellow) are similar to the strain isoline range from 0 to 0.05;
- In subject D4, for T3 load step and cluster no. 2 (yellow) are similar to the strain isoline range of 0.05;
- In subject D7, for T4 load step and cluster no. 1 (navy) are similar to the strain isoline range of 0.1;
- In subject D8, for T4 load step and cluster no. 1 (navy) are similar to the strain isoline range of 0.05;

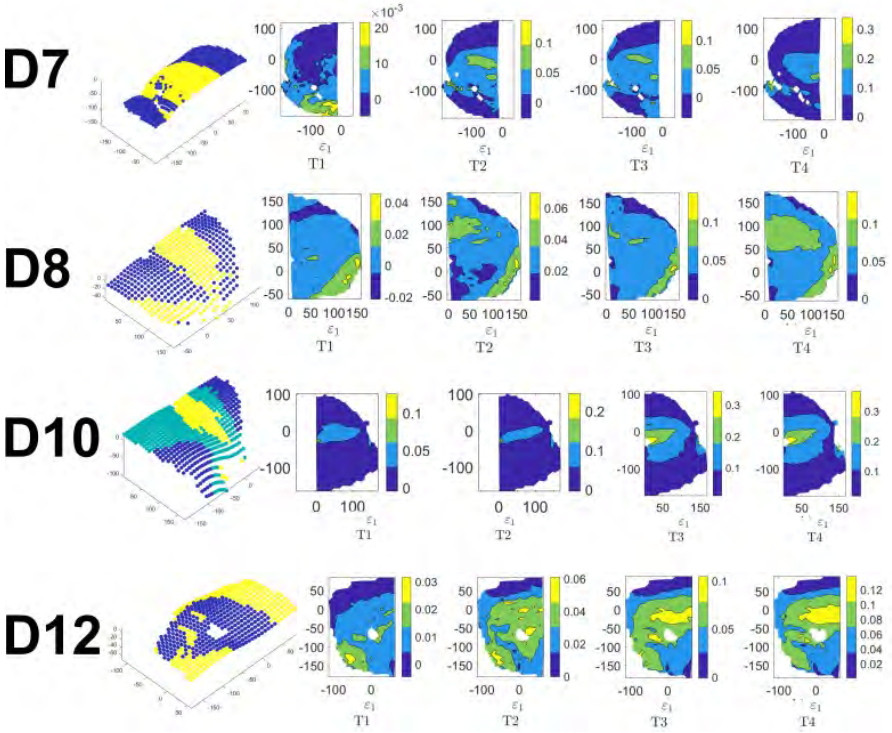

Figure 5.75: Contour maps and respective halves of abdomens of patients (D7–D12) with mapped clusters. On the y axis, different ranges of principal strains (ε_1) are shown in colours, on the horizontal x axis on the left side, grid points of the half the abdomen are shown. Contour maps adapted from Szepietowska et al. (2023).

- In subject D10, in range of T1–T2 load step and cluster no. 2 (celeste colour) are similar to the strain isoline range of 0.1;
- In subject D12, for T1 load step and cluster no. 2 (yellow) are similar to the strain isoline range of 0.01.

The integration of SOM and contour maps could facilitate implications for abdominal wall mechanics. Either it could be identification of dominant mechanical variables influencing deformation in specific regions of the abdominal wall. Or it could contribute to recognition of variability between individuals with an emphasis on the importance of patient-specific approaches in biomechanics.

5.3 Conclusions

This study used full-field measured data obtained from *in vivo* tests on human subjects, with the main focus directed on the strain field of the human abdominal wall under varying pressure conditions. This approach provided valuable information on the mechanical behaviour and distribution of strain across the abdominal wall during loading scenarios and while breathing. The change in directions of principal strains on the surface of a pressurised abdominal wall should be noted as an intriguing observation from the experiment. This phenomenon likely indicates that different components of the abdominal wall dominate depending on whether the muscles are passively or actively engaged. It may also imply the anisotropic characteristics of the abdominal wall.

These fluctuating changes highlight the complexity of the mechanical behaviour of the abdominal wall and underscore the necessity of employing advanced analytical tools to effectively capture such variations. This complexity arises from the interplay between different tissue components, which respond differently under varying intra-abdominal pressure and muscle activation states. Accurately identifying these mechanical nuances is essential for improving patient-specific treatments. Therefore, integrating sophisticated tools like machine learning models is beneficial for addressing these biomechanical challenges.

This research employed Self-Organising Maps to identify regions of the human abdominal wall that exhibit similar deformation states under changing pressure in time. By clustering these regions based on their mechanical responses, it was shown that SOM can reveal patterns of strain distribution that may not be clear

when only one variable or strain field is considered at one moment in time. This approach helps to understand the behaviour of different tissue components. The resulting clustering showed that the deformation state varies not only across different abdominal regions but also between subjects. This variability underscores the necessity for a personalised approach to abdominal wall reconstruction procedures. However, to derive more detailed and reliable indications, a larger test group is essential for future studies.

The presented research provides valuable insights into the interaction between native tissue and load that is being exerted on its parts, emphasising the importance of designing surgical meshes that can withstand these loading conditions. By incorporating non-homogeneous and anisotropic mechanical properties akin to those of human tissues, these meshes could be tailored to specific regions of the abdominal wall, enhancing their compatibility and performance. This is particularly significant, as many currently available surgical meshes, especially those with increased stiffness compared to human tissues, are linked to postoperative pain and discomfort, which can significantly impact the patient's quality of life. Tailoring meshes with mechanical properties more closely aligned to native tissues may help mitigate these negative effects.

Chapter 6

Temporomandibular Joint

6.1 Self-Organising Maps in Analysis of TMJ's Muscle Performance

Dental diagnoses demand extensive expertise and a high level of medical proficiency. However, leveraging accessible and easily acquired data could enhance diagnostic efficiency and broaden its applicability. With access to muscle activity data, analysis can be taken a step further using machine learning methods, particularly Self-Organising Maps. Using SOM, sEMG (surface electromyography) data from multiple patients can be analysed and grouped into clusters.

6.1.1 Datasets for Analyses

Datasets used in this study was provided by a research team that focused on assessing surface muscle activity at the TMJ using sEMG within the project titled "The study of 3D temporo-mandibular joint (TMJ) model of bone-cartilage-ligament system mapping for effective commercialization of results in dental prosthetics, orthodontic and orthognathic surgery" (POIR.04.01.02-00-0029/17). More details about the data acquisition with sEMG as well as other information can be found in Troka et al. (2022), as aspect of data acquisition was outside the scope of this dissertation, it was not addressed or discussed.

In this study, a subset of five volunteers (Table 6.1) from the Project 3D-JAW was selected to investigate muscles activity related to their temporomandibular joint function. Three of them (subsequently marked as VI, VII and VIII) were examined 6 months later for the second time and their entries ID were added as *new*

volunteers as well to show the ability of SOM to pinpoint similarities. Thus, the dataset included sEMG signals from 8 volunteers performing jaw motions, such as opening, closing, and lateral motions (protrusion and retrusion). The sEMG signals of activity were recorded from four superficial muscles: right and left masseters, and the anterior parts of the right and left temporalis (Fig. 6.1).

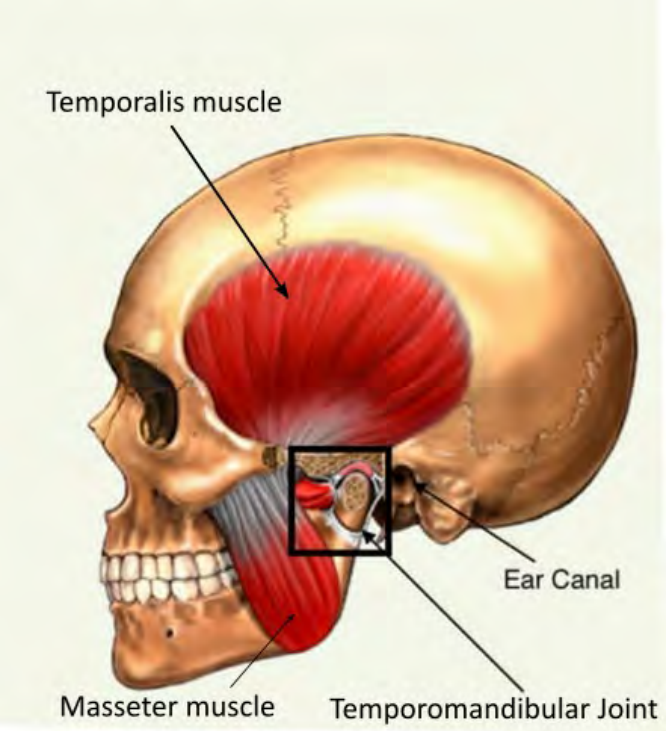

Figure 6.1: TMJ anatomy. Fig. modified from Demerjian et al. (2018b).

The volunteers were chosen based on the absence of systemic diseases or significant pain, indicating overall good health. However, it is worth noting that during the examination, three of the five participants reported mild TMJ issues, which were nonetheless deemed non-severe enough to exclude them from the study. The participants' demographic details, occlusion types, and any TMJ issues they reported are summarised in Table 6.1, which serves as a reference for understanding the cohort.

The sEMG is a non-invasive procedure and appropriate. Ethical considerations were addressed, with all participants providing written informed consent as per the protocols approved by the Ethics Committee (agreement No. KB/111/2018, Medical University of Warsaw). An additional criterion for selection was the thickness of the subcutaneous fat layer in the participants, which was determined to be in the lower range, ensuring that it would not interfere with the surface electromyography signals.

This careful selection process helped to ensure that the study's findings are relevant and that muscle activity patterns are accurately captured, providing valuable insights for further research and potential clinical applications.

Volunteer No.	Entry ID	Gender	Occlusion	Self-reported mild issues
1	I, VI	M	Normal	None
2	II, VIII	M	Anterior	Right disc blockage, increased muscle tension
3	III, VII	M	Deep bite	None
4	IV	M	Anterior	Muscle tension during chewing and yawning
5	V	F	Normal	Clicking in the right TMJ (instability)

Table 6.1: List of volunteers and their details.

6.1.2 Inputs for SOM

Although normalisation in this case is not strictly necessary for SOM due to sEMG data that was acquired and post-processed, but it can improve numerical accuracy and network performance. Thus, to prevent data with larger magnitudes

from disproportionately influencing the SOM, the sEMG data was normalised before being applied to the SOM algorithm.

Moreover, to account for instability and difference in various phases of motions data was also divided into three phases. Here, in the Fig. 6.2 RMS envelopes of the muscle sEMG acquired during jaw opening are presented. Entry ID corresponds to the volunteers' sEMG examination ID (Table 6.1).

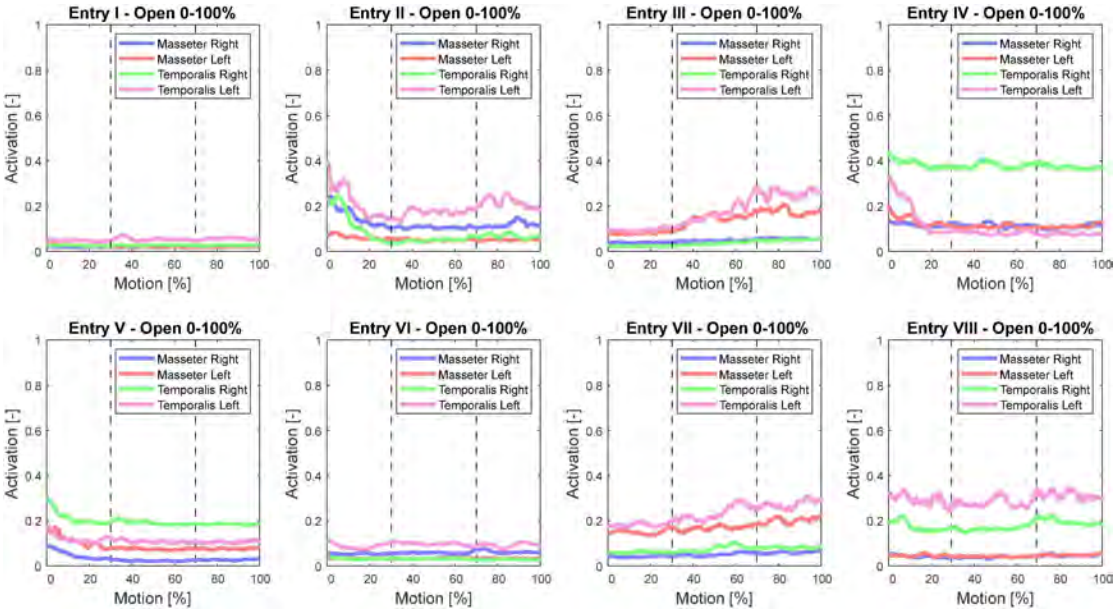

Figure 6.2: RMS envelopes of the muscles sEMG signal during jaw opening with outlines of motion phases (grey dashed lines): acceleration phase 0–30% of motion, middle phase 30–70%, deceleration phase 70–100%. Fig. from Troka et al. (2022).

For the analyses, input data was structured as numerical matrices with 4 variables – for 4 tested muscles. Data points came from each Subject from the data selected for the analysis, with IDs assigned to each test, I-II-III-IV-V-VI-VII-VIII (Table 6.3) respectively. As shown in Fig. 6.3 where rows had a number of samples from each variable for each Subject, here 8 times 1000 sEMG data points from a specific muscle from motion being analysed during current calculation. To account for instability and difference in various phases of motions data was divided into three phases (for analyses no. 1–3 in Table 6.2). First 30% of the motion following next 40% and ending with another 30% of motion.

In Table 6.2 further description of how inputs were structured for each specific analysis are shown.

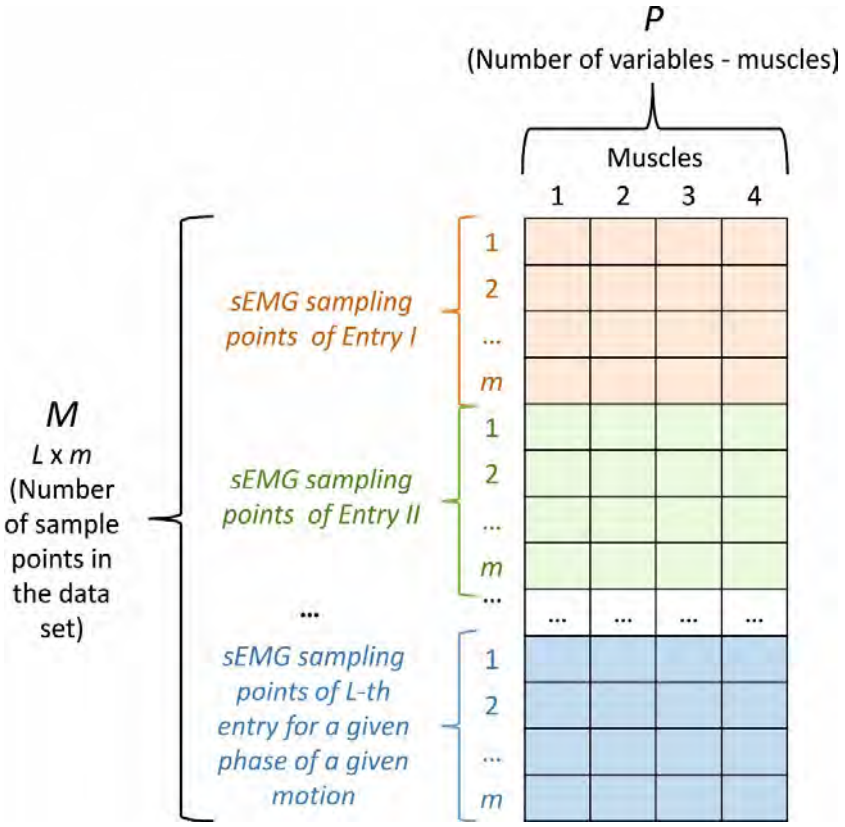

Figure 6.3: Dataset input to the SOM. Fig. from Troka et al. (2022).

No.	variables	no. of data points	analysis range
1	sEMG signal of 4 muscles	first 300 samples x 8 subjects	for each motion
2	sEMG signal of 4 muscles	subsequent 400 samples x 8 subjects	for each motion
3	sEMG signal of 4 muscles	last 300 samples x 8 subjects	for each motion
4	sEMG signal of 4 muscles	1000 samples x 8 subjects	for each motion

Table 6.2: The structure of the input for TMJ analyses with SOM

6.2 Results and discussion

For analyses we followed a guideline mentioned in Chapter 3.2 to determine the size of map (total number of nodes: $M = 5\sqrt{N}$ (Vesanto and Alhoniemi (2000)), where M is the number of samples in the dataset). Training was conducted in batch mode, where the entire dataset was presented to the network simultaneously.

For the analyses with inputs numbered 1–3 the U-matrix map was structured with enclosed borders (2D sheet), to capture essential patterns from the input data, and for analysis no.4 it was borderless (toroidal), to explore data features without restricting the self-organisation.

The number of training epochs–defined as the number of iterations in which each sample is processed by the network until the SOM converges and was set 300 for the rough training and 100 for fine-tuning.

The open-source SOM Toolbox for MATLAB Vesanto et al. (2000) was utilised for performing the training and visualisation tasks in this research.

6.2.1 Results of analysis of separate phases of motions

In this section the results for divided motions are shown and discussed in a comprehensive manner. Figs that show Unified distance matrix resultant maps for input datasets no.1 to 3 of Table 6.2 are presented in Fig. 6.4. Also labelled U-matrix maps of TMJ muscles of sEMG data for examined motions in three phases (divided motions) are presented. Colour bar values represent Euclidean distance between neighbouring neurons, labels (Roman numerals) correspond to Entry IDs. Key information on clustering of the data entries, representing patterns of similarity in muscle sEMG data, are summarised in Table 6.3. Alongside U-matrices, component planes and label maps can be found in supplementary material in Troka et al. (2022).

Motion	Subjects clustered together	Best separated clusters
Opening	III with VII	IV, V
Closing	III with VII, III with VIII	IV, V
Protrusion	I with VI and with III	IV, V
Retrusion	II with III (initial phase), III with VII	IV, V

Table 6.3: Data organisation into clusters of divided motions.

The results show that SOM was able to encode the same volunteers labelled as their subsequent entries IDs (examined in time interval Table 6.1), respectively I and VI, II and VIII, III and VII. Thus, the identification of similar data by SOM is possible.

An interesting finding is a formed cluster of volunteers I, VI and III in protrusion motion and in retrusion motion in the initial phase subjects II and III. The finding suggests data similarity between them. Among best separated clusters are these formed with the majority of data points from Subjects IV and V.

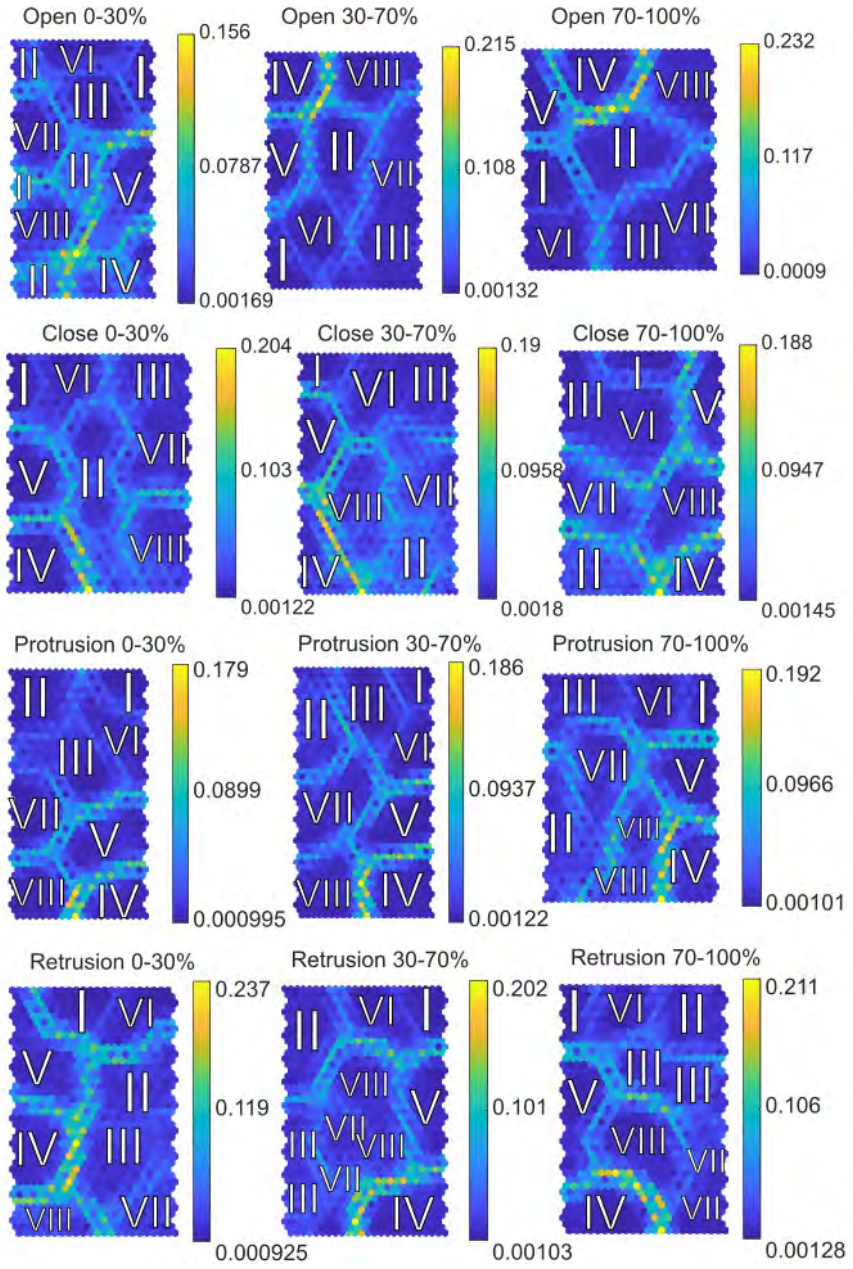

Figure 6.4: Labelled U-matrix maps of TMJ muscles of processed sEMG data for examined motions in three phases, of divided motions, Colour bar values represent Euclidean distance between neighbouring neurons; labels (Roman numerals) correspond to Entry IDs. Figure adapted from Troka et al. (2022).

6.2.2 Results of analysis of full motions

Results presented in this section refer to the analysis no.4 from the Table 6.2, where the whole recorded sEMG signals of performed motions were analysed. Partly this analysis was presented in Troka et al. (2024b). Analysing 100% of the motion data can provide a more comprehensive evaluation, compared to examining individual motion phases separately. Worth noting is whether the whole motion analysis can confirm the one of separate phases, which in turn, can be more applicable in the clinical setting.

Figs 6.5, 6.7, 6.9, 6.11 show data organisation on U-matrix maps next to the cluster maps, which is a suggested division into a fixed number of clusters calculated to be within the best quality as mentioned in Chapter 3.3. Additionally, a colour coded map is presented next to the labels map. It is directly linked to the labels map and shows how many data object marked with matching label was *organised* in that respective node of the map. It can be used to assess if an outlier node is connected to only a fraction of data points or a larger amount which would be of more significance.

Whereas in Figs 6.6, 6.8, 6.10, 6.12 component planes for the analsis are shown. In the context of SOM they represent the values of a single variable (here a specific muscle sEMG activity signal) across the input data. In this case the presented values are denormalised to show the range of input data that were fed into the SOM algorithm.

A summary of the results is presented in the Table 6.4. In contrary to the one based on visual interpretation of labelled U-matrix map as in Table 6.3 the division into clusters was noted from suggested division into clusters provided by the SOM calculation.

Motion	**Subjects clustered together**	**Best separated clusters**
Opening	III with VI	IV, III with VII, VIII
Closing	II with VII with III, I with III with VI	IV, V
Protrusion	I with VI with III, II with III, VII with VIII	IV, V
Retrusion	I with VI with III, II with III with VII with VIII	IV, V

Table 6.4: Data organisation into clusters of whole motions.

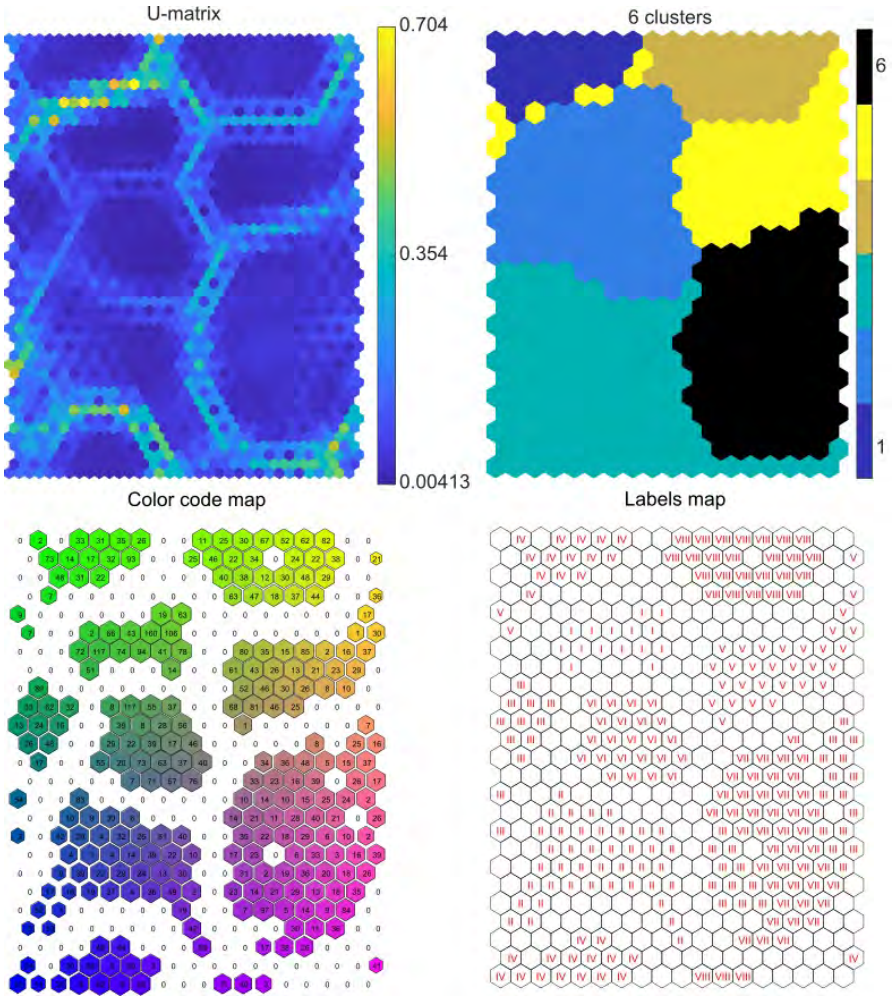

Figure 6.5: Opening 0-100% motion. Shown U-matrix, clusters, colour coded and labels maps respectively.

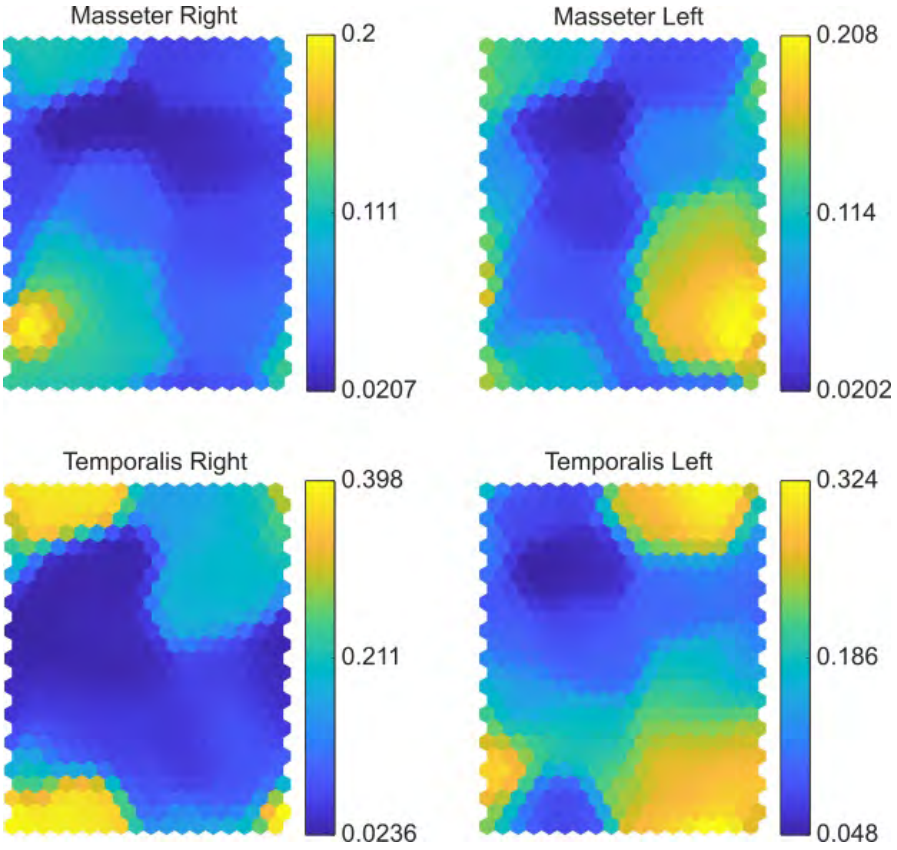

Figure 6.6: Opening 0-100% motion. Maps of variables (masseter right, masseter left, temporalis right, temporalis left) as component planes.

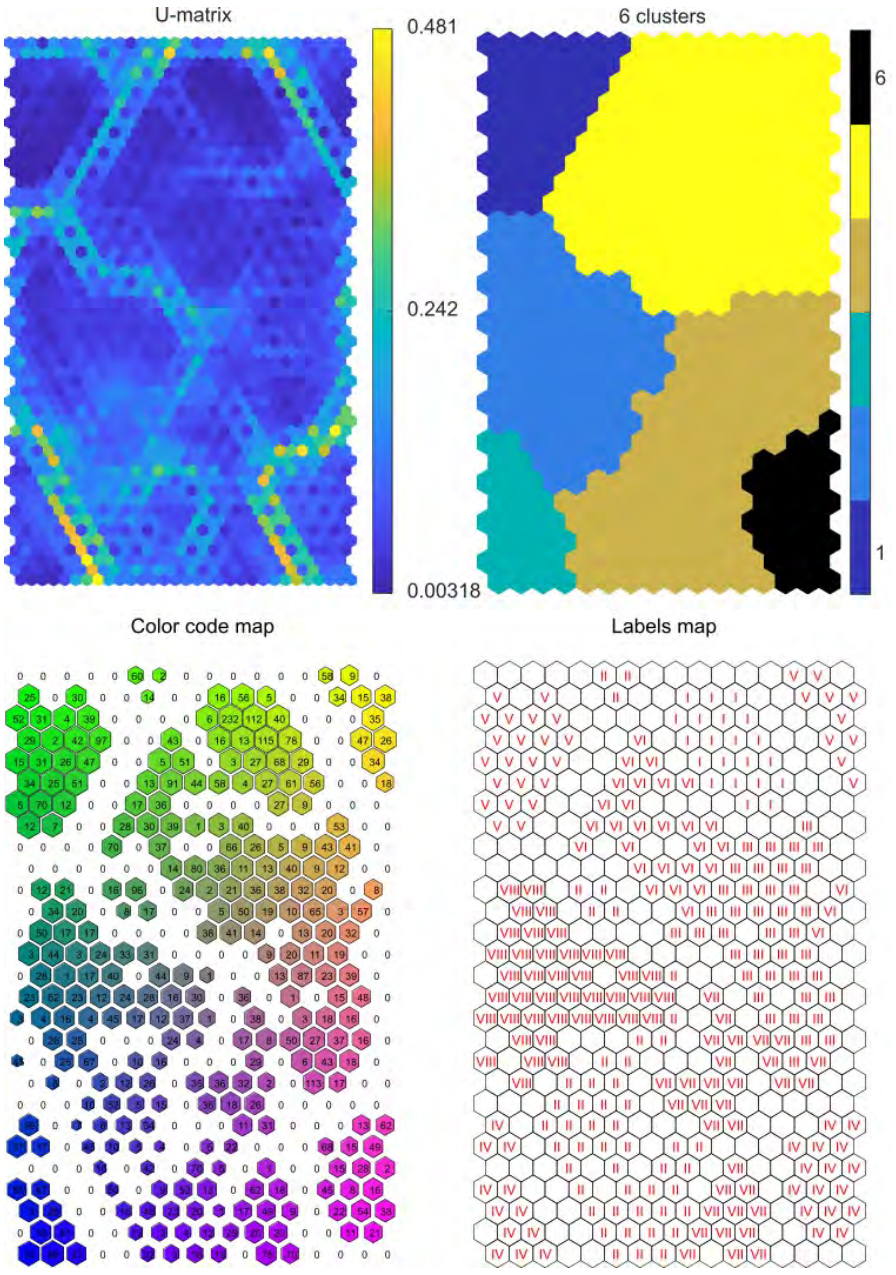

Figure 6.7: Closing 0-100% motion. Shown U-matrix, clusters, colour coded and labels maps respectively.

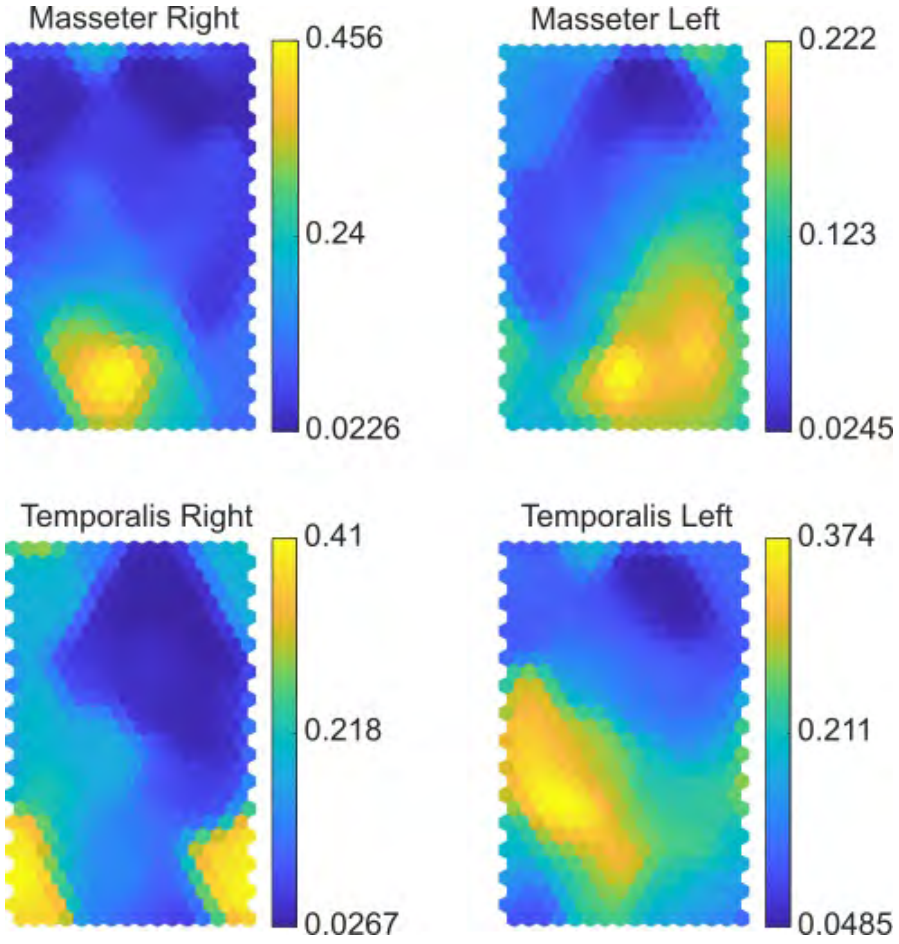

Figure 6.8: Closing 0-100% motion. Maps of variables (masseter right, masseter left, temporalis right, temporalis left) as component planes.

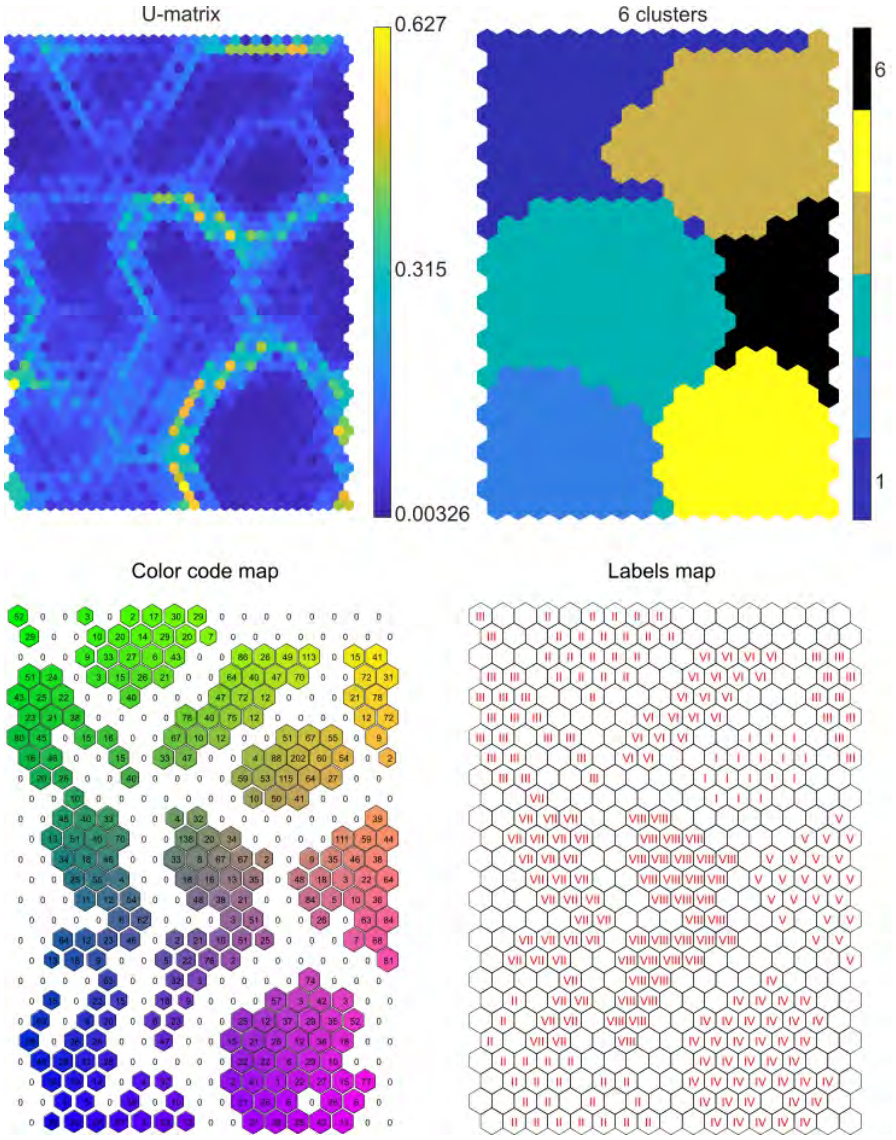

Figure 6.9: Protrusion 0-100% motion. Shown U-matrix, clusters, colour coded and labels maps respectively.

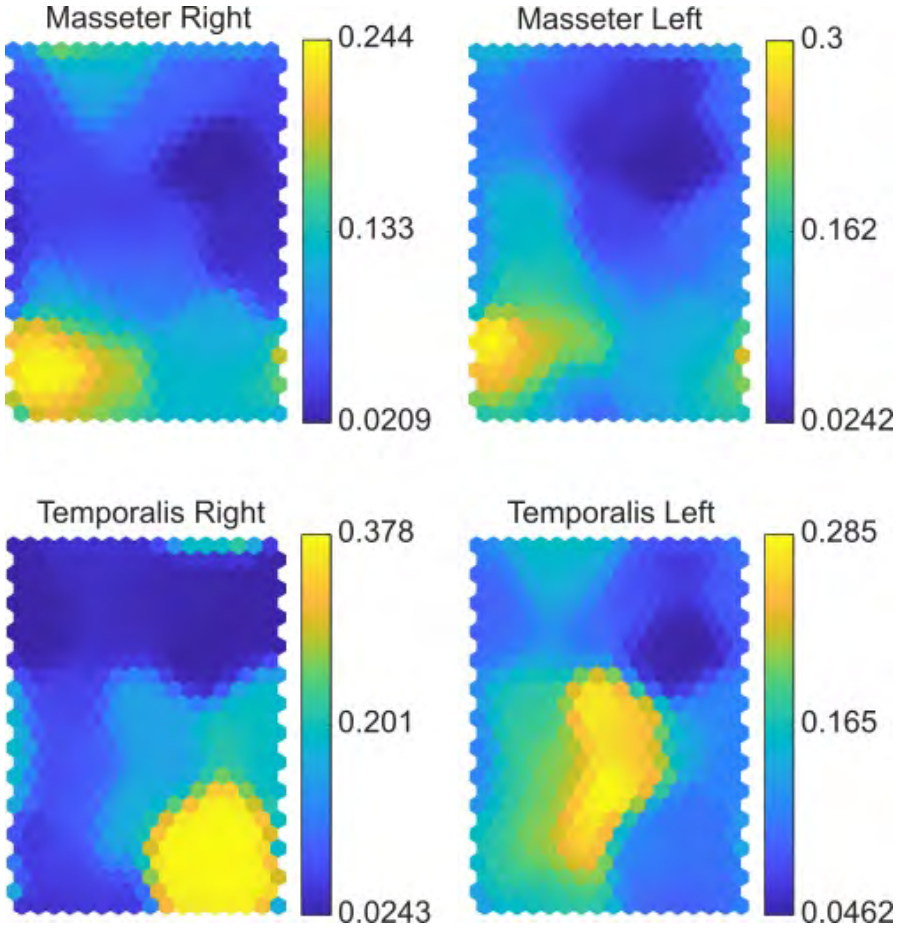

Figure 6.10: Protrusion 0-100% motion. Maps of variables (masseter right, masseter left, temporalis right, temporalis left) as component planes.

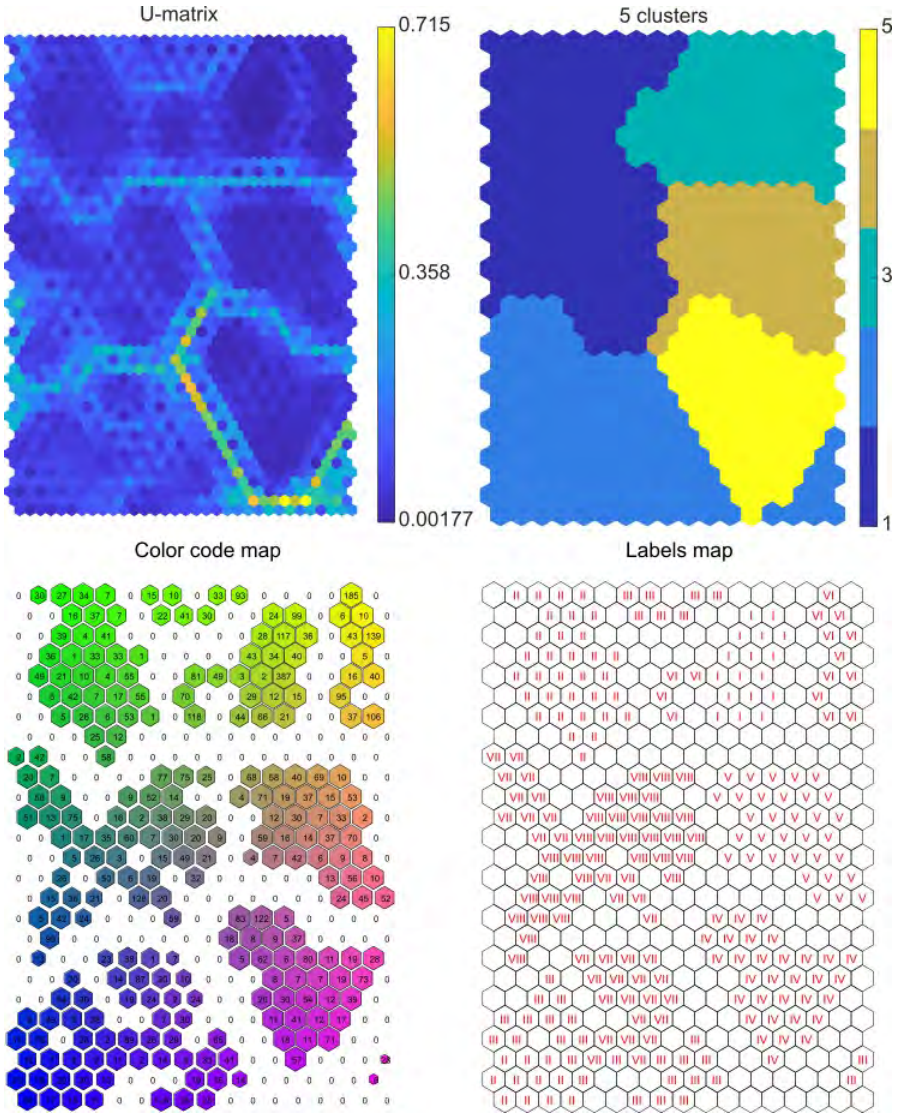

Figure 6.11: Retrusion 0-100% motion. Shown U-matrix, clusters, color coded and labels maps respectively.

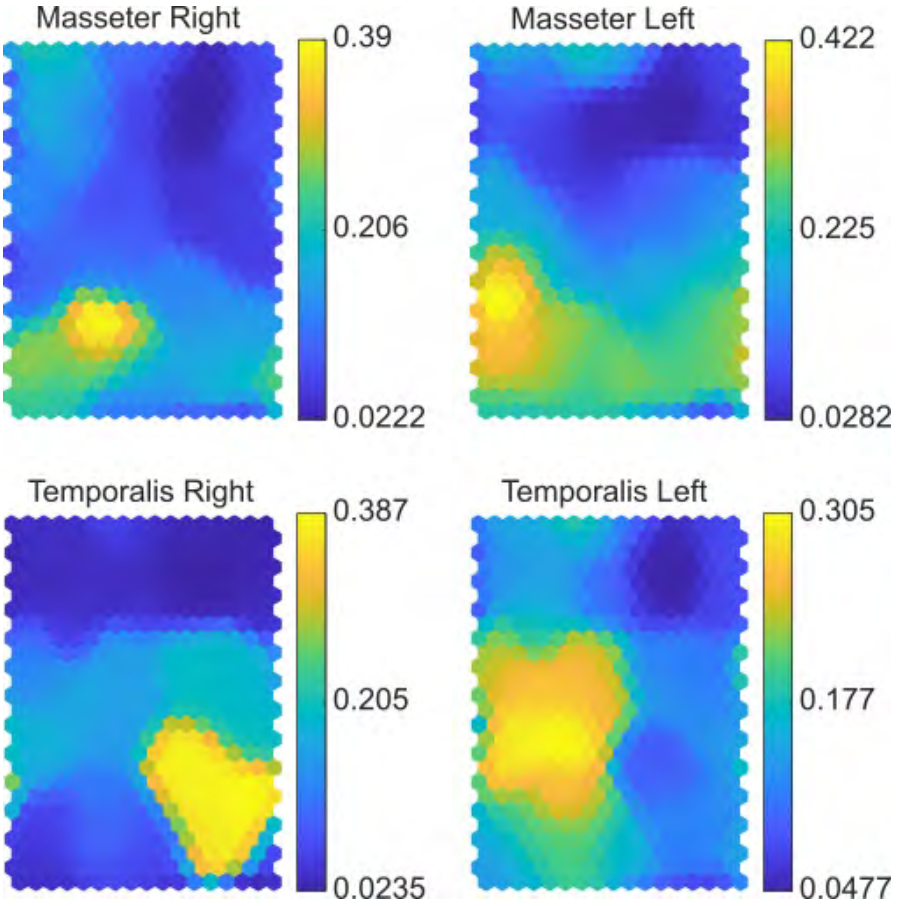

Figure 6.12: Retrusion 0-100% motion. Maps of variables (masseter right, masseter left, temporalis right, temporalis left) as component planes.

6.2.3 Discussion

Using the entirety of the motion data (100%) for the analysis allowed for a more overall and comprehensive evaluation, unveiling more intricate groupings compared to analysing individual motion phases separately. This integrated approach captured the full complexity of muscle activity patterns, offering a deeper insight into interrelations and potential similarities between subjects. In contrast to separate phases analysis it revealed different clustering of subjects.

If we compare Table 6.3 with Table 6.4 we will observe that subjects that formed clusters together are different. It suggests that similarity throughout the whole motions varies to that of when analysing phases of motion.

Interestingly, in both the general and phase-specific analyses, subjects IV and V consistently emerged as the most dissimilar. This could indicate unique patterns

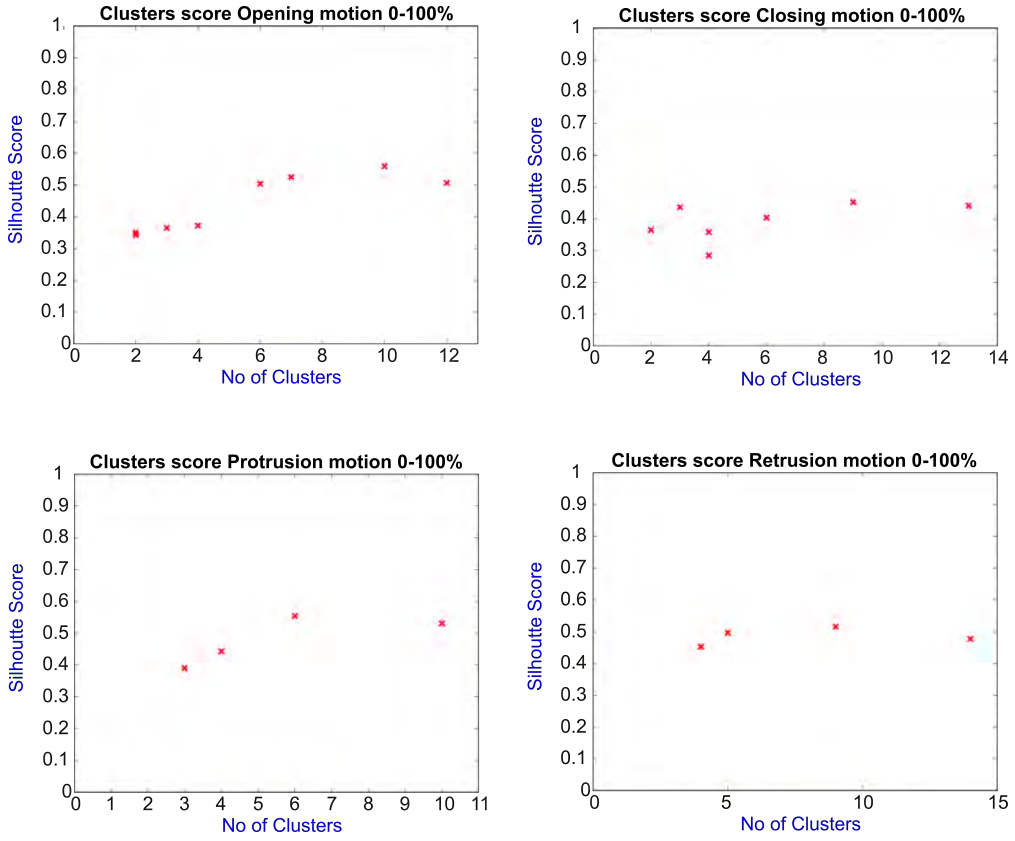

Figure 6.13: Averaged silhouette width for the datasets in respect to the number of clusters obtained. Plots for opening, closing, protrusion and retrusion motions respectively.

of muscle activity in these individuals, potentially signalling outliers or cases with distinct characteristics that merit further investigation.

What is more, the full motions analyses acquired averaged silhouette width score of around or greater than 0.5, except for closing motion (Fig. 6.13) which is according to Kaufman and Rousseeuw (1990); Everitt et al. (2011) a reasonable clustering quality outcome. Although *the best* possible cluster division was found to be into more clusters than shown in Section 6.2.2, regardless, the visual inspection and knowledge about number of different entries were defining factors for accepting a lower quality score in order to have better data explainability and draw meaningful conclusions.

6.3 Conclusions

SOM was used to interpret processed sEMG data obtained during the opening, closing, protrusion, and retrusion motions of the jaw. The SOM method offers a powerful tool for comparing neuromuscular responses by representing multidimensional data inputs, making it applicable in both biomechanical analysis and clinical practice. This approach can aid the development of preventive models to identify dysfunction by analysing muscle activity and capturing jaw motion. Furthermore, the SOM groups can be integrated into personalised predictive models for the stomatognathic system, which are essential in orthognathic treatment planning. The analysis can also be performed in clinical settings to monitor muscle activity during treatments (e.g., using a tooth brace) and provide guidance on whether further corrections are needed.

The analysis underscores the complexity of the stomatognathic system, revealing that while muscle activity varies across individuals, the applied approach successfully identifies similarities between them. The methods used here provide a solid foundation for further research into TMJ dysfunction, considering both muscles activity and dominant sides. Future studies should focus on exploring the effects of connective tissue laxity and bruxism on temporomandibular joint function, as these factors may play significant roles in the development and progression of TMJ disorders.

Moreover, both analyses demonstrated the ability of the Self-Organising Maps to reliably identify repeated entries of the same patients. This consistency reinforces SOM's utility as a robust clustering tool, capable of recognising and grouping similar datasets. Such reliability is critical for ensuring the method's application in clinical and research settings, particularly in identifying patterns across multidimensional datasets. Future research could explore how these findings translate to clinical practice, focusing on their potential for patient-specific diagnostics and treatment planning.

It is worth noting that SOM analysis is relatively user-friendly compared to cross-correlation analysis of sEMG data (presented in Troka et al. (2022)), which requires greater expertise. A significant advantage of SOM is its ability to analyse multiple muscles activity simultaneously, making it an efficient tool for daily clinical practice without over-complicating the diagnostic process. Future advancements should focus on collecting larger data sets from a diverse range of subjects to enable the automated classification of potential health issues. This would further

enhance the applicability of SOM in clinical settings, allowing for more efficient and accurate diagnosis and treatment planning.

Chapter 7

Summary and Future Work

Referring to the thesis of this dissertation, it has been demonstrated that Machine Learning-based methodologies can effectively be applied to the presented problems. In particular where mechanical characterisation of the material as well as loading or boundary conditions are difficult to define and simulate using standard computational techniques, like e.g, using finite element method.

The identification of regions with similar mechanical behaviour in the abdominal walls of multiple patients has been successfully achieved. Similarly, in the analysis of sEMG signals from muscles surrounding the temporomandibular joint, clustering has proven to provide valuable insights into the performance of patients' muscles. These applications demonstrate the versatility and potential of Machine Learning techniques, in particular Self-Organising Maps, in addressing medical application with complex biomechanical challenges.

7.1 Concluding Insights on Abdominal Wall Problem

In the analyses SOM reduced the multi-dimensional data space to the two-dimensional result space by clustering the data points on a 2D map represented by U-matrix. In the abdominal wall problem, clusters, as a SOM output, represent grouped points, of the grid generated on the human abdominal wall that reveal a certain similarity. After grouping, these points are mapped onto the surface of the tested abdomen identifying areas characterised by similar mechanical behaviour. Thanks to SOM, different loading states expressed in terms of strains can be analysed simultaneously.

By analysing multiple variables across load steps, a more comprehensive and nuanced understanding of abdominal wall mechanics is achieved. This multidimensional approach is critical for applications such as surgical mesh design, where an accurate representation of deformation behaviour across regions is main goal. At the same time single-variable analyses may be inadequate for drawing reliable conclusions, as the dominant factors varies across subjects and load steps.

Consequently, the proposed methodology serves as a preliminary step in developing abdominal wall characterisation procedures, paving the way for more tailored and efficient methodology for advancing medical solutions in biomechanics. This approach accounts for variations caused by active behaviours, like muscle engagement during breathing, along with a multidimensional analysis of strain states at different loading stages. Based on the above, several subsequent impactful possibilities emerge:

1. Designing patient-specific implants - by analysing the deformation behaviour of an individual patient's abdominal wall, SOM analysis can guide the creation of customised implants tailored to their unique mechanical responses.

2. Optimised implant selection - using deformation patterns and principal strain directions, the method facilitates selecting the most appropriate implant from existing options, ensuring better mechanical compatibility.

3. Surgical planning - this approach supports precise surgical planning, including determining the optimal orientation and placement of implants at specific angles within designated abdominal zones.

4. Implant design for patient groups - SOM can identify clusters of patients with similar abdominal wall behaviour, enabling the development of implants optimised for these groups rather than a one-size-fits-all approach, which currently is being utilised.

5. Topological optimisation of implants - the technique can aid in refining implant design by optimising shape, thickness, and stiffness to match specific zones of the abdomen, improving overall functionality and comfort.

These novelty underscores the potential of Self-Organising Maps in aiding personalised medical solutions, surgical efficiency, and implant performance. What is more, the proposed SOM analysis of deformation fields could be extended to

study other soft tissue mechanics based on *in vivo* experiments or applied to other challenging anisotropic and non-linear materials, broadening its scope of utility in biomechanical research and material science Troka et al. (2024a).

7.2 Concluding Insights on the Temporomandibular Joint Problem

By applying the methodology based on Self-Organising Maps to sEMG data, the study of identifying patterns and similarities in the data, leading to a more objective and nuanced clustering of sEMG muscle activity signals was possible.

In terms of mechanics of TMJ the study introduces the study introduced several novel aspects. TMJ issues were examined through muscle activation similarities using and Self-Organising Maps. A classification approach, based on TMJ muscle activation patterns was presented enabling the grouping of individuals. SOM was employed to map and visualise muscle activation during real jaw motions across different phases and full motion. It was facilitating the identification of both similarities and differences among subjects while also offering insights into individual-specific patterns. The findings shed light on the activation of the masseter and temporalis muscles in healthy individuals during jaw movements, including opening, closing, protrusion, and retrusion.

SOM analysis can help to compare individual responses by clustering data and using large databases. This approach could classify TMJ performance and serve as a simple starting point for diagnosing similar dysfunctions, which is important for orthodontic and orthognathic treatments Troka et al. (2022).

The differences observed in data groupings may have significant clinical implications, but these findings require validation by medical professionals to determine whether the groupings genuinely reflect physiological or pathological similarities between patients. These groupings can reveal patterns in muscle activity that correlate with specific conditions or dysfunctions, enabling the classification of recurring problems. When combined with medical histories, this approach could support the early diagnosis and management of conditions like temporomandibular joint disorders.

7.3 Final Conclusions and Limitations

The study has some limitations that should be acknowledged. In the abdominal wall problem, the loading conditions considered are restricted by the medical procedure, and to achieve more generalised results. The analysis should be expanded to include a broader range of physiological loading conditions and types. Additionally, while it would be beneficial to include more levels of intra-abdominal pressure measurements, this was limited for patient safety reasons, adhering to standard practice. The measurements were taken on the surface (skin) of the abdominal wall, meaning that any conclusions regarding the mechanics of the entire structure can only be approximate. Furthermore, a larger sample size, particularly including more women, would help to address their under-representation in the current group of subjects.

While a consistent pattern of clusters might be expected across subjects, notable variability emerged, a common observation in biomechanics. Factors contributing to this variability include:

- Demographic differences among subjects, including age, gender, body mass index (BMI), and muscle composition;

- Variations in breathing patterns during data acquisition, potentially influencing mechanical response and clustering outcomes.

This heterogeneity highlights the complexity of abdominal wall mechanics and underscores the importance of incorporating diverse datasets for a comprehensive analysis. The SOM-based approach provides an insightful method for examining these complex patterns and identifying key zones of similar mechanical behaviour, supporting applications in personalised interventions and surgical planning.

The SOM based methodology applied to the TMJ problem offers a significant benefit by enabling the grouping of patients based on muscle activation patterns, independent of pre-existing classification systems. While supervised algorithms are valuable for diagnosing diseases, they lack the ability to uncover and explore novel patterns within the data that go beyond established knowledge.

This study does not encompass all the muscles involved in TMJ function and jaw movements, such as the lateral and medial pterygoid muscles, which represents a limitation. Instead, it focuses exclusively on the activation of superficial muscles that can be tested in non-invasive examination. This approach enhances the

potential for the methodology to be broadly applied in clinical practice, thereby contributing to improved diagnostic processes.

Another limitation of this study is the relatively small sample size of patients. Future research could address this by collecting a larger dataset, including both healthy individuals and patients diagnosed with temporomandibular disorder (TMD) or other issues. However, identifying specific TMDs would require knowledge of the activation patterns characteristic for each disorder. Additionally, expanding the study to include a more diverse group of patients, including individuals of both sexes, would allow for a deeper exploration of sex-related factors as potential contributor.

7.4 Future Work

Due to the fact that our SOM analyses did not always achieve best results in quality assessment, the presented methodology could be enhanced by integrating additional techniques (Gao et al. (2023b)). Also combining it with additional techniques can yield better results e.g., with principal component analysis (PCA) as successfully performed by Das et al. (2016). As Ahmad et al. (2019) shows, before applying clustering algorithms PCA can be used to select features that should be feed into the algorithm. However, as presented by Chattopadhyay et al. (2011), the PCA explains most of the cumulative variance of data but the projection could not provide efficient clustering structure. Then using SOM with additional features of e.g. colour extraction or data samples hit map it can provide very good results. By incorporating additional methods, the SOM-based analysis could achieve higher accuracy, better cluster quality, and more reliable insights, making it a more versatile tool for complex datasets.

The proposed methodologies can be *a ground for* developing diagnostic tools useful for the temporomandibular joint disorders and the abdominal wall insufficiency treatment.

The construction of a methodology for diagnostic tools targeting the temporomandibular joint and the abdominal wall builds on the approaches outlined in this work. In both cases, the methodology integrates experimental measurements, such as surface electromyography for TMJ and full-field Digital Image Correlation for the abdominal wall, with Self-Organising Maps as a core analytical tool.

Bibliography

Ahmad, N. B., Alias, U. F., Mohamad, N., and Yusof, N. (2019). Principal component analysis and self-organizing map clustering for student browsing behaviour analysis. *Procedia Computer Science*, 163:550–559.

Arbelaitz, O., Gurrutxaga, I., Muguerza, J., Pérez, J. M., and Perona, I. (2013). An extensive comparative study of cluster validity indices. *Pattern Recognition*, 46(1):243–256.

Astruc, L., De Meulaere, M., Witz, J.-F., Nováček, V., Turquier, F., Hoc, T., and Brieu, M. (2018). Characterization of the anisotropic mechanical behavior of human abdominal wall connective tissues. *Journal of the mechanical behavior of biomedical materials*, 82:45–50.

Ayuso, S. A., Elhage, S. A., Zhang, Y., Aladegbami, B. G., Gersin, K. S., Fischer, J. P., Augenstein, V. A., Colavita, P. D., and Heniford, B. T. (2023). Predicting rare outcomes in abdominal wall reconstruction using image-based deep learning models. *Surgery*, 173(3):748–755.

Batool, F. (2019). *Optimum Average Silhouette Width Clustering Methods*. PhD thesis, University College London.

Berardo, A., Bonaldi, L., Stecco, C., and Fontanella, C. G. (2024). Biomechanical properties of the human superficial fascia: Site-specific variability and anisotropy of abdominal and thoracic regions. *Journal of the Mechanical Behavior of Biomedical Materials*, 157:106637.

Bianchi, J., Ruellas, A., Gonçalves, J., Paniagua, B., Prieto, J., Styner, M., Li, T., Zhu, H., Sugai, J., Giannobile, W., Benavides, E., Soki, F., Yatabe, M., Ashman, L., Walker, D., Soroushmehr, S., Najarian, K., and Cevidanes, L. (2020). Osteoarthritis of the temporomandibular joint can be diagnosed earlier using biomarkers and machine learning. *Scientific Reports*, 10.

Carbonaro, M., Rohlén, R., Seoni, S., Meiburger, K. M., Vieira, T., Grönlund, C., and Botter, A. (2023). Combining high-density electromyography and ultrafast ultrasound to assess individual motor unit properties in vivo. *biorxiv*.

Chattopadhyay, M., Dan, P. K., and Mazumdar, S. (2011). Principal component analysis and self-organizing map for visual clustering of machine-part cell formation in cellular manufacturing system. *Systems Research Forum*, 05(01):25–51.

Das, G., Chattopadhyay, M., and Gupta, S. (2016). A comparison of self-organising maps and principal components analysis. *International Journal of Market Research*, 58(6):815–834.

Deeken, C. R. and Lake, S. P. (2017). Mechanical properties of the abdominal wall and biomaterials utilized for hernia repair. *Journal of the Mechanical Behavior of Biomedical Materials*, 74:411–427.

Demerjian, G., Sims, A., Patel, M., Lee, T., and Sabal, E. (2018a). *Head and Neck Manifestations of Temporomandibular Joint Disorders: A Translational Perspective*, pages 73–93. Springer International Publishing.

Demerjian, G. G., Sims, A. B., Patel, M., Balatgek, T. L., and Sabal, E. B. (2018b). *Head and Neck Manifestations of Temporomandibular Joint Disorders*, pages 73–93. Springer International Publishing, Cham.

Deza, M. and Deza, E. (2016). *Encyclopedia of Distances*. Springer Berlin Heidelberg.

Donmazov, S., Saruhan, E., Pekkan, K., and Piskin, S. (2024). Review of machine learning techniques in soft tissue biomechanics and biomaterials. *Cardiovascular Engineering and Technology*, 15.

Elhage, S., Deerenberg, E., Ayuso, S., Murphy, K., Shao, J., Kercher, K., Smart, N., Fischer, J., Augenstein, V., Colavita, P., and Heniford, B. T. (2021). Development and validation of image-based deep learning models to predict surgical complexity and complications in abdominal wall reconstruction. *JAMA surgery*, 156.

Everitt, B., Landau, S., Leese, M., and Stahl, D. (2011). *Cluster analysis. 5th edition*. John Wiley and Sons, Ltd.

Ezugwu, A. E., Ikotun, A. M., Oyelade, O. O., Abualigah, L., Agushaka, J. O., Eke, C. I., and Akinyelu, A. A. (2022). A comprehensive survey of clustering algorithms: State-of-the-art machine learning applications, taxonomy, challenges, and future research prospects. *Engineering Applications of Artificial Intelligence*, 110:104743.

Fung, Y. (1993). *Biomechanics, Mechanical Properties of Living Tissues*. Springer-Verlag, second edition.

Gao, C. X., Dwyer, D., Zhu, Y., Smith, C. L., Du, L., Filia, K. M., Bayer, J., Menssink, J. M., Wang, T., Bergmeir, C., Wood, S., and Cotton, S. M. (2023a). An overview of clustering methods with guidelines for application in mental health research. *Psychiatry Research*, 327:115265.

Gao, C. X., Dwyer, D., Zhu, Y., Smith, C. L., Du, L., Filia, K. M., Bayer, J., Menssink, J. M., Wang, T., Bergmeir, C., Wood, S., and Cotton, S. M. (2023b). An overview of clustering methods with guidelines for application in mental health research. *Psychiatry Research*, 327:115265.

Ghezelbash, F., Hossein Eskandari, A., Robert-Lachaine, X., Cao, S., Pesteie, M., Qiao, Z., Shirazi-Adl, A., and Lariviere, C. (2024). Machine learning applications in spine biomechanics. *Journal of Biomechanics*, 166:111967.

Gräßel, D., Prescher, A., Fitzek, S., Keyserlingk, D. G. v., and Axer, H. (2005). Anisotropy of human linea alba: a biomechanical study. *Journal of Surgical Research*, 124(1):118–125.

Hassan, A., Lu, S.-C., Asaad, M., Liu, J., Offodile, A., Sidey-Gibbons, C., and Butler, C. (2022). Novel machine learning approach for the prediction of hernia recurrence, surgical complication, and 30-day readmission after abdominal wall reconstruction. *Journal of the American College of Surgeons*.

Haykin, S. S. (2009). *Neural Networks and Learning Machines*. Pearson Education, third edition.

Hennig, C., Meilă, M., Murtagh, F., and Rocci, R. (2015). Handbook of cluster analysis. In *Handbook of Cluster Analysis*.

Horst, F., Lapuschkin, S., Samek, W., Müller, K.-R., and Schöllhorn, W. (2019). Explaining the unique nature of individual gait patterns with deep learning. *Scientific Reports*, 9:2391.

Humphrey, J. and Delange, S. (2015). *An Introduction to Biomechanics: Solids and Fluids, Analysis and Design*. Springer.

Janneke Schwaner, M., Mayfield, D. L., Azizi, E., and Daley, M. A. (2024). Linking in vivo muscle dynamics to force–length and force–velocity properties reveals that guinea fowl lateral gastrocnemius operates at shorter than optimal lengths. *Journal of Experimental Biology*, 227(15):jeb246879.

Jones, E. and Iadicola, M. E. (2018). *A Good Practices Guide for Digital Image Correlation*. International Digital Image Correlation Society.

Joppin, V., Jourdan, A., Bendahan, D., Soucasse, A., Guye, M., Masson, C., and BEGE, T. (2024). Towards a better understanding of abdominal wall biomechanics: In vivo relationship between dynamic intra-abdominal pressure and magnetic resonance imaging measurements. *Clinical Biomechanics*, 121:106396.

Jourdan, A., Dhume, R., Guérin, E., Siegel, A., Le Ruyet, A., and Palmer, M. (2024). Numerical investigation of a finite element abdominal wall model during breathing and muscular contraction. *Computer Methods and Programs in Biomedicine*, 244:107985.

Karrech, A., Ahmad, H., and Hamdorf, J. M. (2023). Biomechanical stability of hernia-damaged abdominal walls. *Scientific reports*, 13:4936.

Kaufman, L. and Rousseeuw, P. J. (1990). *Finding Groups in Data. An Introduction to Cluster Analysis*. John Wiley and Sons, Inc., New York.

Kim, M., Kim, J., Lee, C., and Kang, B.-K. (2021). Detection of pneumoperitoneum in the abdominal radiograph images using artificial neural networks. *European Journal of Radiology Open*, 8:100316.

Kind, M. and Brunner, R. (2013). Somz: Photometric redshift pdfs with self-organizing maps and random atlas. *Monthly Notices of the Royal Astronomical Society*, 438.

Kingsnorth, A. and LeBlanc, K. (2003). Hernias: inguinal and incisional. *The Lancet*, 362(9395):1561–1571.

Kohonen, T. (1982). Self-organized formation of topologically correct feature maps. *Biological Cybernetics*, 43.

Kohonen, T. (1997). *Self-Organizing Maps*. Springer, Berlin, Heidelberg.

Kohonen, T. (2013). Essentials of the self-organizing map. *Neural Networks*, 37:52–65.

Kohonen, T. (2014). *MATLAB Implementations and Applications of the Self-Organizing Map*. Unigrafia.

Kreiner, M. and Viloria, J. (2022). A novel artificial neural network for the diagnosis of orofacial pain and temporomandibular disorders. *Journal of Oral Rehabilitation*, 49(9):884–889.

Kriener, K., Lala, R., Homes, R., Finley, H., Sinclair, K., Williams, M., and Midwinter, M. (2023). Mechanical characterization of the human abdominal wall using uniaxial tensile testing. *Bioengineering*, 10:1213.

Le Ruyet, A., Yurtkap, Y., den Hartog, F., Vegleur, A., Turquier, F., Lange, J., and Kleinrensink, G.-J. (2020). Differences in biomechanics of abdominal wall closure with and without mesh reinforcement: A study in post mortem human specimens. *Journal of the Mechanical Behavior of Biomedical Materials*, 105:103683.

Lee, Y.-H., Jeon, S., Won, J.-H., Auh, Q.-S., and Noh, Y.-K. (2024). Automatic detection and visualization of temporomandibular joint effusion with deep neural network. *Scientific Reports*, 14.

Lima, D., Kasakewitch, J., Nguyen, D., Nogueira, R., Cavazzola, L., Heniford, B., and Malcher, F. (2024). Machine learning, deep learning and hernia surgery. are we pushing the limits of abdominal core health? a qualitative systematic review. *Hernia*, 28:1–8.

Liu, W., Xie, Y., Zheng, Y., He, W., Qiao, K., and Meng, H. (2021). Regulatory science for hernia mesh: Current status and future perspectives. *Bioactive Materials*, 6:420–432.

Lötsch, J. and Ultsch, A. (2014). Exploiting the structures of the u-matrix. In Villmann, T., Schleif, F.-M., Kaden, M., and Lange, M., editors, *Advances in Self-Organizing Maps and Learning Vector Quantization*, pages 249–257, Cham. Springer International Publishing.

Lubowiecka, I., Szepietowska, K., Tomaszewska, A., Bielski, P. M., Chmielewski, M., Lichodziejewska-Niemierko, M., and Szymczak, C. (2022). A novel in vivo approach to assess strains of the human abdominal wall under known intraabdominal pressure. *Journal of the Mechanical Behavior of Biomedical Materials*, 125:104902.

Mayol, J. (2023). Transforming abdominal wall surgery with generative artificial intelligence. *Journal of abdominal wall surgery : JAWS*, 2:12419.

Michael S. Detamore, K. A. A. (2003). Structure and function of the temporomandibular joint disc: Implications for tissue engineering. *Journal of Oral and Maxillofacial Surgery*, 61(4):494–506.

Micomyiza, C., Zou, B., and Li, Y. (2022). An effective automatic segmentation of abdominal adipose tissue using a convolution neural network. *Diabetes and Metabolic Syndrome: Clinical Research and Reviews*, 16(9):102589.

Mikołajowski, G., Pałac, M., and Linek, P. (2022). Automated ultrasound measurements of lateral abdominal muscles under controlled breathing phases. *Computer Methods and Programs in Biomedicine*, 221:106936.

Mills, K. (2005). The basics of electromyography. *Journal of neurology, neurosurgery, and psychiatry*, 76 Suppl 2.

Mujakperuo, H., Watson, M., Morrison, R., and Macfarlane, T. (2010). Pharmacological interventions for pain in patients with temporomandibular disorders. *Cochrane Database of Systematic Reviews*, (10).

Nazari, F., Nahavandi, D., Mohajer, N., and Khosravi, A. (2021). Human activity recognition from knee angle using machine learning techniques. In *2021 IEEE International Conference on Systems, Man, and Cybernetics (SMC)*, pages 295–300.

Nguyen, Q. and Lejeune, E. (2024). Segmenting mechanically heterogeneous domains via unsupervised learning. *Biomechanics and Modeling in Mechanobiology*, 23:1–24.

Ozsari, S., Güzel, M. S., Yılmaz, D., and Kamburoğlu, K. (2023a). A comprehensive review of artificial intelligence based algorithms regarding temporomandibular joint related diseases. *Diagnostics*, 13(16).

Ozsari, S., Yapicioglu, F. R., Yilmaz, D., Kamburoglu, K., Guzel, M. S., Bostanci, G. E., Acici, K., and Asuroglu, T. (2023b). Interpretation of magnetic resonance images of temporomandibular joint disorders by using deep learning. *IEEE Access*, 11:49102–49113.

Pachera, P., Pavan, P., Todros, S., Cavinato, C., Fontanella, C., and Natali, A. (2016). A numerical investigation of the healthy abdominal wall structures. *Journal of Biomechanics*, 49(9):1818–1823.

Palanca, M., Tozzi, G., and Cristofolini, L. (2016). The use of digital image correlation in the biomechanical area: a review. *International Biomechanics*, 3(1):1–21.

Pérez Díaz, V., Sanz Ballesteros, S., Hernández García, E., Descalzo Casado, E., Herguedas Callejo, I., and Ferrer Perales, C. (2017). Intraperitoneal pressure in peritoneal dialysis. *Nefrologia : Publicacion Oficial de la Sociedad Española de Nefrologia*, 37:579–586.

Peña, E., Hernández-Gascón, B., and Calvo, B. (2017). Chapter 12 - human abdomen: Mechanical modeling and clinical applications. In Payan, Y. and Ohayon, J., editors, *Biomechanics of Living Organs*, volume 1 of *Translational Epigenetics*, pages 267–285. Academic Press, Oxford.

Podwojewski, F., Ottenio, M., Beillas, P., Guérin, G., Turquier, F., and Mitton, D. (2014). Mechanical response of human abdominal walls ex vivo: effect of an incisional hernia and a mesh repair. *Journal of the Mechanical Behavior of Biomedical Materials*, 38:126–133.

Potthast, W. (2024). *Biomechanical Data*, pages 11–18. Springer Berlin Heidelberg, Berlin, Heidelberg.

Rath, A., Zhang, J., and Chevrel, J. (1997). The sheath of the rectus abdominis muscle: an anatomical and biomechanical study. *Hernia*, 1(3):139–142.

Remus, R., Sure, C., Selkmann, S., Uttich, E., and Bender, B. (2024). Soft tissue material properties based on human abdominal in vivo macro-indenter measurements. *Frontiers in Bioengineering and Biotechnology*, 12.

Reu, P. L., Toussaint, E., Jones, E., Bruck, H. A., Iadicola, M., Balcaen, R., Turner, D. Z., Siebert, T., Lava, P., and Simonsen, M. (2018). Dic challenge: developing

images and guidelines for evaluating accuracy and resolution of 2d analyses. *Experimental Mechanics*, 58:1067–1099.

Rezapour, M., Seymour, R. B., Sims, S. H., Karunakar, M. A., Habet, N., and Gurcan, M. N. (2024). Employing machine learning to enhance fracture recovery insights through gait analysis. *Journal of Orthopaedic Research*, 42(8):1748–1761.

Sadikine, A., Badic, B., Tasu, J.-P., Noblet, V., Ballet, P., Visvikis, D., and Conze, P.-H. (2024). Improving abdominal image segmentation with overcomplete shape priors. *Computerized Medical Imaging and Graphics*, 113:102356.

Sharma, N., Dar, I. G., Kumar, J., Khan, A., and Thakur, A. (2019). Temporomandibular joint syndrome prediction using neural network. In Ray, K., Sharan, S. N., Rawat, S., Jain, S. K., Srivastava, S., and Bandyopadhyay, A., editors, *Engineering Vibration, Communication and Information Processing*, pages 1–7. Springer Singapore.

Simón-Allué, R., Calvo, B., Oberai, A., and Barbone, P. (2017). Towards the mechanical characterization of abdominal wall by inverse analysis. *Journal of the Mechanical Behavior of Biomedical Materials*, 66:127–137.

Spadoni, S., Todros, S., and Pavan, P. (2024). Numerical modeling of the abdominal wall biomechanics and experimental analysis for model validation. *Frontiers in Bioengineering and Biotechnology*, 12.

Stergiou, N. (2020). Chapter 1 - introduction to biomechanics. In Stergiou, N., editor, *Biomechanics and Gait Analysis*, pages 1–16. Academic Press.

Sutton, M., Orteu, J.-J., and Schreier, H. (2009). *Image Correlation for Shape, Motion and Deformation Measurements. Basic Concepts, Theory and Applications*. Springer.

Szepietowska, K., Troka, M., Lichodziejewska-Niemierko, M., Chmielewski, M., and Lubowiecka, I. (2023). Full-field in vivo experimental study of the strains of a breathing human abdominal wall with intra-abdominal pressure variation. *Journal of the Mechanical Behavior of Biomedical Materials*, 147:106148.

Szymczak, C., Lubowiecka, I., Tomaszewska, A., and Śmietański, M. (2012). Investigation of abdomen surface deformation due to life excitation: implications

for implant selection and orientation in laparoscopic ventral hernia repair. *Clinical Biomechanics*, 27:105–110.

Taha, A., Enodien, B., Frey, D., and Taha-Mehlitz, S. (2022). The development of artificial intelligence in hernia surgery: A scoping review. *Frontiers in Surgery*, 9:908014.

Tanaka, E., Kawai, N., Tanaka, M., Todoh, M., Eijden, T., Hanaoka, K., Dalla-Bona, D., Takata, T., and Tanne, K. (2004). The frictional coefficient of the temporomandibular joint and its dependency on the magnitude and duration of joint loading. *Journal of dental research*, 83:404–7.

Tang, H., Dai, Y., Zhao, D., Sun, Z., Chen, F., Zhu, Y., Liang, H., Cao, H., and Zhang, L. (2022). Deep domain adaptation for predicting intra-abdominal pressure with multichannel attention fusion radar chip. *Advanced Intelligent Systems*, 4:2100209.

Tanteri, G., Tanteri, E., Tanteri, C., and Slavicek, G. (2020). *TMJ Dynamics*, pages 57–90. Springer International Publishing, Cham.

Taşkıran, U. and Çunkaş, M. (2021). A deep learning based decision support system for diagnosis of temporomandibular joint disorder. *Applied Acoustics*, 182:108292.

Tomaszewska, A., Lubowiecka, I., Szymczak, C., Smietański, M., Meronk, B., Kłosowski, P., and Bury, K. (2013). Physical and mathematical modelling of implant-fascia system in order to improve laparoscopic repair of ventral hernia. *Clinical Biomechanics (Bristol, Avon)*, 28:743–51.

Troka, M., Szepietowska, K., and Lubowiecka, I. (2024a). Self-organising maps in the analysis of strains of human abdominal wall to identify areas of similar mechanical behaviour. *Journal of the Mechanical Behavior of Biomedical Materials*, 156:106578.

Troka, M., Wojnicz, W., Szepietowska, K., and Lubowiecka, I. (2024b). *Unsupervised Learning for Biomechanical Data Using Self-organising Maps, an Approach for Temporomandibular Joint Analysis*, pages 233–240. Springer Nature Switzerland, Cham.

Troka, M., Wojnicz, W., Szepietowska, K., Podlasiński, M., Walerzak, S., Walerzak, K., and Lubowiecka, I. (2022). Towards classification of patients based on surface emg data of temporomandibular joint muscles using self-organising maps. *Biomedical Signal Processing and Control*, 72:103322.

Urquhart, D. M., Barker, P. J., Hodges, P. W., Story, I. H., and Briggs, C. A. (2005). Regional morphology of the transversus abdominis and obliquus internus and externus abdominis muscles. *Clinical Biomechanics*, 20(3):233–241.

Vesanto, J. and Alhoniemi, E. (2000). Clustering of the self-organizing map. *IEEE Transactions on Neural Networks*, 11(3):586–600.

Vesanto, J., Himberg, J., Alhoniemi, E., and Parhankangas, J. (1999). Self-organizing map in matlab: the som toolbox. In *In Proceedings of the Matlab DSP Conference*, pages 35–40.

Vesanto, J., Himberg, J., Alhoniemi, E., and Parhankangas, J. (2000). Som toolbox for matlab. *Technical Report A57*, 59.

Vogel, R. and Mück, B. (2024). Artificial intelligence—what to expect from machine learning and deep learning in hernia surgery. *Journal of Abdominal Wall Surgery*, 3.

Whitehead-Clarke, T., Brown, C., Ail, G., Mudera, V., Smith, C., and Kureshi, A. (2023). Characterisation of human posterior rectus sheath reveals mechanical and structural anisotropy. *Clinical Biomechanics*, 106:105989.

Wojnicz, W., Lubowiecka, I., Tomaszewska, A., Szepietowska, K., and Bielski, P. M. (2019). Jaw biomechanics: Estimation of activity of muscles acting at the temporomandibular joint. *AIP Conference Proceedings*, 2078(1):020105–.

Wu, C., Xu, Y., Fang, J., and Li, Q. (2024). Machine learning in biomaterials, biomechanics/mechanobiology, and biofabrication: State of the art and perspective. *Archives of Computational Methods in Engineering*.

Xiang, L., Wang, A., Gu, Y., Zhao, L., Shim, V., and Fernandez, J. (2022). Recent machine learning progress in lower limb running biomechanics with wearable technology: A systematic review. *Frontiers in Neurorobotics*, 16:913052.

Yin, H. (2008). *The Self-Organizing Maps: Background, Theories, Extensions and Applications*, pages 715–762. Springer Berlin Heidelberg, Berlin, Heidelberg.